



Lehrstuhl für Experimentelle Genetik

Characterization of a novel mouse line with an immunological phenotype, identification of the causative mutation and the underlying pathomechanism

Irina Treise

Vollständiger Abdruck der von der Fakultät Wissenschaftszentrum Weihenstephan für Ernährung, Landnutzung und Umwelt der Technischen Universität München zur Erlangung des akademischen Grades eines Doktors der Naturwissenschaften (Dr. rer. nat.) genehmigten Dissertation.

Vorsitzender: Prof. Dr. Johannes Beckers

Prüfer der Dissertation:

1. Prof. Dr. Martin Hrabě de Angelis
2. Prof. Dr. Dirk H. Busch
3. Prof. Dr. Michael Groll

Die Dissertation wurde am 31.08.2016 bei der Technischen Universität München eingereicht und durch die Fakultät Wissenschaftszentrum Weihenstephan für Ernährung, Landnutzung und Umwelt am 22.11.2016 angenommen.

dedicated to Artur and Lars
tempus fugit - amor manet

Table of Contents

INDEX OF FIGURES	8
1 SUMMARY	11
2 INTRODUCTION	13
2.1 ENU SCREENING IN THE MOUSE	13
2.2 MURINE PERIPHERAL BLOOD LEUKOCYTE SUBTYPES AND THEIR PHENOTYPIC CHARACTERISTICS	14
2.2.1 THE PERIPHERAL MYELOID COMPARTMENT	15
2.2.2 THE PERIPHERAL LYMPHOID COMPARTMENT	17
2.3 HEMATOPOIESIS	22
2.4 T CELL DEVELOPMENT IN THE THYMIC MICROENVIRONMENT	23
2.5 ANTIGENS IN T CELL IMMUNITY	25
2.6 THE PROTEASOME	26
2.6.1 IMMUNE FUNCTIONS OF PROTEASOMES	28
2.6.2 PROTEASOME BIOGENESIS PATHWAY	29
2.6.3 PROTEASOME-ASSOCIATED HUMAN DISEASES	30
3 OBJECTIVE OF THIS PHD THESIS	32
4 MATERIAL AND METHODS	34
4.1 MATERIALS	34
4.1.1 EQUIPMENT	34
4.1.2 CHEMICALS AND REAGENTS	35
4.1.3 BUFFERS AND MEDIA	37
4.1.4 ANTIBODIES	38
4.1.5 PEPTIDES AND MHC MULTIMERS	40
4.1.6 PRIMERS	40
4.1.7 PLASMIDS	40
4.2 METHODS	41
4.2.1 MICE	41
4.2.2 GENERAL STATISTICAL EVALUATION	41
4.2.3 INFECTION	42
4.2.4 CELL PREPARATION AND FLOW CYTOMETRY	42
4.2.5 IRRADIATION AND BONE MARROW TRANSPLANTATION	44
4.2.6 PLASMA IMMUNOGLOBULIN, CYTOKINE AND AUTOANTIBODY ESTIMATION	44
4.2.7 GROSS PATHOLOGY, NECROPSY, HISTOLOGY AND IMMUNOHISTOCHEMISTRY	45

4.2.8	EXOME SEQUENCING	46
4.2.9	GENOTYPING	46
4.2.10	YEAST MUTAGENESIS, PROTEASOME PURIFICATION, CRYSTALLIZATION AND STRUCTURE DETERMINATION	47
4.2.11	DNA AND PROTEIN SEQUENCES	48
4.2.12	GENERATION OF OVEREXPRESSION CONSTRUCTS	49
4.2.13	RETROVIRUS PRODUCTION AND T CELL TRANSDUCTION	49
5	RESULTS	50
5.1	CHARACTERIZATION OF HETEROZYGOUS TUB006 MUTANTS	50
5.1.1	ANALYSIS OF THE IMMUNE COMPETENCE OF HETEROZYGOUS TUB006 MICE IN THE <i>LISTERIA MONOCYTOGENES</i> INFECTION MODEL	55
5.2	HOMOZYGOUS TUB006 MUTANTS EXHIBIT A SEVERE IMMUNOLOGICAL PHENOTYPE	58
5.2.1	SEVERE COMBINED IMMUNODEFICIENCY	58
5.2.2	GRANULOCYTOSIS	60
5.2.3	HISTOPATHOLOGICAL EXAMINATION	63
5.2.4	DERMATOSIS	64
5.2.5	INFLAMMATORY MILIEU IN HOMOZYGOUS TUB006 MICE	64
5.2.6	ALTERED HEMATOPOIESIS IN THE BONE MARROW	65
5.3	IDENTIFICATION OF THE UNDERLYING GENETIC ALTERATION	68
5.4	ESTABLISHMENT OF GENOTYPING PROTOCOLS	70
5.5	T AND NK CELL DEFICIENCY IS INBORN, WHILE B CELL DEFICIENCY AND GRANULOCYTOSIS DEVELOP LATER	72
5.6	THYMUS IS PRESENT BUT ABNORMAL IN NEWBORN TUB006 HOMOZYGOTES	74
5.7	BONE MARROW TRANSPLANTATION EXPERIMENTS	76
5.8	IMPACT OF COMMENSALS ON TUB006 PHENOTYPE	81
5.9	VALIDATION OF THE MUTATION	82
5.10	WORKING HYPOTHESIS: MECL-1^{G170W} MUTATION CAUSES PROTEASOME ASSEMBLY DEFECT	86
5.11	LETHAL EFFECT OF MECL-1^{G170W}-OVEREXPRESSION	87
5.12	YEAST MUTAGENESIS AND STRUCTURAL DATA	90
6	DISCUSSION	94
6.1	DIVERSE ASPECTS OF T-LYMPHOPENIA AND SCID IN TUB006 MICE	95
6.2	GRANULOCYTOSIS AND INFLAMMATION IN TUB006 MICE	100
6.3	HEMATOPOIETIC DEFECT	103
6.4	ANALYSIS OF THE CELL-SPECIFIC ROLES IN THE PATHOGENESIS OF TUB006 BY GENERATION OF CONDITIONAL KNOCK IN MOUSE MODEL	105

6.5	MOLECULAR IMPACT OF THE MECL-1^{G170W} MUTATION	106
6.6	HUMAN RELEVANCE	109
7	REFERENCES	113
8	INDEX OF ABBREVIATIONS	132
9	CONTRIBUTIONS	137
10	ACKNOWLEDGEMENT	139

Index of Figures

<i>Figure 1: Classical hematopoiesis model describes stepwise differentiation from pluripotent hematopoietic stem cells to lineage-restricted progeny</i>	22
<i>Figure 2: Mammalian proteasome diversity shown as schematic illustration of the three mammalian proteasome types and their catalytic subunit composition</i>	28
<i>Figure 3: Reduced T cell frequencies in peripheral blood from heterozygous TUB006 mutants</i>	50
<i>Figure 4: Normal body weight, B cell, NK cell and granulocyte counts, as well as immunoglobulin concentrations in heterozygous TUB006 mutants</i>	51
<i>Figure 5: CD3 staining of spleen sections confirms T-lymphopenia</i>	52
<i>Figure 6: Terminal deoxynucleotidyl transferase (Tdt) staining of thymus sections from heterozygous TUB006 mutants</i>	53
<i>Figure 7: Flow cytometric analysis of surface marker expression on splenic T cells from wild type (WT) and heterozygous (het) TUB006 mice</i>	54
<i>Figure 8: Heterozygous TUB006 mutants are highly susceptible to L.m. infection</i>	55
<i>Figure 9: Analysis of the Listeria-specific T cell response on day seven after low-dose infection</i>	56
<i>Figure 10: Homozygous TUB006 mutants present severe phenotype</i>	58
<i>Figure 11: Lack of lymphocytes in homozygous TUB006 mutants</i>	59
<i>Figure 12: Histopathological analysis of spleen sections confirms severe combined immunodeficiency (SCID)</i>	59
<i>Figure 13: T cells of homozygous TUB006 mice show activated surface marker expression pattern</i>	60
<i>Figure 14: Granulocytosis in homozygous TUB006 mutants</i>	61
<i>Figure 15: Myeloid infiltrates in spleen, liver and lung of homozygous TUB006 mutants point towards inflammation</i>	62
<i>Figure 16: Histological analysis of skin sections</i>	64
<i>Figure 17: Cytokine profile in plasma of homozygous TUB006 animals</i>	65
<i>Figure 18: Alteration of hematopoietic precursors in the bone marrow</i>	66
<i>Figure 19: Identification of the hematopoietic stem cell (HSC) compartment in the bone marrow</i>	67
<i>Figure 20: Genetic mapping of the TUB006 mutation by SNP analysis between C57BL/6J and C3HeB/FeJ strains.</i>	68
<i>Figure 21: Location of the TUB006 mutation</i>	69
<i>Figure 22: TUB006 genotyping</i>	71
<i>Figure 23: Phenotype of neonatal TUB006 mutants</i>	73

<i>Figure 24: Thymic stroma defect in thymi from newborn TUB006 homozygotes</i>	74
<i>Figure 25: Impaired thymocyte maturation in homozygous TUB006 neonates</i>	75
<i>Figure 26: Bone marrow from homozygous TUB006 donors does not reconstitute wild type recipients</i>	77
<i>Figure 27: Wild type bone marrow cells give rise to B cells, NK cells and granulocytes in homozygous TUB006 hosts</i>	78
<i>Figure 28: WT→TUB006 bone marrow chimera present granulocytosis</i>	80
<i>Figure 29: Persistence of the TUB006 phenotype under germ-free breeding conditions</i>	81
<i>Figure 30: Phenotype of homozygous TUB006 mutants on different genetic backgrounds</i>	82
<i>Figure 31: Validation of the mutation by phenotyping of the TUB006 × MECL-1 KO offspring</i>	83
<i>Figure 32: Mutational strategy of introduction of the G>T substitution in Psmb10 using CRISPR/Cas9 technology</i>	84
<i>Figure 33: Basic structure of the 20S proteasome and structural modeling of the wild type and TUB006 immunoproteasome</i>	86
<i>Figure 34: Overexpression of mutated MECL-1 causes cell death in murine splenocytes</i>	88
<i>Figure 35: Schematic illustration of the plasmid shuffling technique in yeast</i>	90
<i>Figure 36: Crystal structure of the yeast $\beta 2^{G170A}$ intersubunit contacts</i>	92
<i>Figure 37: Schematic illustration of the construction of the conditional knock in mouse mutant</i>	106

1 Summary

In an effort to unravel novel genes or gene functions related to primary immunodeficiencies, the Immunology Screen of the German Mouse Clinic participated in a large-scale mouse mutagenesis program. Mouse mutants generated using the compound *N*-ethyl-*N*-nitrosourea (ENU) were screened for abnormalities in peripheral blood. Novel mouse mutant lines with immunological phenotypes were identified, and the most impressive mutant line TUB006 has moved into the main focus of this thesis.

The immunological defect was analyzed in detail: Flow cytometric analyses, electrochemiluminescence assays, *in vivo* challenge with the intracellular pathogen *Listeria monocytogenes*, histology and immunohistochemistry revealed that heterozygous mutants exhibit a selective T cell defect. Heterozygous TUB006 mice have a normal life span under specific pathogen-free mouse housing conditions, but they succumb to *Listeria* infection. Homozygous TUB006 mutants lack T-, B- and NK lymphocytes and develop systemic sterile autoinflammation, dermatosis and lipodystrophy. The pathophysiology was analyzed at different levels: from the stem cell in the bone marrow to the phenotype in the skin. The unraveled pathogenesis aspects were complex and based on diverse interweaved factors.

Genetic analysis identified the causative point mutation resulting in the exchange from glycine to tryptophan in a highly conserved position of multicatalytic endopeptidase complex subunit-1 (MECL-1). MECL-1 represents a catalytic subunit of the immuno- and thymoproteasome. In contrast to TUB006, MECL-1 knockout mice can compensate the protein loss by redundant subunits and do not present severe immunodeficiency.

To clarify the molecular basis of the TUB006 disease, a multidisciplinary collaboration was initiated, and the gained molecular data indicate that the TUB006 mutation causes structural changes impeding the biogenesis of functional thymo- and immunoproteasomes. Proteasomes are essential for cell survival, and the selective elimination of cells expressing mutated MECL-1 leads to the immunodeficiency in TUB006 mice. Systemic sterile inflammation together with combined T-, B- and NK- cell deficiency has not yet been annotated to a proteasome subunit mutation. Therefore, the proteasome assembly defect in TUB006 mutants provides a novel molecular pathomechanism for primary immunodeficiency that may also be relevant in humans with immunological defects of unknown etiology.

2 Introduction

2.1 ENU screening in the mouse

For improving our understanding of the mammalian immune system, as well as for discovering novel genes or gene functions relevant to human disorders, mouse models with spontaneous (Shultz and Sidman 1987, Joliat and Shultz 2001) or induced mutations (Nelms and Goodnow 2001, Beutler, Jiang et al. 2006, Hoyne and Goodnow 2006, Rutschmann and Hoebe 2008, Soewarto, Klaften et al. 2009) have proven to be invaluable. A large number of mutant mouse lines have been produced by knockout of known genes. In contrast to such a ‘gene driven’ approach, the ‘phenotype driven’ approach allows identification of new genes or gene functions by screening of chemically induced random mutants for phenotypes of interest. The synthetic mutagen *N*-ethyl-*N*-nitrosourea (ENU) causes alkylation of nucleotides, thereby inducing genome-wide point mutations (Barbaric, Wells et al. 2007). This mirrors human single nucleotide variants (SNVs) causative for numerous monogenic disorders (*Online Mendelian Inheritance in Man* database, <http://www.omim.org>). Thus, ENU became the standard mutagen used in phenotype-driven mutagenesis screens worldwide in diverse model organisms such as drosophila or zebra fish.

The pioneer large-scale ENU mutagenesis and phenotypic screening project in the mouse model was launched in Munich (Hrabě de Angelis, Flaswinkel et al. 2000, Rathkolb, Fuchs et al. 2000). The program of random genome-wide germline mutagenesis particularly aimed at discovering mutant mouse lines with clinical phenotypes as models for human diseases. Male mice were injected with ENU. After injection, ENU distributes systemically and in particular targets early stem cell spermatogonia. ENU alkylates genomic DNA during cell division by transferring its ethyl group to nucleophilic sites of nucleic acids. The toxicity of ENU leads to temporal sterility of ENU-treated males, but the fertility recovers in a dose- and strain-dependent manner. The inbred strain C3HeB/FeJ was chosen for the Munich ENU mutagenesis program due to its ability to tolerate high doses of ENU and to regain fertility to relatively high percentage of 50% of injected males. ENU-treated males were mated with untreated wild type female mice, leading to production of heterozygous offspring, which were then screened for phenotypes of interest.

It was calculated that each individual first-generation offspring is carrying an average of approx. 30 independent protein-changing mutations (Beutler, Jiang et al. 2006, Cook, Vinuesa et al. 2006). Most mutations represent A:T to T:A transversions at the nucleotide level, leading to missense mutations at the protein level (Justice, Noveroske et al. 1999). Analysis of the genomic distribution of ENU-induced SNVs showed that resulting SNVs are not randomly distributed, but are overrepresented in genes with high G+C content, and the mutated nucleotide is often flanked directly by C or G nucleotides (Barbaric, Wells et al. 2007).

For many years, the bottleneck in ENU mutagenesis approaches remained the identification of the underlying genetic alteration (Nelms and Goodnow 2001). The most time-consuming part comprised the out- and backcrossing of the affected carrier to wild types of a different genetic background to narrow down the chromosomal region of the mutation by linkage of the phenotype to genetic markers (Soewarto, Klaften et al. 2009). As genetic markers, SNPs (single nucleotide polymorphisms) - inheritable genomic variations among different mouse strains - have proven to be an important tool (Klaften and Hrabě de Angelis 2005). Even though this tool helps to reduce the chromosomal region of the mutation, most cases still exhibit a variety of remaining candidate genes. The former bottleneck has recently been overcome by development on Next generation deep sequencing techniques (Metzker 2010, Fairfield, Gilbert et al. 2011).

2.2 Murine peripheral blood leukocyte subtypes and their phenotypic characteristics

As part of the ENU mutagenesis program at the Helmholtz Zentrum München, the Immunology Screen of the German Mouse Clinic (GMC) analyzed blood samples from ENU-treated offspring for alterations in immune cell populations (Flaswinkel, Alessandrini et al. 2000). Analysis of the peripheral blood is a minimally-invasive method to evaluate the immune status. Furthermore, it facilitates serial analyses over time and mirrors the standard diagnostic method for human immunodeficiencies.

Circulating blood is the primary transportation system within the body. It transports oxygen and carbon dioxide, nutrients and metabolites, as well as signal molecules such as hormones. Blood is composed of the liquid part (plasma) and the cellular part, which has three primary components: red blood cells (erythrocytes), white blood cells (leukocytes) and platelets (thrombocytes). Non-nucleated hemoglobin-containing

erythrocytes transport oxygen to the tissues. Thrombocytes are irregularly shaped particles responsible for blood coagulation. The various leukocyte types with specialized functions and their essential role in the immune system are shortly reviewed in the following chapters. Under baseline conditions, leukocyte subsets are strictly regulated and genetically controlled (Petkova, Yuan et al. 2008, Lynch, Naswa et al. 2010). However, physiological changes in the leukocyte frequencies occur depending on sex-, ageing-, stress- or diet-related factors.

Polychromatic flow cytometry is a powerful method to investigate the heterogenic complexity of leukocytes, since it allows for the definition and proportional assessment of various subsets. In the next chapters, a short overview of the flow cytometric characteristics of the respective leukocyte population is given.

2.2.1 The peripheral myeloid compartment

Myeloid cells of the peripheral blood (granulocytes and monocytes) are crucial components of the innate immune system. Granulocytes are leukocytes containing granules full of effector molecules. There are three types of granulocytes distinguished by their staining capabilities: eosinophils, basophils and neutrophils. Granulocytes patrol in the blood circulation as terminally differentiated cells, until they are recruited into tissues in response to specific stimuli. The life span of short-lived granulocytes in peripheral blood spans only hours to a maximum of several days (Ohnmacht and Voehringer 2009, Bratton and Henson 2011). The eosinophil and rare basophil granulocytes contribute to the development of allergic responses, and play a role in protective immunity against parasites. Furthermore, they interact with other immune cells and modulate immune responses (Mukai, Matsuoka et al. 2005, Rothenberg and Hogan 2006, Karasuyama, Obata et al. 2011). Neutrophils are by far the most abundant granulocyte type. From peripheral blood, neutrophils are recruited into tissues in response to injury or infection (McDonald, Pittman et al. 2010). Within tissues, neutrophils act as major effectors of acute inflammation either triggered by pathogens or in their absence (sterile inflammation). The immediate release of aggressive effector molecules such as reactive oxygen species (ROS), antimicrobial peptides, and proteases efficiently eliminates pathogens, but also possess a host tissue-destructive potential (Nathan 2006). After accomplishing the effector functions, neutrophils undergo apoptosis and are recognized and cleared by macrophages (Rowe, Allen et al. 2002,

Bratton and Henson 2011). Thereby, neutrophils are usually cleared very rapidly to protect the host from overt tissue damage. Detection of morphologically dead neutrophils is rare in tissues during resolution of inflammation. Thus, in the absence of clearance defects, neutrophil removal is an efficient process that actively promotes restoration of tissue structure and function .

Circulating monocytes are a heterogeneous population of precursor cells, which can be further differentiated into tissue macrophages and dendritic cells (DCs; Auffray, Sieweke et al. 2009, Epelman, Lavine et al. 2014). Likewise granulocytes, monocytes are recruited to tissues and promote inflammatory response against microbial triggers (Henderson, Hobbs et al. 2003, Serbina, Jia et al. 2008, Shi and Pamer 2011).

In classic flow cytometry, neutrophils were identified by their high side scatter (SSC) signal that mirrors high granularity of these leukocytes (Robinson and Carter 1993). Currently, the common strategy to identify myeloid cells in murine peripheral blood is the combination of the surface markers Gr-1 and CD11b. Antibodies targeting the myeloid differentiation antigen Gr-1 bind both Ly6C and Ly6G. The surface markers Ly6G and Ly6C have been used extensively for flow cytometric analysis of the myeloid compartment in mice. Co-expression of Ly6G and Ly6C is a sign of neutrophils (Rose, Misharin et al. 2012), whereas Ly6C is expressed on dendritic cells, and subpopulations of lymphocytes and monocytes. For further subdivision of myeloid cells, surface expression of the integrin CD11b is used. Neutrophils express high levels of Gr-1 and intermediate levels of CD11b, whereas mouse blood monocytes are commonly defined by the surface co-expression of high levels of CD11b and intermediate levels of Gr-1 (Lagasse and Weissman 1996, Zhao, Evans et al. 2008). Alternatively, the marker 7/4 in combination with intermediate Gr-1 levels can be used for monocyte identification (Henderson, Hobbs et al. 2003).

The heterogeneous monocyte population can be subdivided into phenotypically and functionally distinct subpopulations by the surface expression of Ly6C. Ly6C^{high} “inflammatory” monocytes are recent emigrants from the bone marrow and show the capacity to migrate into sites of inflammation (Geissmann, Jung et al. 2003, Sunderkotter, Nikolic et al. 2004). In contrast, Ly6C^{low} monocytes have lost this potential. Ly6C^{low} “resident” monocytes show patrolling behavior in the blood vessels and healthy tissues (Auffray, Fogg et al. 2007). Moreover, Ly6C^{high} monocytes mature in the circulation and are the precursors of Ly6C^{low} monocytes (Sunderkotter, Nikolic et al.

2004). Blood DCs, another small subset of monocytic cells in peripheral blood, are characterized by the expression of the integrin CD11c (Auffray, Sieweke et al. 2009).

2.2.2 The peripheral lymphoid compartment

Lymphocytes are categorized into three principle types: natural killer (NK) cells, T and B cells. NK cells are component of the innate immune system and kill cancer cells and virus-infected cells. T and B lymphocytes are components of the adaptive immune system. B cells produce antibodies, while T cells can directly kill or modulate immune responses against foreign cells, including cancer cells and virus-infected cells.

NK cells

NK cells are large granular lymphocytes that are able to recognize and kill transformed, infected and foreign cells. NK cells share some features with T cells, for example the requirement of major histocompatibility complex MHC class I (Yokoyama and Kim 2006, Orr and Lanier 2010) and transcription factors T-bet and Eomes for maturation (Gordon, Chaix et al. 2012).

Using flow cytometry, NK cells can be identified by their surface expression of markers NKp46 and NK1.1 (Karlhofer and Yokoyama 1991, Walzer, Blery et al. 2007). Notably, NK receptors show allelic divergence among different mouse strains, complicating the flow cytometric identification of NK cells. For example, NK1.1 can be used to identify NK cells on C57BL/6, but not on C3H or BALB/c backgrounds (Carlyle, Mesci et al. 2006).

Diverse NK cell subpopulations can be identified upon their expression of specific markers such as CD11b, CD44, or Ly6C: CD11b-expressing NK cells represent the mature population (Chiossone, Chaix et al. 2009); CD44 is an activation marker, which is upregulated to high levels upon activation (Sague, S. L., et al. 2004); and Ly6C is higher expressed in NK cells with memory-like properties (Sun, Beilke et al. 2009).

T cells

The T cell compartment in peripheral blood is a dynamic pool of cells that undergo maturation, antigen encounter, acquisition of effector functions and memory cell formation and maintenance (Woodland and Dutton 2003). The two most abundant functionally distinct T cell lineages – CD4⁺ and CD8⁺ T cells - are discriminated by the expression of co-receptors CD4 or CD8.

CD4⁺ T lymphocytes are referred to as T helper cells. T helper cells modulate the activity of other leukocytes by cytokine secretion, and play an essential role in B cell antibody class switching as well as activation of CD8⁺ T cells and innate immune cells. Functionally distinct subsets of CD4⁺ T cells develop in the context of infections or other inflammatory conditions, distinguished by characteristic cytokine signatures. Although the exact number of T helper subsets is still disputed, the physiological relevance of subsets T_H1, T_H2 and T_H17 is widely accepted (Grogan, Mohrs et al. 2001, Murphy and Reiner 2002, Stockinger and Veldhoen 2007). Another subset of CD4⁺ T cells - regulatory T (T_{reg}) cells - have critical function in suppression of autoimmunity (Williams and Rudensky 2007). Many T_{reg} cells express T cell receptors with high affinity for self-peptide:MHCs (Apostolou, Sarukhan et al. 2002, Pacholczyk, Ignatowicz et al. 2006). In adult mice, the regulatory T cell pool is maintained by self-renewal of mature regulatory T cells (Rubtsov, Niec et al. 2010), but T_{reg} differentiation can be also induced by administration transforming growth factor (TGF)- β to CD4⁺ effector cells (Chen, Jin et al. 2003).

CD8⁺ T cells harbor cytolytic and cytotoxic potential and are therefore termed cytolytic T lymphocytes (CTL). The effector molecules secreted or expressed on the cell surface of CD8⁺ T cells mediate cell death by forming of pores in the cell membrane or pro-apoptotic signaling (Bossi, Trambas et al. 2002, Russell and Ley 2002). Therefore, generation of robust CD8⁺ T cell responses is crucial for immune defense against infections with viruses and intracellular bacteria as well as some tumors. Beside their cytotoxic activity, activated CD8⁺ T cells also secrete immune-stimulatory cytokines such as interferon (IFN)- γ , tumor necrosis factor (TNF)- α and interleukin (IL)-2. These cytokines promote antiviral defense mechanisms, enhance effector functions of innate immune cells, and induce further proliferation and activation of T cells.

The course of a T cell response begins with a naïve T cell that encounters its correspondent antigen for the first time. Within this priming phase, the T cell gets activated and subsequently proliferates to produce numerous daughter cells with the same specificity (clonal expansion). Thereby, a large effector cell population is generated that is responsible for effector functions (e.g. cytokine secretion, acute elimination of the pathogen). Thereafter, the effector phase is terminated by a dramatic reduction of the effector cell population, leaving behind a small number of memory cells

that continuously patrol various tissues and provide long-term immunity (Busch and Pamer 1999, Reiner, Sallusto et al. 2007, Williams and Bevan 2007).

For flow cytometric identification of all mature T cells the expression of the T cell receptor (TCR), but also the Pan-T cell markers CD3 or CD5 are appropriate (Azzam, Grinberg et al. 1998). The T cell pool is divided by the expression of co-receptors CD4 or CD8, and CD4⁺ as well as CD8⁺ T cell populations can be further subdivided upon the cell surface expression of numerous markers. L-selectin (CD62L), for example, is promoting efficient lymphocyte homing to lymph nodes (Arbones, Ord et al. 1994, Catalina, Carroll et al. 1996, Steeber, Green et al. 1996). Ly6C is a surface glycoprotein that was historically considered as a T cell memory marker (Walunas, Bruce et al. 1995). In the meantime, it was shown to be involved in many T cell processes such as cytolysis, proliferation, IL-2 and IFN- γ production, homing, and adhesion to endothelial cells (Gumley, McKenzie et al. 1995, Jaakkola, Merinen et al. 2003, Hanninen, Maksimow et al. 2011). The hyaluronic acid-binding adhesion molecule CD44 mediates T cell trafficking to inflamed sites (DeGrendele, Estess et al. 1997) and also provides co-stimulation (Galandrini, Galluzzo et al. 1994).

A number of phenotypic differences between the different T cell subpopulations have been described. Naïve T cells are characterized by the surface expression of CD62L and CD127 and low expression of the activation marker CD44 (Zhang, Joe et al. 2005, Zhao and Davies 2010). During T cell activation, adhesion molecules, e.g. CD44 and CD11b are upregulated, indicating altered migrating behavior that allows egress into sites of inflammation. Short-living effector T cells lose the expression of CD62L and acquire the CD44⁺CD62L⁻ phenotype. Activation-induced upregulation of CD44 is retained long-term also during memory phase. There are two distinct long-lived memory T cell populations: effector memory (T_{EM}) and central memory T cells (T_{CM}; Sallusto, Lenig et al. 1999). CD127⁺CD62L⁻ T_{EM} preferentially migrate to peripheral tissues, displaying immediate effector functions upon antigen re-encounter, while CD127⁺CD62L⁺ T_{CM} circulate through secondary lymphoid organs, have little effector function, but readily expand and differentiate to secondary effector cells in response to antigen stimulation (Huster, Busch et al. 2004, Masopust, Vezys et al. 2004, Sallusto, Geginat et al. 2004).

Phenotypic identification of memory T cells is further complicated by a process called homeostatic proliferation. Thereby, naïve T cells divide in the periphery without antigen encounter and upregulate activation and memory markers such as CD44 and Ly6C

(Goldrath, Bogatzki et al. 2000, Haluszczak, Akue et al. 2009). In lymphopenic environment, homeostatic proliferation is pronounced, but it is unclear to which extent it contributes to the T cell pool in non-lymphopenic mice (Goldrath and Bevan 1999, Murali-Krishna, Lau et al. 1999).

A CD4⁺ T cell subset expressing high levels of Ly6C was identified that is specialized to regulate plasma cell production (McHeyzer-Williams and McHeyzer-Williams 2004).

Another phenotypic marker for T cells is the IL-2 receptor CD25. In naïve mice, most CD4⁺ T cells expressing CD25 represent T_{reg} cells. However, the definition of T_{reg} cells by co-expression of CD4 and CD25 can be misleading, since the upregulation of CD25 is also observed in non-regulatory CD4⁺ cells upon activation (Malek and Castro 2010). For the definite identification of the T_{reg} subpopulation, intracellular staining of the lineage-specific transcription factor Foxp3 is required (Hori, Nomura et al. 2003).

Besides the predominant CD4⁺ helper and CD8⁺ cytotoxic cells, some small populations of T lymphocytes are present in peripheral blood: CD4 and CD8 double-positive (DP) and double-negative (DN) T cell sublineages, gamma delta T cells, and NKT cells (Zuckermann 1999, Martina, Noel et al. 2015, Fay, Larson et al. 2016). NKT cells form a heterogeneous population of T cells that share some characteristics with NK cells (Godfrey, Hammond et al. 2000). NKT cells influence immune responses in both stimulating or suppressive manner (Kronenberg 2005). The key features of NKT cells include TCR expression, CD1b restriction and rapid production of high cytokine levels, particularly IL-4 and IFN- γ . In mice, NKT cells are commonly defined as NK1.1⁺CD3⁺. Like conventional T cells, NKT cells can be subdivided into functionally distinct CD4⁺, DN and CD8⁺ subsets (Godfrey, Hammond et al. 2000). Most NKT cells are developed in the thymus, but extrathymical generation from T cells by upregulation of NK1.1 in the periphery was also described (Slifka, Pagarigan et al. 2000). The majority of NKT cells have a special type of invariant T cell receptor, which is generated by the rearrangement of V α 14-J α 18 segments. These cells are termed type I or invariant NKT (iNKT) cells. DN T cells, which are not NKT cells, play a role in the development of autoimmune diseases (Shivakumar, Tsokos et al. 1989, Sumida, Sakamoto et al. 1995).

Taken together, the complex T cell compartment is functionally diverse, complicating its analysis by flow cytometry. However, great effort has been made to correlate functional properties with phenotypical characteristics.

B cells

B lymphocytes are the main players of humoral immunity due to their capability to synthesize immunoglobulins (Ig). The B cell receptor (BCR, formed by the membrane-bound form of immunoglobulin and other transmembrane proteins) signaling is essential for the B cell development and activation. B cells are generated in the bone marrow and circulate in the blood and secondary lymphoid tissues. When B cells encounter their specific antigen in the lymphoid tissues and receive stimulatory signals from T helper cells, B cells proliferate and its progeny undergoes alterations of the B cells receptor by isotype switch recombination and somatic hypermutation. Thereafter, B cells differentiate either into short-lived plasma cells, which produce large quantities of antibodies or into long-lived memory B cells that respond rapidly upon re-encounter with the same antigen (McHeyzer-Williams and McHeyzer-Williams 2005).

For the definition of B cells by flow cytometry, the surface expression of CD19 and/or B220 is commonly used. CD19 might be the more reliable B cell marker than B220 (Rolink, ten Boekel et al. 1996). Some B cell subpopulations can be distinguished by levels of surface IgD and IgM expression. IgM is the first antibody isotype expressed during B cell development. Following egress from the bone marrow, B cells start expressing a second Ig isotype, IgD. Thus, naïve mature B cells are characterized as IgM⁺IgD⁺ B cells (Lutz, Ledermann et al. 1998, Geisberger, Lamers et al. 2006). After that, IgM is downregulated and the IgD⁺IgM⁻ B cell compartment represent mature recirculating B cells (Korner, Winkler et al. 2001). During B cell activation, the surface Ig expression is switched to IgG and IgA, thus B cells after class switch appear IgM⁻IgD⁻ B cells (Reynaud, Descatoire et al. 2012).

Besides conventional B cells, a second B cell lineage exists known as B1 cells. (Fagarasan, Watanabe et al. 2000). B1 cells are characterized by surface expression of CD5. B1 cells express a distinctive repertoire of receptors and differ from conventional (sometimes referred to as B2 cells) B cells. B1 cells are present in stable frequencies in immunologically normal mouse strains, but show abnormal frequency alterations in both directions in immunodeficient mouse mutants (Hayakawa, Hardy et al. 1983, Sidman, Shultz et al. 1986).

2.3 Hematopoiesis

The lifespan of terminally differentiated leukocytes is limited, ranging from few hours for granulocytes to several years for memory T cells. To replenish the peripheral compartment, daily billions of leukocytes are generated. The strictly regulated process of blood cell production and homeostasis is termed hematopoiesis. Blood cell production is established during embryogenesis, first in the yolk sac, subsequently in the liver, spleen, and eventually in the bone marrow. After birth, the bone marrow remains the predominant site of hematopoiesis.

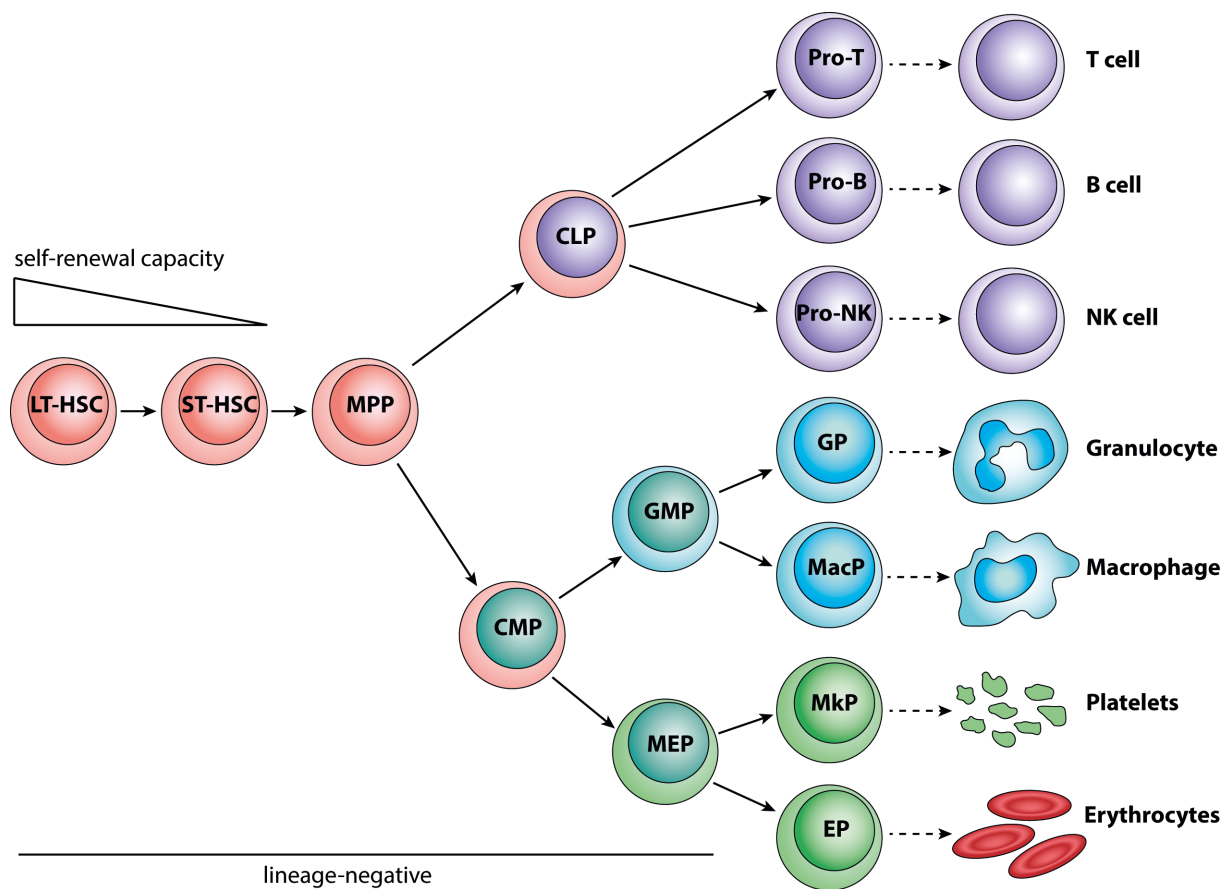


Figure 1: Classical hematopoiesis model describes stepwise differentiation from pluripotent hematopoietic stem cells to lineage-restricted progeny. Solid arrows show irreversible maturation events. Dashed arrows indicate multi-step differentiation to terminally differentiated cells. LT-HSC, long-term hematopoietic stem cell; ST-HSC, short-term hematopoietic stem cell; MPP, multipotent progenitor cell; CLP, common myeloid progenitor; CMP, common myeloid progenitor; GMP, granulocyte-macrophage progenitor; MEP, megakaryocyte-erythrocyte progenitor; EP, erythrocyte progenitor; MkP, megakaryocyte progenitor; GP, granulocyte progenitor; MacP, macrophage progenitor.

Pluripotent hematopoietic stem cells (HSCs) are the origin of the full spectrum of leukocyte lineages (Figure 1; Spangrude, Heimfeld et al. 1988, Weissman 2000). Long-term HSCs (LT-HSCs) have the ability to self-renew and to differentiate to all lineages throughout the entire life span of the organism (Morrison and Weissman 1994, Wilson, Laurenti et al. 2008). Short-term HSCs (ST-HSCs) have a more limited self-renewal

capability. ST-HSCs can reconstitute the hematopoietic system after transplantation into an irradiated recipient, but fail to reconstitute a secondary recipient (Morrison and Weissman 1994). HSCs give rise to non-self-renewing multipotent progenitor cells (MPPs; Morrison, Wandycz et al. 1997), which in turn differentiate into lineage-restricted progenitors. These include common lymphoid progenitors (CLPs; Kondo, Weissman et al. 1997) and common myeloid progenitors (CMPs; Akashi, Traver et al. 2000). CLPs develop to T cells, B cells and NK cells. CMPs undergo differentiation to either megakaryocyte/erythrocyte (MEPs) or granulocyte/macrophage progenitors (GMPs). These committed progenitors in turn give rise to the terminally differentiated erythrocytes and platelets or granulocytes and macrophages, respectively.

Beyond basic homeostasis, hematopoietic stress conditions such as blood loss or infection demand rapid adaptation of the hematopoietic system by increasing cellular output. To ensure production of the required leukocyte lineages, the balance between the diverse hematopoietic differentiation pathways is highly regulated. For example, lymphopoiesis and granulopoiesis show reciprocal regulation (Ueda, Kondo et al. 2005). In response to infection, a program of accelerated granulocyte production is initiated that enables fast defense against pathogenic invaders. Bacterial components and inflammatory cytokines such as IL-1 stimulate granulopoiesis and the release of neutrophils into the blood stream (Cain, Snowden et al. 2011). Such inflammation-induced granulocyte expansion, also known as “emergency granulopoiesis”, engages the total capacity of the bone marrow haematopoietic system and leaves no space for lymphopoiesis (Manz and Boettcher 2014).

Thus, the bone marrow hematopoietic system adopts the needs of an organism and supplies the required blood cell types in a highly orchestrated way during physiological steady-state as well as under emergency conditions.

2.4 T cell development in the thymic microenvironment

As described above, the development of lymphocytes starts in the bone marrow. While B cells differentiate terminally within the bone marrow, T cell precursors are recruited to the thymus to complete their maturation (Perry, Pierce et al. 2003). The thymus is a bilobed organ located above the heart. It is surrounded by a capsule and displays morphological distinction into the outer cortex and inner medulla. The thymic stroma – a network of thymic epithelial cells (TECs) - is essential for T cell differentiation, and

impaired development of TECs leads to complete lack of T cells in the athymic nude mouse (Nehls, Kyewski et al. 1996, Anderson and Takahama 2012).

T cell progenitors enter the thymus at the border of cortex and medulla. The maturing thymocytes migrate outwards the cortex to the subcapsular region and then back through the cortex into the medulla (Petrie and Zuniga-Pflucker 2007). The disparate thymic regions provide specific microenvironments that convey differentiation events such as proliferation, recombination of the TCR, lineage commitment, and clonal selection, as described below in more detail.

Conventional T lymphocytes ($CD4^+$ or $CD8^+$ $TCR\alpha\beta$ T cells) recognize antigens via the TCR, which consists of two chains: α and β . Both TCR chains are not germline encoded, but rather generated during thymocyte maturation by individual somatic recombination events. The most immature T cell progenitors in the thymus lack surface expression of the TCR and the TCR-associated co-receptor complex CD3. Furthermore, they do not express the T cell co-receptors CD4 or CD8 and are thus termed $CD4/CD8$ double-negative thymocytes. While migrating outwards the cortex and accumulating within the subcapsular region, T cell progenitors undergo V(D)J recombination, i.e. random sequential gene rearrangement of the genomic regions encoding components of the β and α TCR chains (Schatz, Oettinger et al. 1992, Livak, Tourigny et al. 1999). V(D)J recombination results in an individual TCR with a unique antigen specificity in each T cell in order to achieve maximal diversity of the T cell repertoire.

Upon successfully rearranged TCRs and the associated complex CD3 on the cell surface, thymocytes start migration back inwards. This developmental stage is associated with the expression of both CD4 and CD8 co-receptors, thus thymocytes show $CD4^+ CD8^+$ double positive signature. Developing DP thymocytes expressing a functional TCR first are screened for their ability to recognize self-peptides in association with MHC class I or class II molecules. Only thymocytes that can bind self-peptide:MHC with low avidity receive a survival signal. This process, also known as positive selection, takes place in the thymic cortex and is mediated by cortical thymic epithelial cells (cTECs; Laufer, DeKoning et al. 1996, Nitta, Murata et al. 2010). T cells, which fail at positive selection, undergo apoptosis. Positive selection eliminates potentially self-reactive high-avidity T cells as well as T cells incapable of MHC recognition (Laufer, DeKoning et al. 1996, Starr, Jameson et al. 2003).

DP thymocytes differentiate into either CD4⁺CD8⁻ (CD4SP) or CD4⁻CD8⁺ (CD8SP) T cells and move then to the thymic medulla. Within the medulla, maturing T cells encounter medullary thymic epithelial cells (mTECs) and thymic dendritic cells. These cell types mediate elimination of self-reactive T cells in a process called negative selection (Starr, Jameson et al. 2003, Perry, Lio et al. 2014). As a result, self-tolerance is established. T cells successfully passed this last differentiation step mature and finally are released into the periphery as naïve CD4⁺ or CD8⁺ T cells.

Most developing thymocytes die by apoptosis without successfully completing the stepwise progression of thymocyte development. The functionally distinct thymic epithelial microenvironments play a pivotal role in the establishment of an effective T cell pool and preventing autoimmunity.

2.5 Antigen in T cell immunity

Each individual T cell carries TCRs of one distinct antigen specificity, and the pool of individual T cells forms the highly diverse T cell repertoire of an organism. The TCRs recognize peptide:MHC complexes, i.e. membrane-bound molecules of the MHC family displaying processed protein antigens (Germain 1994). MHC class I molecules are expressed on the surface of all nucleated cells, while MHC class II expression is limited to professional antigen-presenting cells (APCs). T cell recognition of either peptide:MHC class I or peptide:MHC class II complexes depends not only on the TCR specificity, but also on expression of T cell co-receptors CD4 or CD8, which discriminates the CD8⁺ cytotoxic T cell and CD4⁺ T helper cell compartments (Germain 2002).

Extracellular or endosomal proteins are unselectively degraded by endosomal and lysosomal proteases such as cathepsins. The resulting peptide fragments of 15 to 24 amino acids are preferentially loaded on MHC class II molecules and presented to CD4⁺ T cells (Villadangos 2001, Lennon-Dumenil, Bakker et al. 2002).

In contrast, MHC class I molecules recognized by TCRs of CD8⁺ T cells are loaded with peptides from cytosolic origin. More than 90 % of all cytosolic proteins are degraded by the proteasome – the major protease engaged in the non-lysosomal protein turnover. By shaping the antigenic pool of peptides the proteasome constitutes a key component of the CD8⁺ T cell immunity. From cytosol, putative antigenic peptides are translocated into the endoplasmic reticulum (ER) by the transporter associated with antigen processing (TAP; Townsend and Trowsdale 1993). In the ER peptides associate with the binding

groove of nascent MHC class I molecules. After maturation, stable peptide:MHC complexes are transported to the cell surface for their exposure to the extracellular environment.

2.6 The proteasome

For cellular function and viability, degradation of misfolded and damaged proteins is crucial. Protein homeostasis is mainly maintained by the ubiquitin-proteasome system, the major proteolytic pathway. The key player of this system is the proteasome, acting as the major cytoplasmic protease for controlled degradation of intracellular proteins. Beyond basic protein homeostasis, proteasomes have wide-spread functions such as control of signaling pathways, cell cycle and apoptosis regulators via selective proteolysis (Hershko, Ciechanover et al. 2000), as well as generation of peptides for major MHC class-I presentation (Pamer and Cresswell 1998, Sijts and Kloetzel 2011).

The 26S proteasome complex consists of a barrel-shaped 20S proteolytic core and two 19S regulatory particles located at the brims of the cylinder (Kish-Trier and Hill 2013). The 19S particles bind ubiquitinated proteins, and translocate them into the proteolytic chamber of the 20S core (Finley 2009).

The basic structure of the 20S proteasome is highly conserved among eukaryotes, but it is also present in a simplified form in prokaryotes including archaea and bacteria (Bochtler, Ditzel et al. 1997, Groll, Ditzel et al. 1997, Huber, Basler et al. 2012). The cylindrical proteasome is formed by 28 subunits arranged in four stacked heptameric rings. Proteasomes are formed by the two outer α -rings and two inner β -rings. Each ring of eukaryotic proteasomes contains seven different (but similar) subunits (α 1-7 and β 1-7) located at fixed positions. The proteolytic activity is limited to the three subunits β 1-, β 2-, and β 5.

Whereas simple eukaryotes like yeast express only one type of proteasome (Groll, Ditzel et al. 1997), in vertebrates with adaptive immunity a second class of proteasome has coevolved, termed the immunoproteasome (Groettrup, Kirk et al. 2010). The “classical” proteasome, hereafter referred to as the constitutive proteasome, comprises the constitutive catalytic subunits β 1c, β 2c and β 5c; and is predominantly expressed in all non-hematopoietic cells. The immunoproteasome show a distinct enzymatically active β -subunit composition: β 1i (LMP2, low molecular weight protein 2), β 2i (MECL-1, multicatalytic endopeptidase complex-like-1) and β 5i (LMP7; Figure 2; Groettrup et al.,

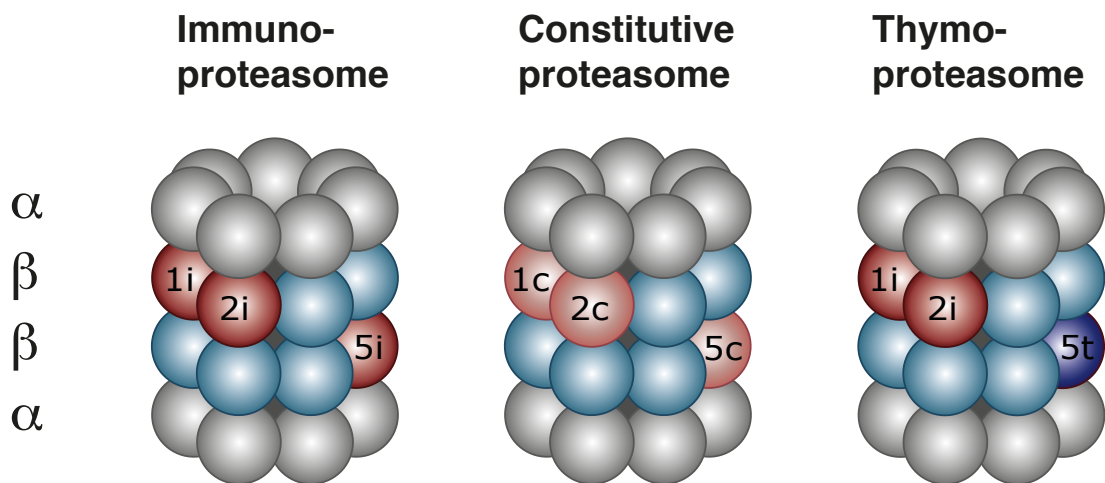
2010). The nomenclature of the different subunits and their encoding genes are summarized in Table 1.

Table 1: Nomenclature of diverse catalytic subunits of proteasomes

	Subunit	LMP-alias	Mouse	Human	Gene
<i>Constitutive subunits</i>					
	β 1c	LMP19	δ	Y	<i>Psmb6</i>
	β 2c	LMP9	MC14	Z	<i>Psmb7</i>
	β 5c	LMP17	MB	X	<i>Psmb5</i>
<i>Specialized subunits</i>					
	β 1i	LMP2	LMP2	LMP2	<i>Psmb9</i>
	β 2i	LMP10	MECL-1	MECL-1	<i>Psmb10</i>
	β 5i	LMP7	LMP7	LMP7	<i>Psmb8</i>
	β 5t				<i>Psmb11</i>

The immunoproteasome is constitutively produced in lymphocytes and professional APCs, but its expression can be induced also in non-immune tissues by the proinflammatory cytokine IFN- γ (Aki, Shimbara et al. 1994, Groettrup, Kraft et al. 1996, Nandi, Jiang et al. 1996, Groettrup, Kirk et al. 2010). In some experimental settings, also TNF- α , IFN- α , IFN- β and lipopolysaccharide (LPS) can induce immuno-subunit expression (Van den Eynde and Morel 2001, Reis, Hassan et al. 2011). The immunoproteasome generates the majority of MHC class-I antigens required for efficient immune surveillance and pathogen clearance by CD8⁺ T cells as proven by knockout mice lacking individual or all three catalytic immuno-subunits (Fehling, Swat et al. 1994, Van Kaer, Ashton-Rickardt et al. 1994, Basler, Moebius et al. 2006, Kincaid, Che et al. 2012).

Some years ago, a third type of specialized proteasome has been discovered in the murine and human thymus and termed thymoproteasome (Murata, Sasaki et al. 2007, Tomaru, Ishizu et al. 2009). It is composed of LMP2, MECL-1 and a third, thymoproteasome-specific catalytic subunit β 5t (Murata, Sasaki et al. 2007; Figure 2). The thymoproteasome is produced exclusively in cTECs, and β 5t knockout studies demonstrated its essential role in positive selection during CD8⁺ T cell maturation (Xing, Jameson et al. 2013).



$\beta 1$	$\beta 1i$ LMP2	$\beta 1c$ δ	$\beta 1i$ LMP2
$\beta 2$	$\beta 2i$ MECL-1	$\beta 2c$ MC14	$\beta 2i$ MECL-1
$\beta 5$	$\beta 5i$ LMP7	$\beta 5c$ MB1	$\beta 5t$

Figure 2: Mammalian proteasome diversity shown as schematic illustration of the three mammalian proteasome types and their catalytic subunit composition. Grey: α -subunit, Light blue: non-catalytic β -subunits, light red: catalytic constitutive β -subunits, dark red: immuno- β -subunits, dark blue: thymoproteasome-specific subunit $\beta 5t$.

Besides the three mentioned eukaryotic proteasome types, mixed-type proteasomes with specific cleavage specificities were reported, incorporating combined subunit composition: LMP2, $\beta 2c$ and LMP7; or $\beta 1c$, $\beta 2c$ and LMP7; or $\beta 1c$, MECL-1 and LMP7 (Dahlmann, Ruppert et al. 2000, De, Jayarapu et al. 2003, Guillaume, Chapiro et al. 2010). To even more complicate the proteasome diversity, proteasomes with asymmetric composition of β subunits were described, bearing two different β -rings (Klare, Seeger et al. 2007).

2.6.1 Immune functions of proteasomes

All three types of proteasomes, the constitutive proteasome, immunoproteasome and thymoproteasome, generate antigenic peptides presented on MHC I molecules (Van den Eynde and Morel 2001, Murata, Takahama et al. 2008). However, they have distinct substrate specificities, resulting in production of different peptide repertoires. Even though the constitutive proteasome can produce immunogenic peptides, the immunoproteasome is more efficient in this process. Viral infections trigger cytokine release, which in turn induce the expression of the immunoproteasome. This leads to enhanced antigen presentation and support clearance of the pathogen. Immunoproteasome-deficient mice exhibit a quantitatively and qualitatively altered

antigen repertoire (Kincaid, Che et al. 2012). Besides, the immunoproteasome plays a crucial role in T cell differentiation, survival and the release of proinflammatory cytokines. The basis of this requirement is not yet understood, but the nuclear factor- κ B (NF- κ B) pathway seems to be not involved (Muchamuel, Basler et al. 2009). Another role assigned to the immunoproteasome is the efficient proteolysis of proteins damaged by cytokine-induced oxidative stress (Seifert, Bialy et al. 2010).

The thymoproteasome in cTECs is involved in selection of thymocytes for the optimal binding of their TCR to MHC:self-peptide complexes. The specific substrate cleavage capability of the thymoproteasome is assumed to produce self-peptides that are bound by TCR with low-affinity (Murata, Takahama et al. 2008). Positively selected T cells show less cross-reaction with self-peptides presented by diverse non-cTEC cells, thereby preventing autoimmunity. In thymoproteasome-deficient mice, the number of CD8⁺ T cells is substantially reduced, demonstrating the importance of the thymoproteasome for thymocyte maturation (Murata, Sasaki et al. 2007). Furthermore, in absence of thymoproteasome-mediated positive selection, mice exhibit severe defects in CD8⁺ T cell response and in the survival following influenza virus infection (Nitta, Murata et al. 2010).

In summary, both the thymo- and the immunoproteasome are key players of the adaptive immune system. The thymoproteasome is essential for shaping of an immunocompetent and self-tolerant T cell repertoire, and the immunoproteasome promotes immune competence and sufficient CD8⁺ T cell responses to pathogens.

2.6.2 Proteasome biogenesis pathway

Proteasome assembly follows a complex, well studied but not yet completely understood biogenesis program. Proteasome formation involves generation of all subunits, their assembly and maturation, and requires numerous regulators and chaperons (Murata, Yashiroda et al. 2009, Gallastegui and Groll 2010, Kunjappu and Hochstrasser 2014). Assembly of the mammalian constitutive, immuno- and thymoproteasome as well as the yeast proteasome basically follows the same principle. The β -subunits are synthesized as inactive precursors with N-terminal propeptides that protect from uncontrolled proteolysis and are essential for proteasome maturation (Jager, Groll et al. 1999). The initial step of the proteasome formation involves the assembly of subunits α 1- α 7 to a heptameric α -ring. The α -ring thereafter serves as a

docking platform for β -subunits (Nandi, Woodward et al. 1997), which are incorporated in a well-defined sequence. One of the first β -subunit that associates with the α -ring is β_2 (De, Jayarapu et al. 2003, Hirano, Kaneko et al. 2008). The C-terminal appendage of β_2 is essential for integration of the neighbor subunit β_3 (Ramos, Marques et al. 2004). Thus, β_2 and its C-terminal tail is highly conserved in structure and sequence among eukaryotic species in constitutive and immuno- β_2 -subunits (Murata, Yashiroda et al. 2009, Huber, Basler et al. 2012).

The resulting precursor complex consists of two rings ($\alpha_{1-7}\beta_{1-7}$) and is termed half-proteasome or hemiproteasome. Final activation of β -subunits by autolytic cleavage of their propeptides requires dimerization of two hemiproteasomes and structural rearrangements (Chen and Hochstrasser 1996, Ditzel, Huber et al. 1998, Murata, Yashiroda et al. 2009).

Readily assembled proteasomes have fix subunit composition and different types of proteasomes have to be formed *de novo*. How the incorporation of constitutive vs. alternative subunits is controlled is not yet completely understood. Immuno-subunits are preferentially incorporated into nascent proteasomes (Griffin, Nandi et al. 1998, Bai, Zhao et al. 2014). The proteasomal β_5 subunit LMP7 undergoes accelerated incorporation/activation compared to constitutive 20S proteasome assembly nearly four-fold (Heink, Ludwig et al. 2005).

2.6.3 Proteasome-associated human diseases

Due to the essential functions of the proteasome, mutations in any of its components are associated with diverse human diseases such as diabetes and cancer (Gomes 2013). Mutations in the proteasome maturation protein (POMP) were associated with the human keratosis linearis with ichthyosis congenitalis and sclerosing keratoderma (KLICK) syndrome. POMP acts as an essential chaperone for proteasome assembly. Differentiating keratinocytes are highly sensitive to proteasome insufficiency, thus POMP mutations can lead to the skin disease (Dahlqvist, Klar et al. 2010).

In several autoimmune disorders, circulating extracellular proteasomes are observed in plasma from patients. Although circulating proteasomes are also present in plasma from healthy donors, a substantial increase is found in patients suffering from systemic lupus erythematoses, mixed connective tissue disease, and rheumatoid arthritis (Zoeger, Blau et al. 2006, Majetschak, Perez et al. 2008). Thus, extracellularly available proteasomal

subunits, among others also the three immuno-subunits, act as autoantigens in systemic autoimmune diseases (Scheffler, Kuckelkorn et al. 2008).

During the last years, three human syndromes have been associated with mutations in LMP7, a catalytic subunit of the immunoproteasome: NKJO (Nakajo- Nishimura syndrome; Arima, Kinoshita et al. 2011, Kitamura, Maekawa et al. 2011), JMP syndrome (joint contractures, muscular atrophy, microcytic anemia, and panniculitis-induced lipodystrophy; Garg, Hernandez et al. 2010), and CANDLE (chronic atypical neutrophilic dermatosis with lipodystrophy and elevated temperature syndrome; Liu, Ramot et al. 2012). Since these syndromes share common features and are associated with mutations in the LMP7 gene, it was suggested to group them under ALDD (autoinflammation, lipodystrophy and dermatosis syndrome; OMIM entry 256040). All these syndromes have in common the autoinflammation, dermatosis, and lipodystrophy. Although the pathogenic mechanisms are not yet resolved, in ALDD patients following observations were made: reduced mature proteasomes and proteasome activity, increased proteasome assembly intermediates and increased ubiquitin accumulation pointing towards inefficient protein turnover (Kitamura, Maekawa et al. 2011). Therefore, an immunoproteasome assembly defect has been suggested as the underlying pathomechanism (Arima, Kinoshita et al. 2011). However, molecular data proving this hypothesis were not yet reported.

3 Objective of this PhD thesis

At the beginning of the project, novel mutant mouse lines with immunological phenotypes were identified in the ENU mutagenesis and screening program, and previously established ENU mutant lines were reanalyzed. TUB006, one of the existent mouse mutant lines, has moved into the focus of this PhD thesis due to its fascinating phenotype. Using the available screening platforms, own establishments of novel methods, as well as multidisciplinary collaborations helped to elucidate multiple aspects of the TUB006 mouse line.

The in-depth characterization of the immune defect of the mutant line TUB006 was the first objective of this study. Diverse elaborated techniques were applied, such as multicolor flow cytometry, electrochemiluminescent detection of immunoglobulin isotypes and cytokines, as well as pathology including histology and immunohistochemistry. The obtained results demonstrated that heterozygous mutants were characterized by a selective T cell defect. In homozygous mutants, SCID was observed, along with dermatosis, lipodystrophy and systemic autoinflammation.

The second aim of this study was establishment of an *in vivo* challenge platform at the Immunology Screen of the GMC. To evaluate the innate and adaptive immune response, the *Listeria monocytogenes* infection model was successfully established (Klymiuk, Kenner et al. 2012, Pozzi, Amodio et al. 2012, Come, Cvrljevic et al. 2016). Heterozygous TUB006 mutants analyzed in the *Listeria* model showed an impaired T cell response and substantial lethality upon infection.

The third major challenge was the identification of the genetic alteration underlying the TUB006 disease. Deep whole exome sequencing revealed the missense point mutation resulting in the single amino acid exchange G170W in MECL-1, the β 2i-subunit of the immuno- and thymoproteasome. This was surprising, since MECL-1 knockout mice do not present the severe phenotype observed in TUB006.

The fourth major aim of this research project was to elucidate the underlying pathomechanisms. Optimal antibody combinations and staining protocols were established for thymocyte maturation patterns and quantification of thymic stromal cell subtypes, as well as for identification of hematopoietic progenitors and stem cells in the

bone marrow. Furthermore, bone marrow transfer experiments were performed in order to deeper understand the pathogenesis in TUB006. All these analyses yielded detailed insights into the underlying mechanisms leading to the severe disease in TUB006 mice. As shown by breeding of the mutant line under sterile conditions, the autoinflammation develops independently from microbiotic triggers. On cellular level, overexpression of the mutant protein proved lethal for murine cells. Proteasomes are essential for cell survival, and the selective elimination of cells expressing mutated MECL-1 leads to the immunodeficiency in TUB006 mice.

In subsequent experiments with collaboration partners, the pathomechanism was resolved on the molecular level. Mutagenesis of the yeast proteasome and X-ray crystallography indicated that the severe TUB006 phenotype is caused by structural changes in the C-terminal appendage of MECL-1, which prevent the biogenesis of functional immuno- and thymoproteasomes. Due to preferential incorporation of MECL-1 into nascent proteasomes, the production of functional proteasomes cannot be rescued by incorporation of the respective constitutive subunit $\beta 2c$.

The ENU program aimed at identification of novel mouse models for human diseases, and TUB006 provides an excellent example. Mutations in other immunoproteasome subunits have been associated with clinical symptoms in humans that closely resemble key features of TUB006 mice. However, so far there is no existent mouse model for these diseases, and TUB006 provides the first mouse model for pathological implications of immuno- and thymoproteasome assembly defects. Diverse mutations in other proteasomal subunits have been annotated to human autoinflammatory disorders; it is probably only a question of time until MECL-1 mutations will be also identified in humans with primary immunodeficiencies.

4 Material and Methods

4.1 Materials

4.1.1 Equipment

Equipment	Model, Supplier
Bioplex reader	Bio-Rad, Hercules, CA, USA
Centrifuges	Biofuge fresco, Heraeus, Hanau, Germany Biofuge 15 table top centrifuge, Heraeus, Hanau, Germany Multifuge 3 SR, Heraeus, Hanau, Germany Varifuge 3.0RS centrifuge, Heraeus, Hanau, Germany
ELISA reader	Sunrise, Tecan, Maennedorf, Switzerland
Flow cytometer	LSR II, Becton Dickinson, Heidelberg, Germany Gallios, Beckman Coulter, Brea, CA, USA
Heating block	Thermomixer compact, Eppendorf, Hamburg, Germany
Incubator	Cytoperm 2, Heraeus, Hanau, Germany
Laminar flow hood	HERA safe, Heraeus, Hanau, Germany
LightScanner	Idaho Technology, Salt Lake City, UT, USA
Microscope	Axiovert S100, Carl Zeiss, Jena, Germany
Microtome	Rotatory microtome HMS35, Zeiss, Jena, Germany
MSD Instrument	SECTOR S 600, MesoScaleDelivery, Rockville, MD, USA
NanoDrop	Thermo Scientific, Braunschweig, Germany
Neubauer counting device	Schubert, München, Germany
PCR cycler	LightCycler, Roche Applied Science, Penzberg, Germany
Photometer	BioPhotometer, Eppendorf, Hamburg, Germany
Radiation facility	Eldorado 78, Helmholtz Zentrum München, Germany
Sequencer	HiSeq2000 system, Illumina, San Diego, CA, USA
Shaker	Multitron Version 2, INFORS AG, Bottmingen, Schweiz
Slide-scanning system	NanoZoomer 2.0 HT (Hamamatsu Photonics K.K.; Hamamatsu City, Japan)
Tissue homogenizer	GentleMACS dissociator, Miltenyi Biotec, Bergisch Gladbach, Germany
Vacuum infiltration processor	TissueTEK VIP 5E-F2, Sakura, Iphen aan den Rijn, Netherlands
Water bath	Ecoline 019, LAUDA, Lauda-Königshofen, Germany

4.1.2 Chemicals and reagents

Reagent	Supplier
Affinity Script cDNA Synthesis Kit	Agilent, Santa Clara, CA, USA
Ammonium chloride (NH ₄ Cl)	Sigma, Taufkirchen, Germany
Annexin AADvanced Apoptosis Kit	Thermo Scientific, Braunschweig, Germany
Ampure Beads	Beckman Coulter, Krefeld, Germany
Big Dye Terminator	ABI PRISM, Carlsbad, CA, USA
Bovine serum albumin (BSA)	Sigma, Taufkirchen, Germany
Brefeldin A (Golgi Plug)	BD Biosciences, Heidelberg, Germany
Calcium chloride (CaCl ₂)	Sigma, Taufkirchen, Germany
CleanSeq beads	Beckman Coulter, Krefeld, Germany
Collagenase VIII	Sigma, Taufkirchen, Germany
Cytofix/Cytoperm kit	BD Biosciences, Heidelberg, Germany
3,3'-diaminobenzidine (DAB)	DCS Innovative Diagnostic Systems, Hamburg, Germany
Dimethyl sulfoxide (DMSO)	Sigma, Taufkirchen, Germany
DMEM	Thermo Scientific, Braunschweig, Germany
EosinY	BioOptica, Milano, Italy
Ethanol	Sigma, Taufkirchen, Germany
Ethidium monazide (EMA)	Molecular Probes, Leiden, Netherlands
Fetal calf serum (FCS)	Biochrom, Berlin, Germany
Gentamycin	Gibco BRL, Karlsruhe, Germany
Goat or rabbit serum	Gibco BRL, Karlsruhe, Germany
Heparin	Roche, Basel, Switzerland
Hydrochloric acid (HCl)	Roth, Karlsruhe, Germany
4-(2-hydroxyethyl)-1-piperazineethanesulfonic acid (HEPES)	Gibco BRL, Karlsruhe, Germany
IFN- γ (XMG1.2)	BD Biosciences, Heidelberg, Germany
IL-2 (Proleukin S)	Novartis, Basel, Switzerland
IL-15	PeptoTech, Hamburg, Germany
Ionomycin	Sigma, Taufkirchen, Germany
L-Arginine	Roth, Karlsruhe, Germany
L-Glutamine	Gibco BRL, Karlsruhe, Germany

Reagent	Supplier
LCGreen Dye	Idaho Technology, Salt Lake City, UT, USA
LiChrosolve solvent	Merck Millipore, Darmstadt, Germany
LightScanner Master Mix	Idaho Technology, Salt Lake City, UT, USA
Lineage cell depletion kit	Miltenyi Biotec, Bergisch Gladbach, Germany
Magnesium chloride (MgCl ₂)	Sigma, Taufkirchen, Germany
Mayers acid Hemalum bluing	BioOptica, Milano, Italy
NaOH	Roth, Karlsruhe, Germany
Paraformaldehyde (PFA)	Sigma, Taufkirchen, Germany
Penicillin	Roth, Karlsruhe, Germany
PermWash	BD Biosciences, Heidelberg, Germany
Pertex mounting medium	Medite, Burgdorf, Germany
Phorbol 12-myristate 13-acetate (PMA)	Sigma, Taufkirchen, Germany
Phosphate buffered saline (PBS)	Biochrom, Berlin, Germany
Proinflammatory Panel 1 Kit	MesoScaleDelivery, Rockville, MD, USA
Propidium iodide (PI)	Molecular Probes, Eugene, OR, USA
Proteinase K	Roche, Basel, Switzerland
Phire Taq polymerase	Thermo Scientific, Braunschweig, Germany
Retronectin	Takara Bio, Saint-Germain-en-Laye, France
RPMI 1640	Gibco BRL, Karlsruhe, Germany
EDTA	Sigma, Taufkirchen, Germany
Streptomycin	Sigma, Taufkirchen, Germany
Streptactin-APC	IBA, Göttingen, Germany
Streptactin-PE	IBA, Göttingen, Germany
SureSelectXT Mouse All Exon kit	Agilent Technologies, Santa Clara, CA, USA
Suc-LLVY-AMC	Bachem, Bubendorf, Switzerland
Thymus DNA	Sigma Aldrich Chemie, Steinheim, Germany
Triton X-100	Biorad, Munich, Germany
TriReagent	Sigma, Taufkirchen, Germany
Trypan Blue solution	Sigma, Taufkirchen, Germany

4.1.3 Buffers and media

All buffers were filtered using a Stericup 0.22 μ M vacuum filtering system (Millipore, Bedford, USA) and pH was adjusted with NaOH or HCl.

Buffer/Medium	Composition	
Ammoniumchloride-Tris (ACT)	0.17 M	NH ₄ Cl
	0.3 M	Tris-HCl, pH 7.5
Collagenase VIII Buffer	95 ml	RPMI
	20.33 mg	MgCl ₂
	14.7 mg	CaCl ₂
	5 ml	FCS
DMEM+ cell culture medium	1x	DMEM
	10% (v/v)	FCS
	0.025% (w/v)	L-Glutamine
	0.1% (w/v)	HEPES
	0.001% (w/v)	Gentamycin
	0.002% (w/v)	Streptomycin
FACS staining buffer, pH 7.45	1x	PBS
	0.5% (w/v)	BSA
	0.02% (w/v)	Sodium azide
RPMI+ cell culture medium	1x	RPMI 1640
	10% (w/v)	FCS
	0.025% (w/v)	L-Glutamine
	0.025% (w/v)	L-Arginine
	0.1% (w/v)	HEPES
	0.001% (w/v)	Gentamycin
	0.002% (w/v)	Streptomycin
YPD	1% (w/v)	Yeast extract
	2% (w/v)	Peptone
	2% (w/v)	Glucose

4.1.4 Antibodies

Unless declared otherwise, all antibodies have been titrated for optimal dilutions.

Antigen	Conjugate	Clone	Supplier
B220	APC-AF750	RA3-6B2	Life Technologies, Carlsbad, CA, USA
B220	BV605	RA3-6B2	BioLegend, San Diego, CA, USA
B220	-	550286	BD Biosciences, San Diego, USA,
CD3e	eF450	17A2	eBioscience, Frankfurt, Germany
CD3e	BV510	17A2	BioLegend, San Diego, CA, USA
CD3e	PE-eF610	145-2C11	eBioscience, Frankfurt, Germany
CD3e	-	A0452	DakoCytomation, Hamburg, Germany
CD3e	-	145.2C11	BD Pharmingen, San Diego, USA
CD4	FITC	H129.19	BD Biosciences, San Diego, CA, USA
CD4	PerCP-Cy.5.5	RM4-5	TONBO Biosciences, San Diego, CA, USA
CD4	APC	L3T4	BD Biosciences, San Diego, CA, USA
CD5	APC	53-7.3	BD Biosciences, San Diego, CA, USA
CD5	eFluor 450	53-7.3	eBioscience, San Diego, CA, USA
CD8 α	APC	5H10	Caltag, Hamburg, Germany
CD8 α	eFlour450	5H10	eBioscience, Frankfurt, Germany
CD8 α	FITC	5H10	Caltag, Hamburg, Germany
CD8 α	Pacific Orange	5H10	Invitrogen, Darmstadt, Germany
CD8 α	PE	5H10	BD Biosciences, San Diego, CA, USA
CD8 α	APC-AF750	5H10	Invitrogen, Carlsbad, CA, USA
CD11b	PB	M1/70.15	Life Technologies, Carlsbad, CA, USA
CD11c	FITC	HL3	BD Biosciences, San Diego, CA, USA
CD16/CD32	-	2.4G2	Caltag, Hamburg, Germany
CD16/CD32	FITC	2.4G2	BD Biosciences, San Diego, CA, USA
CD19	PE-Cy7	1D3	BD Biosciences, San Diego, CA, USA
CD19	PE-CF594	1D3	BD Biosciences, San Diego, CA, USA

Antigen	Conjugate	Clone	Supplier
CD25	APC	PC61	BD Biosciences, San Diego, CA, USA
CD25	PE	PC61	BD Biosciences, San Diego, CA, USA
CD28	-	37.51	BD Pharmingen, San Diego, USA
CD44	FITC	IM7	BD Biosciences, San Diego, CA, USA
CD44	BV570	IM7	BioLegend, San Diego, CA, USA
CD45	AF700	30-F11	BioLegend, San Diego, CA, USA
CD45.1	FITC	A20	BD Biosciences, San Diego, CA, USA
CD62L	PE-Cy7	MEL-14	BD Biosciences, San Diego, CA, USA
CD117 (c-Kit)	PE-Cy7	2B8	eBioscience, Frankfurt, Germany
CD127	APC	A7R34	eBioscience, Frankfurt, Germany
CD150	PE	TC15-12F12.2	BioLegend, San Diego, CA, USA
CD326 (EpCAM)	PE-Cy7	G8.8	BioLegend, San Diego, CA, USA
Gr-1	PO	RB6-8C5	Life Technologies, Carlsbad, CA, USA
$\gamma\delta$ TCR	FITC	GL3	BD Biosciences, San Diego, CA, USA
IFN- γ	APC	XMG1.2	eBioscience, Frankfurt, Germany
Ly-51	AF647	6C3	BioLegend, San Diego, CA, USA
MPO	-	RB-373-R7	NeoMarkers, Fremont, CA, USA
NK1.1	PE	PK136	BD Biosciences, San Diego, CA, USA
NKp46	PE	29A1.4	eBioscience, Frankfurt, Germany
Sca1	BV421	D7	BioLegend, San Diego, CA, USA
TCR β	APC	H57-597	BD Biosciences, San Diego, CA, USA
Tdt	-	A3524	DakoCytomation, Hamburg, Germany
TNF- α	PE-Cy7	MP6-XT22	BD Biosciences, San Diego, CA, USA
mouse IgG, IgA, IgM	(H+L)-Peroxidase	polyclonal	Sigma, Taufkirchen, Germany
goat IgG	Biotin	BA5000	Vector Lab, Burlingame, USA
rabbit IgG	Biotin	BA100	Vector Lab, Burlingame, USA

4.1.5 Peptides and MHC multimers

Peptides were purchased from Biosynthan GmbH, Berlin, Germany and dissolved in DMSO at a concentration of 1 µg/µl. LLO₉₁₋₉₉ (GYKDGNEYI) peptide from listerial Listeriolysin O (LLO) was used for restimulation of antigen-specific T cells. Conventional MHC-I multimers for the detection of antigen-specific CD8⁺ T cells were routinely produced in our laboratory according to well-established protocols (Busch, Pilip et al. 1998). The H2-K^d/ LLO₉₁₋₉₉ Streptavidin-PE peptide-loaded MHC-I multimer was used for detection of *Listeria*-specific CD8⁺ T cells in BALB/c mice.

4.1.6 Primers

All oligonucleotides were synthesized and HPLC-purified by Sigma (Taufkirchen, Germany) or Eurofins MWG Operon (Ebersberg, Germany). Primers were dissolved in ddH₂O to a final concentration of 100 pmol/µl.

Primer	Sequence
Psmb10 LS L	GTGGAAGCCATCACAGC
Psmb10 LS R	CCTGCAGTGATCACACAG
Psmb10 seq L	CAGCCTTTTAGAATGCAGCC
Psmb10 seq R	CCTCATTTTCCACTACCCAGC
MECL-1 Not1 fwd	ATTAGCGGCCGCGCCACCATGCTGAAGCAGGCAGTGG
MECL-1 P2A rev	AGTTCGTGGCTCCGGAACCTTCCACCTCCATGGCCTGC
MECL-1 P2A fwd	GCAGGCCATGGAGGTGGAAGGTTCCGGAGCCACGAACT
GFP EcoR1 rev	TAATGAATTCTTACTTGTACAGCTCGTCC
Pup1 fwd	CCATCTAGACAGTCTGCTTTGTAGTGGGG
Pup1 rev	CCAAAGCTTATATTACCCTGTTATCCCTAGC

4.1.7 Plasmids

Plasmids	Description	Source
pRS315	CEN LEU2	Sikorski et al., 1989
mP71	mP71 retroviral vector	Gift from Wolfgang Uckert

4.2 Methods

4.2.1 Mice

Unless stated otherwise, mice were derived from in-house breeding. Prtpc (congenic CD45.1⁺ BALB/c mice) were purchased from the Jackson Laboratory (Bar Harbor, ME, USA). MECL-1 knockout mice were kindly provided by Prof. Dr. Marcus Groettrup (Universität Konstanz). Hemizygous MECL-1^{-/G170W} mice were generated by crossing heterozygous TUB006 mice with MECL-1 knockout mice.

If not stated otherwise, mice were bred and housed under specific pathogen-free (SPF) conditions at the mouse facility at the Technical University of Munich and the German Mouse Clinic. Mice were kept in a 12/12-hour dark/light cycle and provided ad libitum water and standard chow (total pathogen-free chow 1314: calcium content, 0.9%; phosphate, 0.7%; and vitamin D3, 600 international units (IU); Altromin, Lage, Germany). Hygienic monitoring was performed following Federation of European Laboratory Animal Science Associations (FELASA) recommendations. Handling was performed according to the federal animal welfare guidelines, and the local authorities approved all animal studies.

TUB006 mutants were originally tentatively grouped into wild type, heterozygous and homozygous groups according to their phenotype. Genotyping was performed retrospectively after the mutation was identified.

For generation of germ-free TUB006 mice, 4-6 week old heterozygous TUB006 females were superovulated by intraperitoneal (i.p.) injection of 7.5 IU pregnant mare serum gonadotropin (PMSG), and 4 hours later 7.5 IU human chorionic gonadotropin (hCG), and on the same evening paired with heterozygous TUB006 males. On the following morning, successful mating was controlled by plug check; plug positive females were shipped to Clean Mouse Facility (CMF), University of Bern (Bern, Switzerland). Upon arrival, the females were euthanized and the transfer of two-cell embryos into pseudopregnant female recipients was performed as described previously (Slack et al. 2009).

4.2.2 General statistical evaluation

Box plots indicate the median, the first and third quartiles, and the minimum and maximum values. Statistical differences between groups were determined by the Mann-

Whitney rank-sum using Prism v.6 (GraphPad Software, Inc., La Jolla, CA). Asterisks indicate P values * <0.05 , ** <0.01 , *** <0.001 , **** <0.0001 .

4.2.3 Infection

Infection experiments were performed with the wild type *L.m.* strain 10403s (Bishop and Hinrichs 1987) using standard protocols (Busch, Vijn et al. 2001). Briefly, brain-heart infusion (BHI) medium was inoculated with 10 μ l *Listeria* stock solution and incubated under gentle shaking at 37°C until an OD₆₀₀ of 0.05 – 0.1. After adjustment of the bacterial dose with phosphate-buffered saline (PBS) to an injection volume of 200 μ l, the infection of mice was performed by i.v. injection into the lateral tail vein. For primary infection of BALB/c mice an infection dose of 0.5 \times LD₅₀ (1000 colony-forming units, CFU for analysis on day seven) or 2.5 \times LD₅₀ (5000 CFU for analysis on day three) was applied (Cheers, McKenzie et al. 1978). The exact infection dose was controlled by plating of the injection solution triplicates on BHI agar plates and counting of the colonies on the next day.

To estimate bacterial burden of organs, three or seven days after infection mice were sacrificed. Spleens and livers were homogenized in the gentleMACS homogenizer according to manufacturer's recommendation. Serial dilution triplicates of Triton-lysed organ homogenates (ranging from 1:10 to 1:1000) were plated on BHI agar plates. After an overnight incubation at 37°C, CFU were quantified by counting colonies and taking into account the dilution factor. Using this approach, the detection limit of living bacteria is approximately 5 \times 10³ CFU per organ.

4.2.4 Cell preparation and flow cytometry

Peripheral blood leukocytes were obtained using heparinized capillaries through retro-orbital bleeding of isofluran-anesthetized mice. Single cell suspensions from spleens and thymocytes were prepared by homogenizing spleen tissue with the gentleMACS homogenizer according to manufacturer's recommendations. Thymic stroma cells were obtained by mincing of thymi and subsequent digestion in 0.4 mg/ml collagenase VIII and DNase for 30 minutes.

For erythrocyte lysis, cell suspensions were treated with NH₄Cl-Tris for 10 minutes. Lysis was stopped by adding cold RPMI+, then cells were washed with fluorescence-activated cell sorting (FACS) buffer. Numbers of cells were determined by counting

appropriate dilutions in a Neubauer counting chamber, using Trypan Blue staining for discrimination of dead cells.

Surface marker staining was performed in FACS buffer in 96 well U-bottom plates. Cells were pre-incubated for 10 minutes with Fc block (anti-CD16/32, 1:400 of stock solution 2.5 µg/µl). Optionally, MHC multimer staining was performed for 30 minutes at 4°C in the dark. Subsequently, staining with a combination of fluorescence-conjugated antibodies was performed for 20-40 minutes at 4°C in the dark. Live/dead discrimination was either performed with EMA (1:1000, stock at 2 µg/µl, 20 minutes under light on ice) prior to staining procedure, or with propidium iodide (PI; 1:500, stock at 2 µg/µl, 2 minutes in the dark at 4°C) after the staining procedure. Finally, samples were washed three times in a total volume of 200 µl FACS buffer and resuspended in FACS buffer for acquisition.

For intracellular cytokine staining, splenocytes were restimulated *in vitro* for 5 hours at 37°C in RPMI+ medium supplemented with 1 µg/ml LLO₉₁₋₉₉ (GYKDGNEYI) or with 0.5 µmol/L PMA and 0.25 µg ionomycin, or kept without stimulation (negative control with DMSO). After 1 hour of incubation time, Brefeldin A (Golgi Plug) was added at 2 µg/ml. Subsequently, cells were washed with PBS, incubated with Fc block, followed by surface staining as described above. Subsequently, fixation and permeabilization was performed using the Cytofix/Cytoperm kit according to the manufacturer's recommendations, followed by intracellular staining with anti-IFN-γ in PermWash buffer for 30 minutes at 4°C. Subsequently, cells were washed once with PermWash buffer and twice with FACS buffer, and resuspended in FACS buffer for acquisition.

Bone marrow cells were flushed thoroughly with PBS from mouse femurs and tibiae and filtered through nylon cell strainer. Cells were preincubated with CD16/32-FITC, and thereafter stained with biotinylated primary lineage antibody cocktail (Gr-1, CD11b, B220, CD3, Ter119) for depletion of committed cell lineages. Thereafter, hematopoietic progenitor cells were enriched using the lineage cell depletion kit and streptavidin-bead magnetic cell separation (MACS) columns according to manufacturer's recommendations. After MACS enrichment, the standard staining procedure with surface antibodies was performed as described above.

Analysis of retrovirally transduced cells was performed as follows: one day after transduction (see 4.2.13), initial transduction efficacies were assessed by measurement

of GFP producing cells by flow cytometry. GFP expression was analyzed after 24, 36, and 48 hours as a surrogate marker for MECL-1^{WT} or MECL-1^{G170W} expressing cells. Annexin V staining was performed 36 hours after transduction using Pacific Blue Annexin V/SYTOX AADvanced Apoptosis Kit.

Flow cytometry data acquisition was performed using Gallios or LSR II flow cytometers and further analyzed with FlowJo (Tree Star Inc., Ashland, OR; USA) software. Fluorescence minus one (FMO) controls were used for gating to distinguish positive and negative cell populations. Compensation was performed using single color controls. Compensation matrices were calculated and applied using FlowJo software. Biexponential transformation of the axes was adjusted manually when necessary.

4.2.5 Irradiation and bone marrow transplantation

For bone marrow chimera experiments, a license for animal testing has been applied for and approved by the Regierung von Oberbayern (TVA 55.2-1-54-2532-57-12). Recipient mice underwent total body irradiation delivered in 2 dose fractions of 5 or 3 Gy using the ⁶⁰Co facility Eldorado78. The dosimetry was calculated on the basis of the measured air kerma K_a within the cage used for irradiation of mice. K_a was measured using a 1cm³ ionisation chamber. The measured K_a can be converted into the energy dose in tissues (D_{tissue}) according to the US-National Institute of Standards. The conversion factor for ⁶⁰Co radiation is 1.102, thus the administered dose was calculated using the following equation:

$$D_{\text{tissue}} = K_a \times 1.102$$

Both fractions of irradiation were applied with a 4 hours break, and after the second irradiation 1.5×10^6 bone marrow cells from donor mice were injected i.v. into the lateral tail vein.

4.2.6 Plasma immunoglobulin, cytokine and autoantibody estimation

Blood samples were obtained from non-fasted anesthetized mice by puncture of the retro-orbital sinus (Rathkolb, Decker et al. 2000). Plasma samples were obtained immediately after blood withdrawal by centrifugation and were stored at -80°C before analysis.

Plasma concentrations of immunoglobulin isotypes IgG1, IgG2a, IgG2b, IgG3, IgM, and IgA were determined by using bead-conjugated monoclonal anti-mouse Ig antibodies in

a bead-based multiplex assay. Data was acquired using a BioPlex reader. The level of each isotype was calculated over a standard curve fitted with Four-Parameter-Logistic regression using Bio-Plex manager software.

Plasma autoantibody levels were quantified using standard enzyme-linked immunosorbent assay (ELISA). ELISA plates were coated with rheumatoid factor or calf thymus DNA for both single- and double-stranded DNA antibody detection. Serum was diluted and loaded along with a positive control serum of MRL/MpJ-Fas(lpr) mice and negative control sample. Subsequently, goat anti-mouse secondary antibody (polyvalent IgG, IgA, and IgM) was added. After incubation with the secondary antibody, substrate was added and plates were read in an ELISA plate reader.

For determination of the cytokine concentrations (TNF- α , IFN- γ , IL-1 β , IL-4, IL-5, IL-6, CXCL1, IL-12), the commercial MSD Proinflammatory Panel 1 (mouse) Kit was used according to the manufacturer's instructions. Data were acquired and analyzed using the MSD instrument and the included MSD discovery workbench software.

4.2.7 Gross pathology, necropsy, histology and immunohistochemistry

Mice were sacrificed with CO₂, body weight was measured before starting the necropsy as described by Fuchs, Gailus-Durner et al. 2012. Briefly, mice underwent a visual inspection of the integument followed by opening of the abdominal and thoracic cavities. Organs were removed, weighted and immersion-fixed in 4% neutral buffered formalin. Organs were trimmed according to the GMC-specific standard operating procedure (SOP) and embedded in paraffin using a vacuum infiltration processor. Histo-slides were prepared using a rotatory microtome to a thickness of 4 μ m for hematoxylin and eosin (HE) staining or 1 μ m for immunohistochemistry.

HE staining was performed as follows: rehydration was done in a decreasing ethanol series, rinsing with tap water, 2 minutes Mayers Acid Hemalum bluing in tap water followed by 1 minute incubation with EosinY. Subsequent steps were dehydration in increasing ethanol series, mounting with Pertex mounting medium and coverslips.

For immunohistochemistry, 1 μ m thick sections were rehydrated until deionized water. Heat induced antigen retrieval was performed (0.1 M EDTA pH 8.0, 25 minutes at 96 °C/0.1 M citrate pH 6.0 10 minutes at 100°C under pressure) or enzyme-induced antigen retrieval with Proteinase K (diluted 1:200, 8 minutes at RT). Serum block was carried

out in 5% goat or rabbit serum for 1 hour. Primary antibodies used were: CD3, B220, MPO, or Tdt, diluted 1:100 each, incubated overnight at 4°C. Secondary antibodies α -goat-biotin (1:200) and α -rabbit-biotin (1:750) were incubated for 1 hour at room temperature. Detection was performed by incubation with streptavidin-peroxidase for 15 minutes and incubation with DAB for 3 minutes. Counterstaining was performed using Mayers Acid Hemalum for 10 seconds and bluing in tap water. Rehydration and mounting was performed as described above. Images were taken by the NanoZoomer slide-scanning system.

4.2.8 Exome sequencing

In-solution targeted enrichment of exonic sequences from two homozygous TUB006 mice and one wild type littermate control was performed using the SureSelectXT Mouse All Exon 50 Mb kit. The generated libraries were indexed, pooled and sequenced as 100 bp paired-end runs on a HiSeq2000 system.

Read alignment to the mouse genome assembly mm9 was done with Burrows-Wheeler Aligner (BWA, version 0.6.1) and yielded 10.6 Gb, 9.1 Gb and 8.3 Gb of mapped sequence data corresponding to an average coverage of 109x, 103x and 76x for the two mutants and the wild type mouse, respectively. SNVs and small insertion and deletions (indel) detection with SAMtools (version 0.1.18) yielded 14,278, 14,256 and 14,254 good quality non-synonymous coding variants. After filtering for homozygous variants present in the two TUB006 mice but not in the wild type mouse and 145 control mice with unrelated phenotypes, a single missense variant in the gene *Psmb10* remained.

4.2.9 Genotyping

For LightScanner genotyping, a 77-bp genomic fragment was amplified from the *Psmb10* gene in a LightCycler by polymerase chain reaction (PCR) using 50 ng of genomic DNA as template, 200 μ M of each deoxynucleotide triphosphate (dNTP), 0.4 U of PhireTaq polymerase, 0.5 μ M primers (*Psmb10* LS L and *Psmb10* LS R) in presence of 1 μ M LCGreen dye. PCR cycling conditions were as follows: 40 cycles of 98°C for 5 seconds, 63°C for 5 seconds, and 72°C for 5 seconds. After PCR amplification, melting curve was acquired while heating from 84 to 94 °C in the high-resolution LightScanner melting instrument. Analysis of the melting curves was performed using the LightScanner software.

For Sanger sequencing (Sanger et al. 1977), PCR was performed in 10 µl volumes in a LightCycler. The amplification mixture included 50 ng of genomic DNA as template, 200 µM of each deoxynucleotide triphosphate (dNTP), 0.4 U of PhireTaq polymerase, 0.5 µM primers (Psmb10 seq L and Psmb10 seq R), and LCGreen at 1 µM. PCR cycling conditions were as follows: 40 cycles of 98°C for 5 seconds, 66°C for 5 seconds, and 72°C for 5 seconds. PCR products were purified using AmPure beads and the preparation for sequencing was performed using the BigDye Terminator Cycle Sequencing v.3.1 Kit according to manufacturer's protocol. Dye-terminator was removed using CleanSEQ beads following the manufacturer's recommendations, the DNA was resuspended in LiChrosolve solvent and sequenced at the Genome Analysis Center (GAC) sequencing facility at the Helmholtz Zentrum München. Analysis was performed using the MacVector software, the Sequencher software or CLC Genomic Workbench 8 software.

4.2.10 Yeast mutagenesis, proteasome purification, crystallization and structure determination

This part was performed in the laboratory of Michael Groll, Technical University of Munich. The *PUP1-TEV-ProA-His₇* cassette (Knop, Siegers et al. 1999) including 503 bps of the endogenous *PUP1* promoter and 229 bps of the tADH1 terminator was amplified from genomic DNA isolated from the yeast strain W303-*PUP1-TEV-ProA-H₇* (M. Groll, unpublished results) using the primers Pup1 fwd and Pup1 rev. The *Xba*I and *Hind*III digested PCR product was inserted into the vector pRS315, carrying the *LEU2* selection marker, to create pRS315-*PUP1-TEV-ProA-His₇*. Point mutants were created by QuikChange site-directed mutagenesis using either the plasmid pRS315-*PUP1* or pRS315-*PUP1-TEV-ProA-His₇* as template DNA. Introduction of point mutations was confirmed by sequencing. The mutant pRS315-*pup1-TEV-ProA-His₇* and pRS315-*pup1* plasmids were introduced into the yeast strain YWH10 *pup1*Δ::HIS3 [pRS316-PUP1] (Heinemeyer, Fischer et al. 1997), which is chromosomally deleted for the *PUP1* gene and instead carries a *URA3-PUP1*-episome. After growth on synthetic complete medium without leucine (CM leu⁻) transformants were selected on 5'fluoro-orotic acid (5'FOA) for loss of the wild type *URA3-PUP1*-plasmid. Hereby, only yeasts encoding a mutant but functional *pup1* gene can survive.

Mutant yeast strains were grown in 18 l cultures at 30 °C in YPD into early stationary phase. Cells were resuspended in 100 mM Tris/HCl pH 7.5, 500 mM NaCl, 20 mM

imidazole and disrupted by French Press. Cellular debris was pelleted by centrifugation for 30 minutes at 21,000 rpm and the cleared cellular extract was loaded onto a Ni²⁺-NTA chromatography column. The proteasome was eluted by applying a linear gradient to 500 mM imidazole. The eluted protein fractions were immediately diluted in 100 mM Tris/HCl pH 7.5 and 20% (v/v) glycerol in a 1:1 ratio, dialyzed against 20 mM Tris/HCl pH 7.5 and 50 mM NaCl and loaded onto an anion exchange chromatography column. To identify proteasome-containing fractions, protein samples were tested for their proteolytic activity against the fluorogenic substrate Suc-LLVY-AMC (N-Succinyl-Leu-Leu-Val-Tyr-7-Amino-4-methylcoumarin). Active fractions were pooled and subjected to size exclusion chromatography (Superose 6 10/300; 20 mM Tris/HCl pH 7.5, 100 mM NaCl). After incubation with TEV protease in a molar ratio of 1:100 for 15 hours at 4°C to remove the ProteinA-H₇-tag, the samples were concentrated with a 100 kDa cut-off filter. This procedure separated the mutant proteasome from the TEV protease and the cleaved tag and allowed buffer exchange to 10 mM 2-(N-morpholino)ethanesulfonic (MES) pH 6.8.

Crystals were grown by the hanging drop vapour diffusion technique at 20°C. Protein (33 mg/ml) and reservoir solutions (100 mM MES pH 6.8, 20 mM Magnesium acetate pH 6.8, 13% (v/v) 2-Methyl-2,4-pentanediol (MPD)) were mixed in a 2:1 ratio. Crystals were cryoprotected with 5 µl 100 mM MES pH 6.8, 20 mM magnesium acetate pH 6.8, 30% (v/v) MDP and either immediately vitrified in liquid nitrogen or after soaking with bortezomib for 24 hours in a final concentration of 1.5 mM.

Diffraction data were collected using synchrotron radiation of $\lambda = 1.0 \text{ \AA}$ at the beamline X06SA, Swiss Light Source (SLS), Villigen, Switzerland. X-ray intensities were analysed with the program package XDS. The yeast wild type proteasome structure (PDB ID 1RYP) served as a search model for structure determination.

4.2.11 DNA and protein sequences

DNA and protein sequences were obtained from the NCBI nucleotide database¹⁾ or Universal protein resource Uniprot²⁾. The ProtParam tool³⁾ was used to calculate physical and chemical parameters such as molecular mass, pI and the extinction coefficient of protein sequences. For *in silico* processing of DNA and protein sequences, design of cloning strategies, alignments of multiple DNA or protein sequences, the MacVector software of CLC genomic Workbench 8 were used. For the calculation of

protein surface areas the online tool PISA⁴⁾ (Protein interfaces, surfaces and assemblies service) at European Bioinformatics Institute was used.

1) <https://www.ncbi.nlm.nih.gov/nuccore>

2) <http://www.uniprot.org>

3) <http://www.expasy.ch/tools/protparam.html>

4) http://www.ebi.ac.uk/pdbe/prot_int/pistart.html

4.2.12 Generation of overexpression constructs

For overexpression experiments in murine cells, spleen mRNA from a heterozygous TUB006 mouse was isolated using TriReagent and transcribed to cDNA using Affinity Script Multiple Temperature cDNA Synthesis Kit. MECL1^{WT} and MECL-1^{G170W} cDNA was amplified and linked to P2A GFP using an overlap extension method. MECL-1^{WT}-P2A-GFP and MECL-1^{G170W}-P2A-GFP were subsequently cloned into the mP71 retroviral expression vector.

4.2.13 Retrovirus production and T cell transduction

Platinum E cells cultured in DMEM+ medium were transiently transfected with the MECL-1^{WT}-P2A-GFP and MECL-1^{G170W}-P2A-GFP constructs using a calcium phosphate precipitation based method. Virus supernatant was harvested after 48 hours. Subsequently a second virus supernatant with RPMI+ medium was produced for 24 hours. 24-well plates were coated with retronectin (6.25 µg/ml), anti-CD3e (0.5 µg/ml) and anti-CD28 (0.1 µg/ml) diluted in PBS at 4°C overnight. Splenocytes were cultured in RPMI+ containing anti-CD3e (0.5 µg/ml), anti-CD28 (0.1 µg/ml) and IL-2 (20 U/ml) for 24 hours prior to transduction. On the day of transduction, diluted retronectin was removed and plates were coated with DMEM virus supernatant by centrifugation with 3000 g at 4°C. DMEM virus supernatant was removed and splenocytes were resuspended in RPMI virus supernatant supplemented with human IL-2 (25 U/ml). Spinoculation was performed at 800 g, 32°C for 1.5 hours. Transduced T cells were subsequently cultured in RPMI+ with 25 ng/ml IL-15 and 25 U/ml IL-2 or left in the anti-CD3e, anti-CD28 coated plates replacing the medium every two days with fresh medium containing 25 U/ml IL-2.

5 Results

As part of the ENU mutagenesis program, the Immunology Screen of the German Mouse Clinic analyzed peripheral blood from offspring of ENU-treated mice to identify mutants with immunological defects (Flaswinkel, Alessandrini et al. 2000, Hrabě de Angelis, Flaswinkel et al. 2000, Gailus-Durner, Fuchs et al. 2005, Fuchs, Gailus-Durner et al. 2012). In order to identify immunological phenotypes in mutant mouse lines, multi-color flow cytometry, ELISA and multiplex bead-based techniques were applied. Thereby, peripheral blood was characterized in detail for proportions of main leukocyte subsets and T cell subpopulations, immunoglobulin levels and autoantibodies.

5.1 Characterization of heterozygous TUB006 mutants

Initially, heterozygous TUB006 mutants caught attention due to significantly reduced proportions of CD8⁺ and CD4⁺ T cells in peripheral blood (Figure 3). Otherwise, they did not display any visually apparent physical abnormalities and had a normal body weight (Figure 4 A), behavior, and life expectancy.

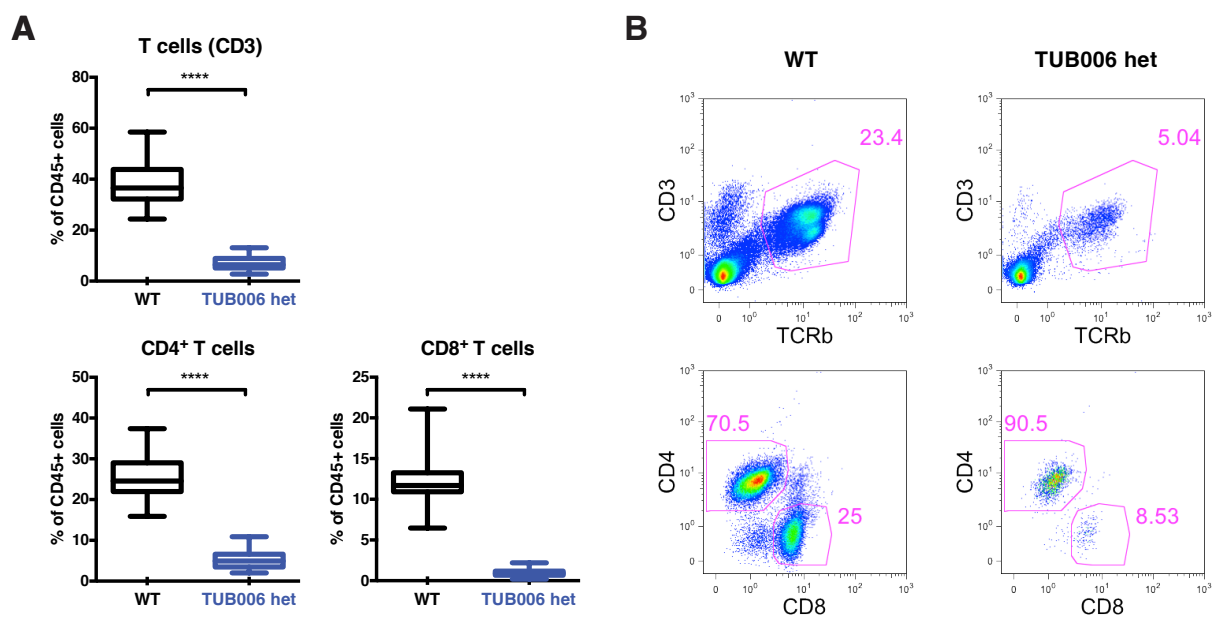


Figure 3: Reduced T cell frequencies in peripheral blood from heterozygous TUB006 mutants. T cell frequencies in peripheral blood from heterozygous (het) mutants and wild type (WT) littermate controls shown as box plots (A) of pooled data from different experiments, n=40 (WT), n=71 (het) and representative dot plots (B) of the T cell gate in the upper panel (pregated on living CD45⁺ cells, T cells defined as CD3⁺ TCRβ⁺ cells), and CD4 versus CD8 profiles of T cells (B, lower panel, gated on living CD45⁺ CD3⁺ TCRβ⁺ cells).

B, NK cell and granulocyte counts were comparable to that of wild type mice (Figure 4 B). No differences in immunoglobulin levels (IgM, IgA, IgG1, IgG2a, IgG2b, IgG3) were

found between heterozygous TUB006 animals and wild type littermates (Figure 4 C). Anti-DNA, and rheumatoid factor autoantibodies were below detection limit.

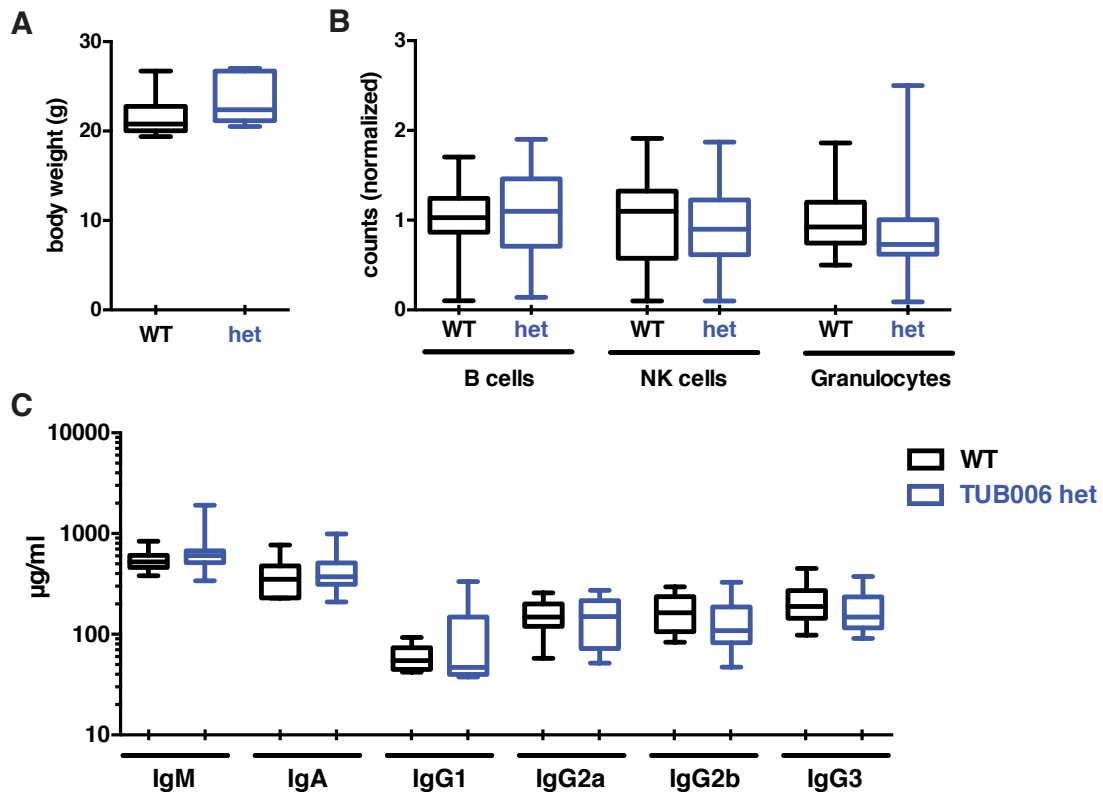


Figure 4: Normal body weight, B cell, NK cell and granulocyte counts, as well as immunoglobulin concentrations in heterozygous TUB006 mutants. A) Body weights of 6-8 weeks old males (n=21). B) Peripheral blood leukocytes: B cell (CD19⁺ B220⁺), NK cell (NKp46⁺) and granulocyte (CD11b⁺ Ly6C⁺) counts were normalized to the mean of the wild type group; n=44 (WT), 76 (het). C) Plasma immunoglobulin titers from 12-week old mice (n=12).

To characterize the phenotype of heterozygous TUB006 mice, a histopathological analysis was performed on seven heterozygous mice and six wild type littermate controls at the age of 10 to 12 weeks. Spleen and thymus showed a clear phenotype, other than that, no abnormalities were observed.

The normal murine spleen is a capsuled organ of a prolonged shape that comprises two morphologically and functionally distinct compartments: the red and the white pulp. The local distribution of lymphocytes in the white pulp follows a typical pattern: the inner T lymphocyte-rich region is arranged around blood vessels, surrounded by the outer B cell-rich region. The red pulp, that surrounds the white pulp, is devoid of lymphocytes (Cesta 2006). Splens from heterozygous TUB006 mutants showed a clear morphological distinction of the white pulp (Figure 5 C and D). However, the T cell numbers in the white pulp identified by immunohistological CD3 staining were strongly reduced compared to the wild type controls (Figure 5 C and D), in line with the flow cytometry data of peripheral blood.

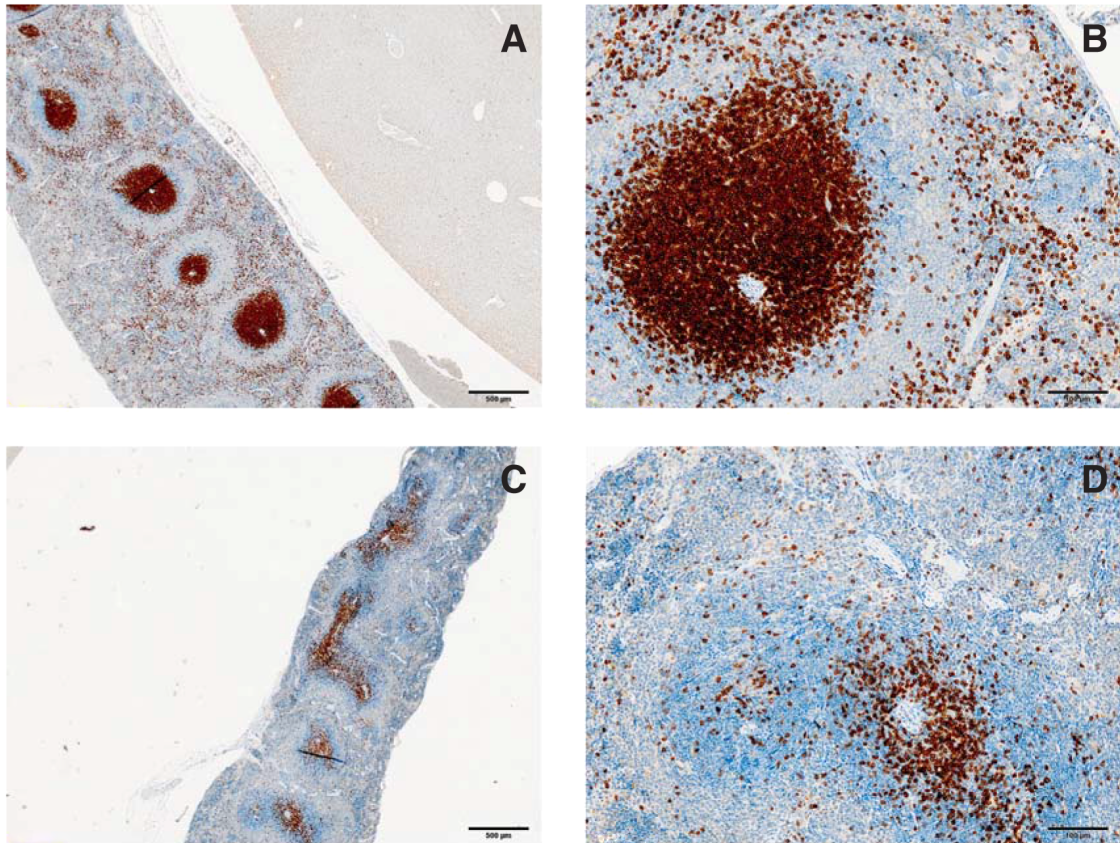


Figure 5: CD3 staining of spleen sections confirms T-lymphopenia. Representative wild type (A and B) and heterozygous TUB006 mutant (C and D) are shown. Ascending magnifications from left to right. CD3-positive cells (T cells) appear brown.

Due to reduced T cell frequencies in blood and spleens of heterozygous TUB006 animals it was of special interest to evaluate the thymic phenotype. For this purpose, an immunostaining for Tdt (terminal deoxynucleotidyl transferase) of thymus sections was performed. Tdt is expressed in immature thymocytes during the V(D)J recombination of the TCR and thus was used as marker for the developing thymocytes in the thymic cortex.

As already determined during necropsy, three of seven heterozygotes were athymic. In three of seven mutants, the thymus was normally sized and displayed regular thymus morphology and a normal distribution of Tdt positive thymocytes in the cortex (Figure 6 A and B). One heterozygous TUB006 mutant displayed thymus atrophy with an abnormal Tdt staining pattern (Figure 6 C and D).

More detailed flow cytometric characterization of splenic T cells from heterozygous TUB006 mice confirmed the results obtained previously. T cell frequencies were markedly decreased in heterozygous spleens. The remaining T cells presented the key attributes of T cells, i.e. expression of the pan-T cell markers CD3, CD5 and TCR beta chain (Figure 7 A). The effect on CD8⁺ T cells was more profound, since the majority of mutant T cells were CD4⁺ (Figure 7 A).

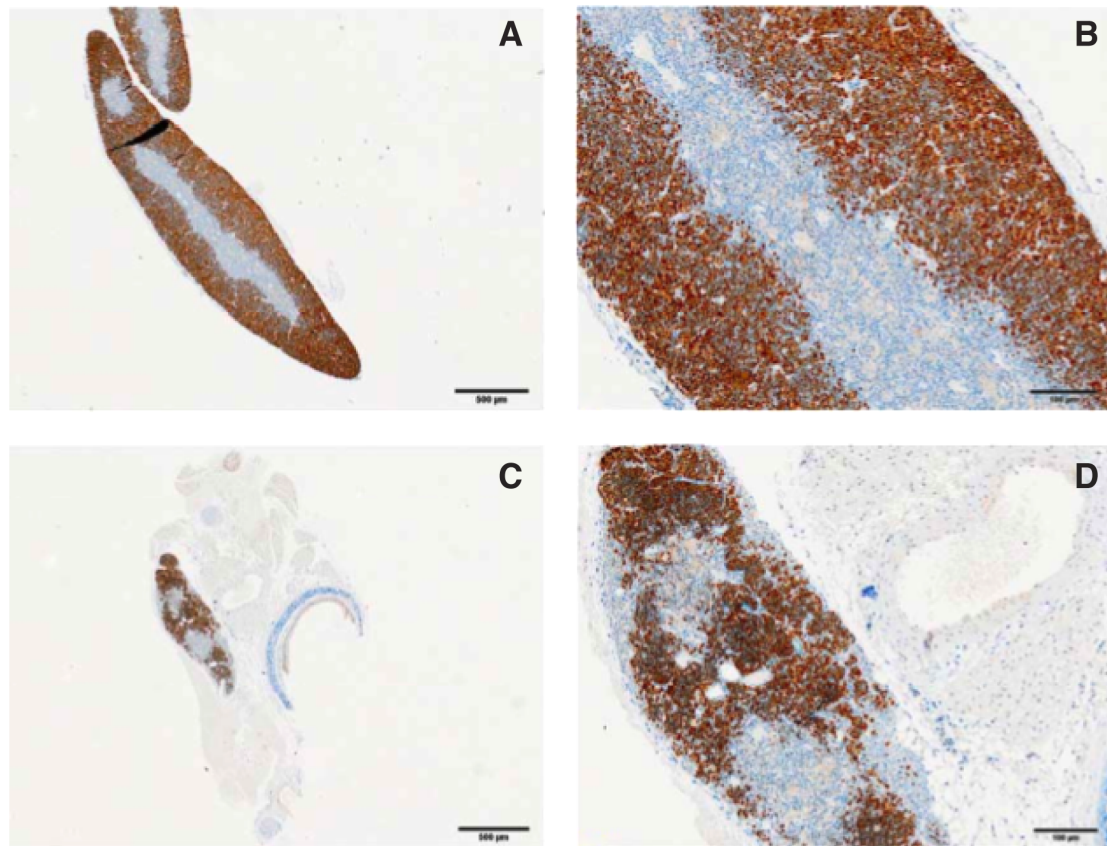


Figure 6: Terminal deoxynucleotidyl transferase (Tdt) staining of thymus sections from heterozygous TUB006 mutants. A and B show a thymus without any abnormalities. C and D show an atrophic thymus. Ascending magnifications from left to right. Tdt-positive cells (developing thymocytes) appear brown.

CD4⁺ and CD8⁺ T cells were subdivided by their surface expression of phenotypic markers CD25, CD44, CD62L and Ly6C. Compared to the wild types, a higher proportion of mutant CD4⁺ T cells were positive for CD25. These CD25⁺ CD4⁺ T cells co-expressed high levels of CD44 (Figure 7 B, top panel). The CD62L⁺ CD44⁻ naïve-phenotype compartment was decreased in mutant CD4⁺ T cells, skewed towards higher expression of CD44. In particular, the frequency of CD44⁺ CD62L⁻ population was markedly increased in CD4⁺ T cells from heterozygous TUB006 mutants (Figure 7 B, bottom panel). In line with the CD4⁺ T cell phenotype, mutant CD8⁺ T cells also presented an increased proportion of CD44 expressing cells and a clear decrease of the CD62L⁺ CD44⁻ population (Figure 7 C, bottom panel). Furthermore, a markedly higher frequency of mutant CD8⁺ T cells was positive for the surface marker Ly6C⁺ (Figure 7 C, top panel).

In both the CD4⁺ and CD8⁺ T cells the cell-surface signatures point towards an activated phenotype. The observed upregulation of activation and memory markers CD44 and Ly6C could be due to the peripheral T cell division in the absence of antigen encounter. In particular, considering the T-lymphopenic environment in heterozygous TUB006 mutants, homeostatic proliferation would be the most likely explanation for the

revealed T cell surface marker pattern (Goldrath, Bogatzki et al. 2000, Haluszczak et al. 2009).

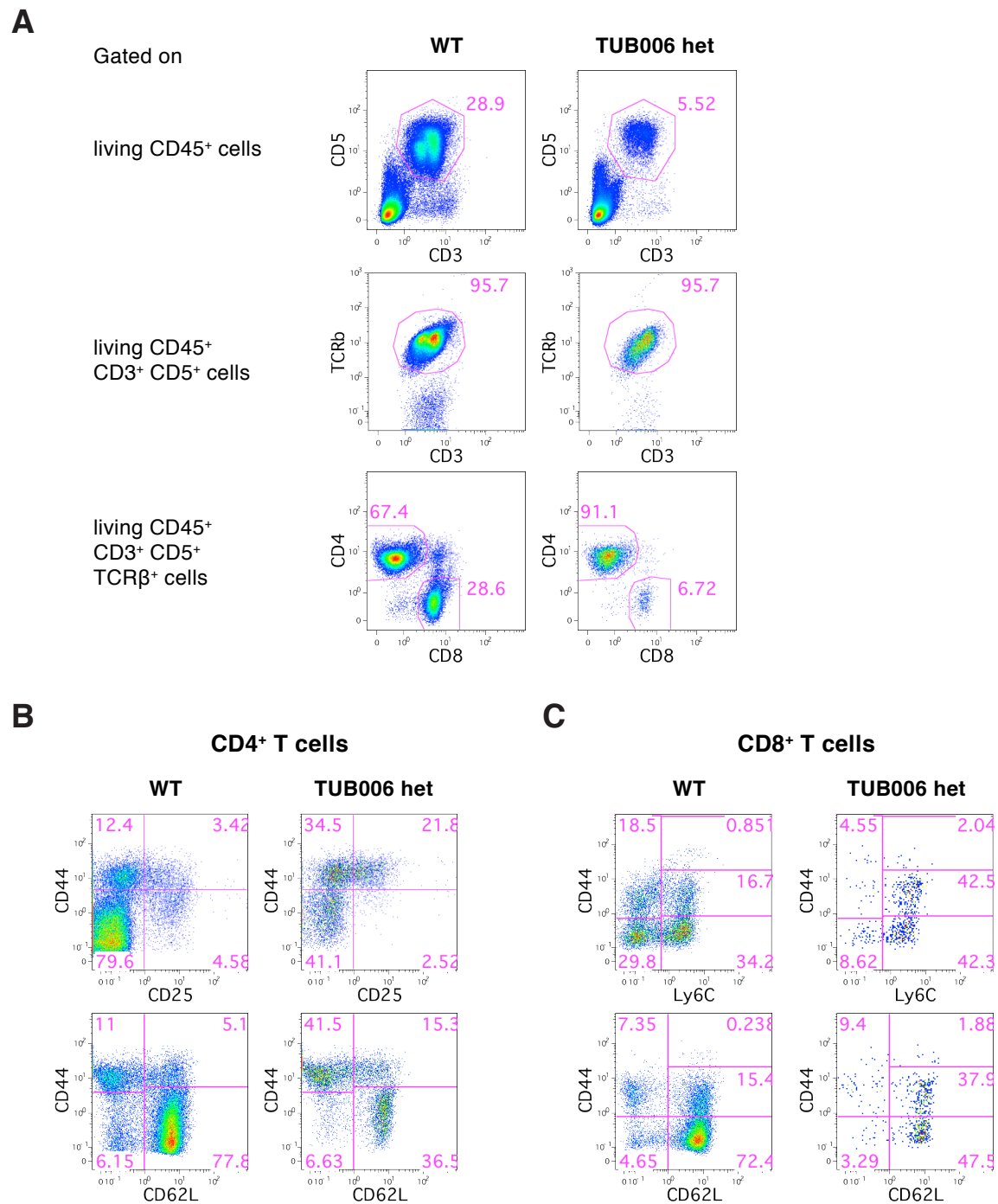


Figure 7: Flow cytometric analysis of surface marker expression on splenic T cells from wild type (WT) and heterozygous (het) TUB006 mice. Representative dot plots are shown; numbers within the gates indicate percentages of parent gate.

CD4⁺ as well as CD8⁺ T cells from heterozygous mutants showed phenotypic characteristics clearly distinct from the wild type controls. However, the phenotypic differences do not assure functional implications. To assess the functionality of the mutated T cells, *in vivo* infection as described below is an excellent model.

5.1.1 Analysis of the immune competence of heterozygous TUB006 mice in the *Listeria monocytogenes* infection model

The immune competence of heterozygous TUB006 mutants was assessed *in vivo* by evaluation of the immune response to i.v. infection with *Listeria monocytogenes*. *Listeria* infection induces an inflammatory response involving neutrophil granulocytes, NK cells, and macrophages during the first 24 to 72 hours of infection. It substantially restricts bacterial growth and is essential for early survival of infected mice (Pamer 2004). After the early innate phase, *Listeria*-specific T cell responses become detectable, reaching peak expansion around day seven p.i. (post infection; Busch, Pilip et al. 1998, Badovinac and Harty 2002). In particular IFN- γ -producing *Listeria*-specific CD8⁺ effector T cells and memory T cells are crucial for complete bacterial clearance and subsequent long-term protection (Bancroft, Schreiber et al. 1987). Therefore, it is possible to assess the competence of innate immunity by quantifying bacteria 48 to 72 hours after infection, and the competence of T cell immunity at later points of time (e.g. day 7 p.i.; Busch, Pilip et al. 1998, Busch, Vijn et al. 2001).

Heterozygous TUB006 mice and wild type littermates were infected with a low dose of *L.m.*. In the early phase of infection (day three), bacterial burden in spleens and livers of heterozygous mutants did not differ significantly from infected controls (Figure 8 A), and mice of both genotypes were vital. Thus, the innate immune defense was not substantially affected in heterozygous TUB006 mutants.

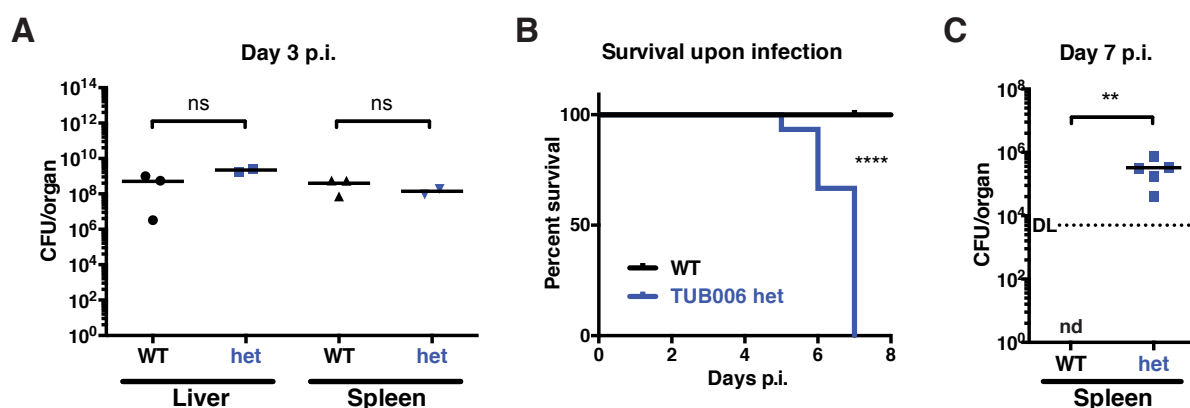


Figure 8: Heterozygous TUB006 mutants are highly susceptible to *L.m.* infection. A,C) Bacterial burden in indicated organs from heterozygous TUB006 mice and wild type littermates on day three (B) or seven (C) after infection. B) Survival curve of heterozygous TUB006 mice and wild type controls.

However, later during the course of infection, heterozygous TUB006 mice showed a significantly higher susceptibility to the pathogen. In fact, five to seven days p.i., all infected heterozygous mice (n=14) failed to further control the infection and succumbed

(Figure 8 B), whereas all littermate controls survived and showed good health conditions. On day seven p.i., heterozygous TUB006 mice failed to eliminate the pathogen, displaying considerable bacterial loads in spleen, while numbers of viable bacteria recoverable from spleens of wild type mice were below detection limit, showing sufficient clearance of the pathogen (Figure 8 C).

Since lack of *L.m.* clearance points towards a T cell defect, the antigen-specific T cell response was analyzed in more detail. In BALB/c mice, the immunodominant *Listeria* epitope – the antigen that provokes a stable and protective immune response by a large population of CD8⁺ T cells - is the peptide LLO₉₁₋₉₉ presented on the H-2K^d MHC I molecule (Pamer, Sijts et al. 1997). Therefore, for identification of *L.m.*-specific CD8⁺ T cells H-2K^d/LLO₉₁₋₉₉ multimer staining was employed (Busch, Pilip et al. 1998). Additionally, to assess the effector functions, splenocytes were restimulated *in vitro* with LLO₉₁₋₉₉ and stained for cytokines.

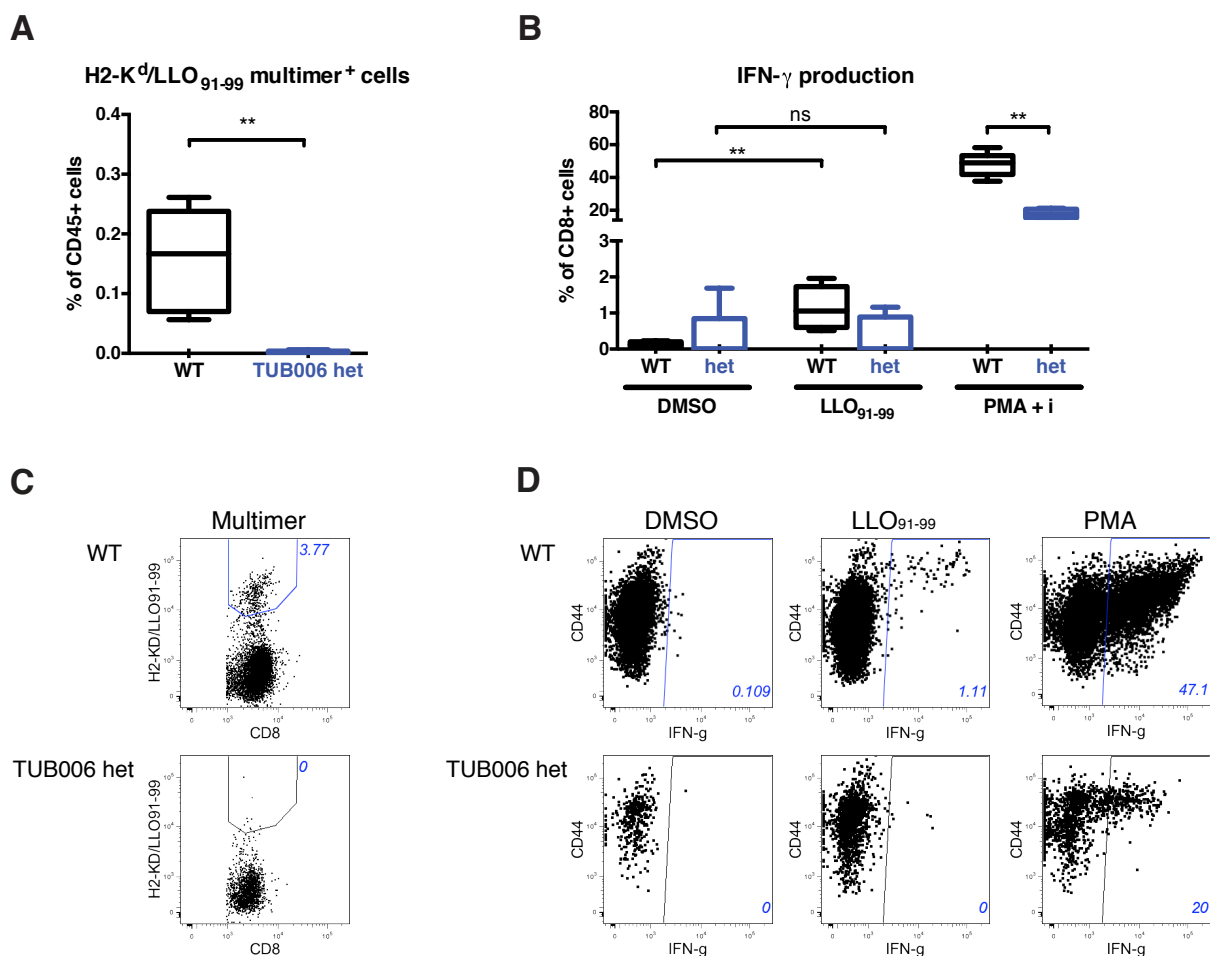


Figure 9: Analysis of the *Listeria*-specific T cell response on day seven after low-dose infection. A,C) H-2K^d/LLO₉₁₋₉₉ multimer⁺ CD8⁺ T cells. B,D) Proportions of IFN- γ producing CD8⁺ T cells detected by intracellular cytokine staining upon stimulation with DMSO (negative control), LLO₉₁₋₉₉ or PMA and ionomycin (positive control). Numbers within the gates indicate percentages of parent gate.

In heterozygous TUB006 splenocytes, it was hard to detect any H-2K^d/LLO₉₁₋₉₉⁺ CD8⁺ T cells (Figure 9 A and C). In accordance with this finding, CD8⁺ T cells from heterozygous TUB006 mice failed to produce IFN- γ upon restimulation with LLO₉₁₋₉₉ peptide (Figure 9 B and D). In response to peptide simulation, in samples from heterozygous TUB006 mice proportions of IFN- γ ⁺ producing CD8⁺ T cells remained as low as in the unstimulated DMSO control, whereas in wild type CD8⁺ T cells a ~10fold induction was observed. However, CD8⁺ T cells from heterozygous TUB006 mice were not generally deficient in cytokine production, as demonstrated by the ability of a substantial T cell population (although lower than in wild types) to produce IFN- γ upon antigen-independent stimulation with PMA and ionomycin (Figure 9 B and D). Noteworthy, some of the infected heterozygotes died prior to day seven, and the T cell response and cytokine production could be analyzed only in the survivors. Thus, a bias cannot be excluded, e.g. a lethal effect of IFN- γ production in mutants would lead to survival of low-producers.

In summary, in all analyzed heterozygous animals T cells in peripheral blood and spleens were reduced, whereas the thymus phenotype was more heterogeneous. In seven mice, three were athymic, three showed a normal T cell maturation pattern, and one animal showed an atrophic thymus with loss of corticomedullary distinction and an atypical Tdt staining pattern. The thymic defect is not of high penetrance in all mutants, meaning that the reduced T cell frequencies are (at least partly) independent of the thymus atrophy. Upon *L.m.* infection, T cells from heterozygous TUB006 mutants fail at priming a sufficient and protective immune response.

5.2 Homozygous TUB006 mutants exhibit a severe immunological phenotype

Mice showing the phenotype of reduced T cells were intercrossed to generate homozygous mutants. In about 25% of the offspring a postnatal lethal phenotype occurred, matching the predicted Mendelian frequencies and thus implying homozygous genotype of these mice. The earliest time point for visual identification of homozygous mutants was day 7-8, when fur growth is set off. Homozygous mutants showed disruption of the fur by loci of irregular hair growth. At the weaning age of three weeks all homozygous TUB006 were clearly distinguishable from their heterozygous or wild type littermates by the general appearance, reduced body size, deformed ears and a characteristic skin phenotype (Figure 10, dermatosis is described in section 5.2.4).

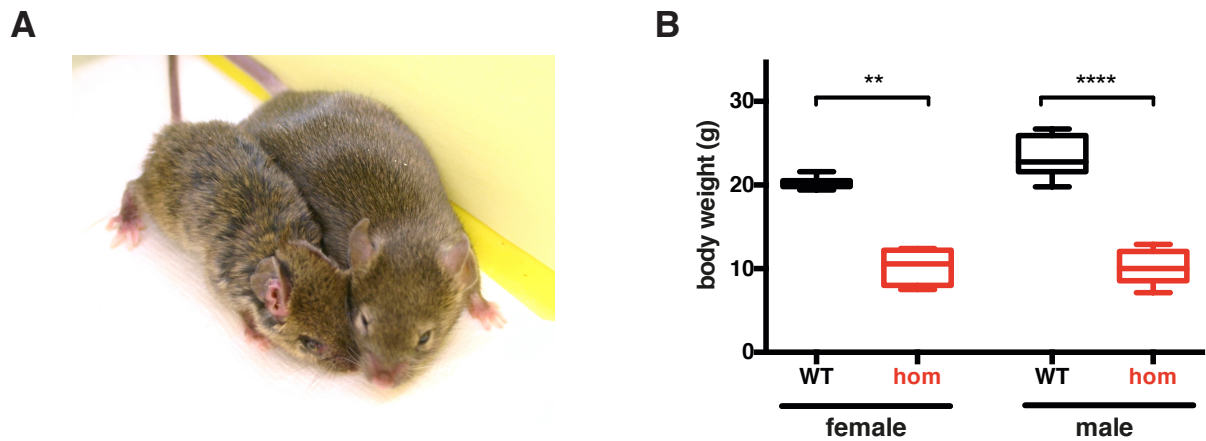


Figure 10: Homozygous TUB006 mutants present severe phenotype. A) Macroscopic appearance of a TUB006 homozygous mutant (left) and wild type littermate (right). B) Body weight data of 5-8 week old homozygous TUB006 mutants and wild type littermates (n=8-10 per group).

At the age of six to ten weeks, the homozygotes developed moribund appearance and died or had to be euthanized due to ethical reasons. During necropsy, neither thymus nor lymph nodes were detectable in any of homozygous TUB006 mutants.

5.2.1 Severe combined immunodeficiency

To characterize the homozygous TUB006 phenotype in detail, flow cytometric and histopathological analyses were performed. Thereby, profound lymphopenia was observed. As demonstrated by flow cytometry, all major types of lymphocytes – T cells, B cells and NK cells - were substantially reduced in blood samples from homozygous TUB006 mice (Figure 11). Histopathological examination confirmed, that spleens of mutant mice were devoid of lymphocytes and did not display the normal morphology of red and white pulp distinction (Figure 12; for detailed description of the wild type spleen architecture refer to section 5.1).

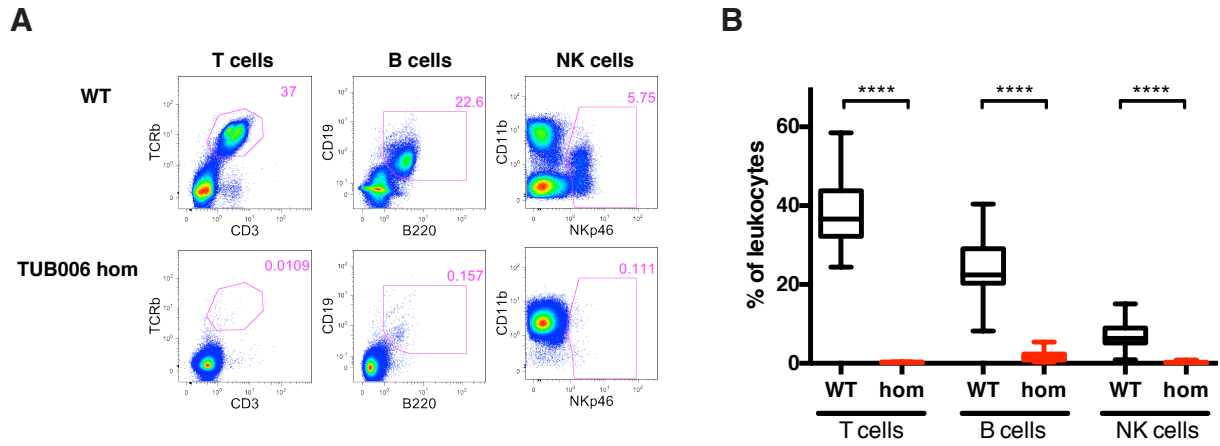


Figure 11: Lack of lymphocytes in homozygous TUB006 mutants. Peripheral blood from wild type (WT) and homozygous TUB006 (hom) animals was analyzed by flow cytometry. T, B and NK cell stainings are shown as representative dot plots (A), plots are gated on living CD45⁺ cells, numbers indicate percentages of parent gate; or box plots of pooled data (B), n=44 (WT), n=11 (hom).

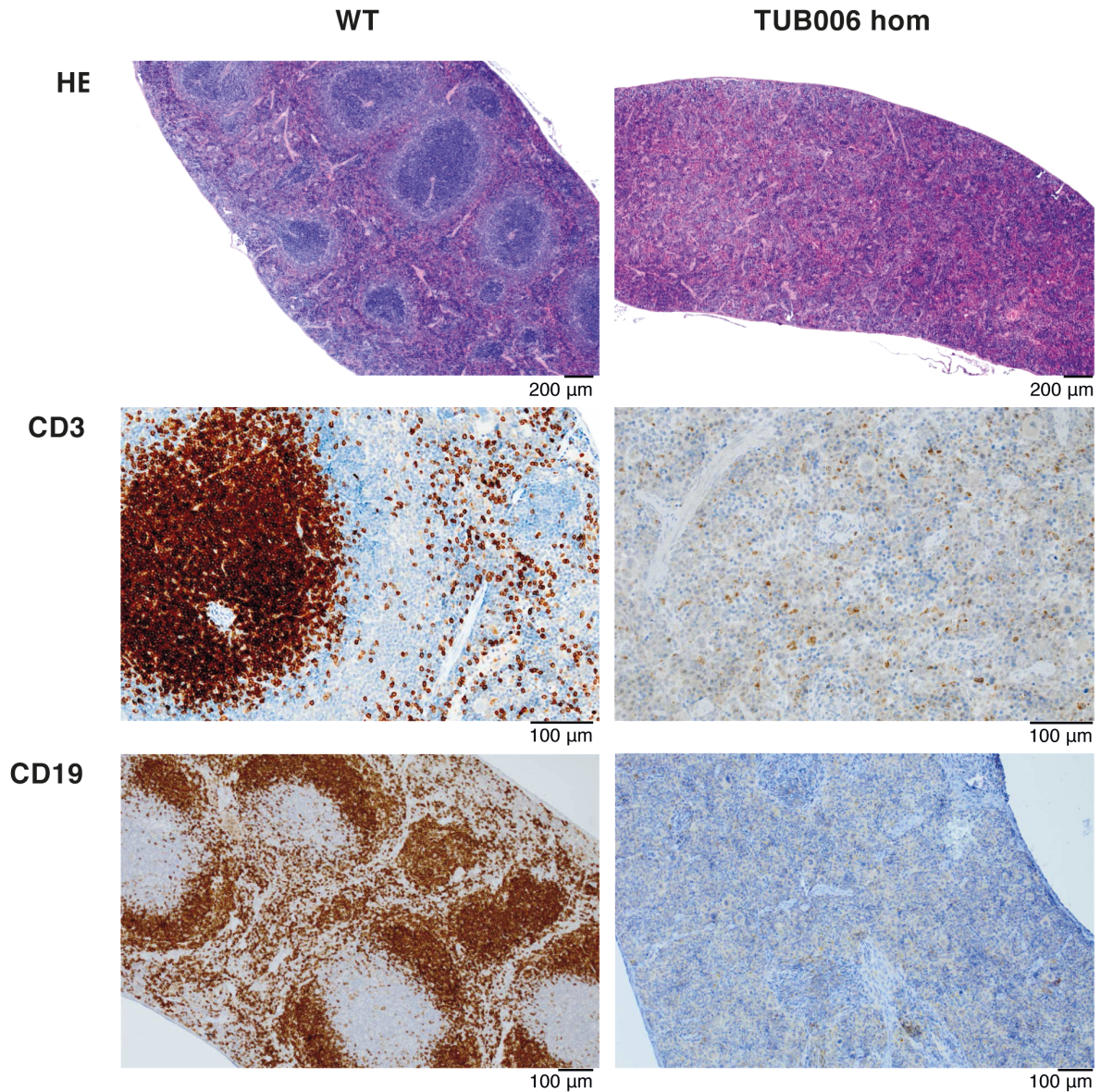


Figure 12: Histopathological analysis of spleen sections confirms severe combined immunodeficiency (SCID). HE (top panel) and immunohistological stainings of spleen sections for T cells (CD3, central panel) and B cells (CD19, bottom panel) of a representative homozygous TUB006 mouse and wild type control are shown. Positively stained cells for CD3 or CD19 appear brown.

Taken together, homozygous TUB006 mice display T⁻ B⁻ NK⁻ severe combined immunodeficiency (SCID). In accordance with the B cell deficiency, immunoglobulin levels (IgM, IgA, IgG1, IgG2a, IgG2b, IgG3) were below detection limits.

The remainder of T cells was analyzed for phenotypic characteristics by flow cytometry. Surface expression of CD3, CD5 and TCR β chain was observed on a small number of cells from homozygous TUB006 mutants, proving their belonging to the T cell lineage. Virtually the entire remaining T cell population consisted of CD4⁺ T cells, CD8⁺ T cells were extremely rare (0.002% of all splenocytes, Figure 13). A high proportion of T cells from TUB006 homozygous animals displayed a CD25⁺ CD44⁺ CD62L⁻ phenotype (Figure 13). CD25⁺ CD4⁺ cells co-expressed high levels of CD44, reflecting an activated state of CD4⁺ T cells rather than an increased frequency of regulatory T cells.

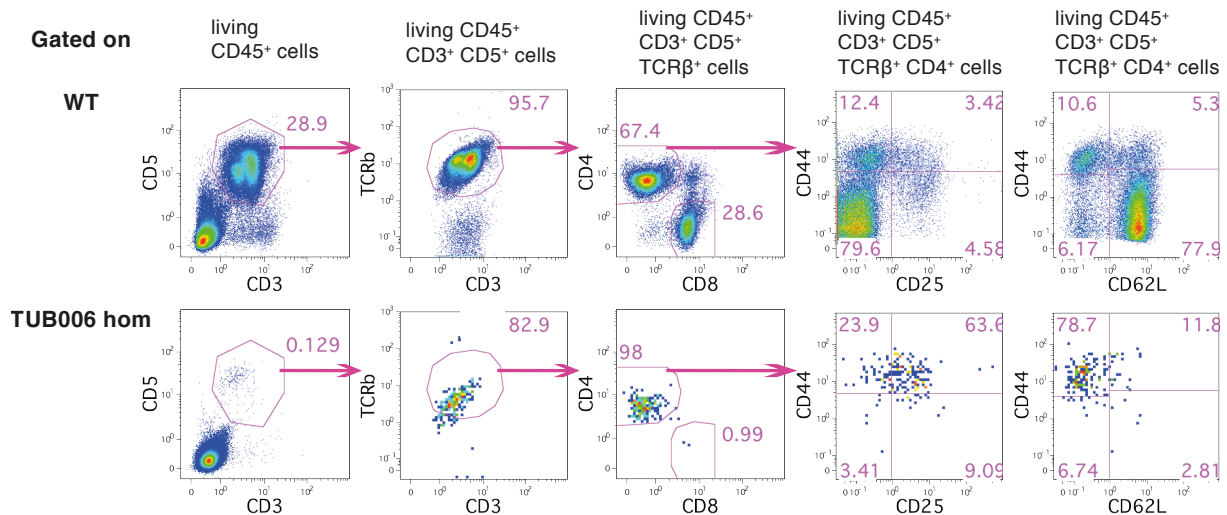


Figure 13: T cells of homozygous TUB006 mice show activated surface marker expression pattern. Flow cytometry data is presented as dot plots of splenic T cells from a representative homozygous TUB006 mouse and wild type littermate. Numbers indicate percentages of parent gate. The first two columns on the left show definition of T cells (CD3⁺ CD5⁺ cells in the first column are further gated for TCR β ⁺ cells in the second column). In the central column the CD4 vs. CD8 profile is shown, CD4⁺ T cells are then further gated for the surface marker analysis in the two columns on the right.

Reminiscent of the T cell phenotype in heterozygotes, the homozygous T cell surface marker signature is typical for activated T cells, but also for homeostatic proliferation as a consequence of repopulating lymphopenic hosts.

5.2.2 Granulocytosis

Immensely increased proportions of granulocytes (Gr-1⁺ CD11b⁺ cells) were observed by flow cytometry in peripheral blood and spleens of homozygous TUB006 animals. Not only the proportions, but also the absolute numbers of granulocytes were dramatically increased in peripheral blood (Figure 14). Microscopic analysis of Giemsa stained blood

smears confirmed that the increased cell population detected by flow cytometry morphologically represents *bona fide* neutrophil granulocytes (Figure 14 B). Interestingly, the nuclei of blood neutrophils show an atypical pattern of numerous lobes. Such neutrophil hypersegmentation is usually not observed in healthy animals.

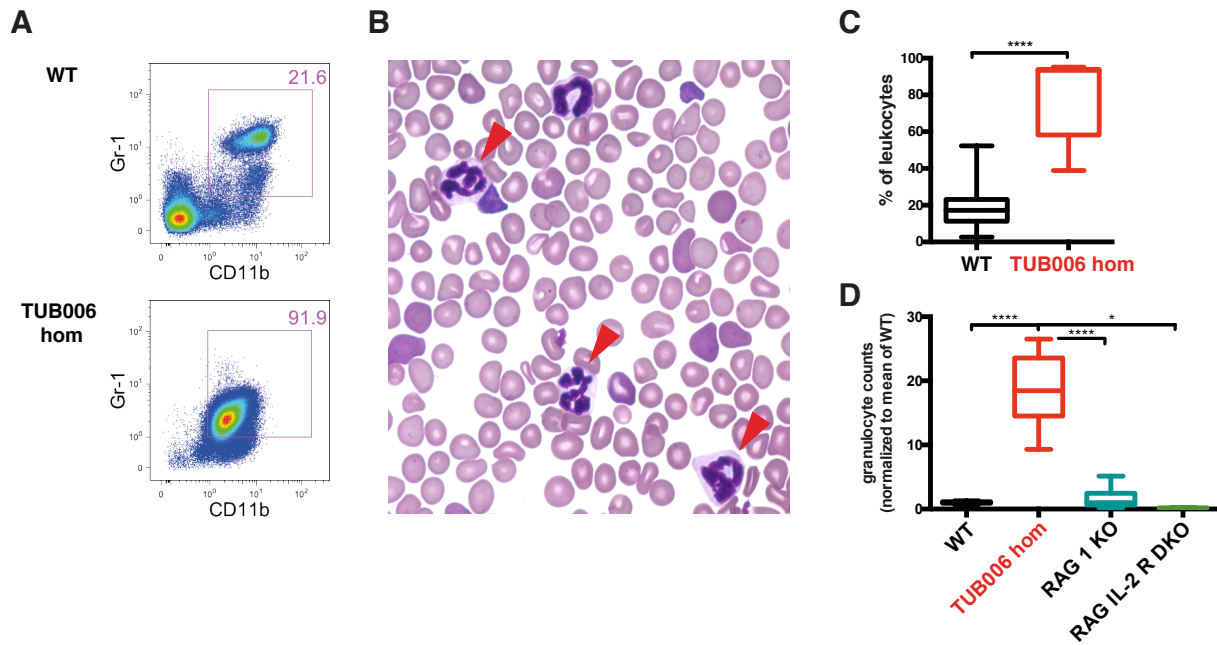


Figure 14: Granulocytosis in homozygous TUB006 mutants. Gr1⁺CD11b⁺ cells in peripheral blood from homozygous TUB006 mutant animals and wild type controls shown as a representative dot plot (A), box plot of pooled experiments as relative percentages of CD45⁺ cells (C) or absolute counts, normalized to the mean of the wild type controls (D). n=11 (hom), n=44 (WT), n=15 (RAG1 KO), n=2 (RAG IL-2 RG DKO). B) Representative blood smear from a homozygous TUB006 mouse. Four neutrophil granulocytes are shown, three of them presenting hypersegmentation of the nucleus (indicated by red triangles).

To assess the question whether the granulocytosis is a compensational consequence of the lymphocyte deficiency, peripheral blood leukocyte counts were compared to other lymphocyte-deficient mouse lines. Recombinase-activating gene 1 (RAG1) knockout mice (RAG1 KO) lack mature T and B lymphocytes (Mombaerts, Iacomini et al. 1992). The interleukin-2 receptor subunit gamma (IL-2 RG), also known as common gamma chain or CD132, is a receptor subunit of at least six different interleukin receptors: IL-2, IL-4, IL-7, IL-9, IL-15 and IL-21 receptor. In RAG1 and IL-2 RG double knockout mice (RAG IL-2 RG DKO) the growth and maturation of lymphocytes is defective resulting in lack of T cells, B cells, and NK cells (Lemischka and Moore 2003). Both RAG1 KO and RAG IL-2 RG DKO mice displayed considerably lower granulocyte counts than the homozygous TUB006 mutants (Figure 14 D). Thus, the granulocytosis in peripheral blood of homozygous TUB006 mice is not a compensatory result of the lack of lymphocytes.

As a target for immunohistological identification of neutrophil granulocytes, the characteristic lysosomal enzyme myeloperoxidase (MPO) was used. During the neutrophil's respiratory burst, MPO produces the cytotoxic hypochlorous acid to kill bacteria and other pathogens. MPO staining of tissue sections from homozygous TUB006 mice revealed granulocyte infiltrates in varying degrees and penetrance in liver, spleen and lungs (Figure 15).

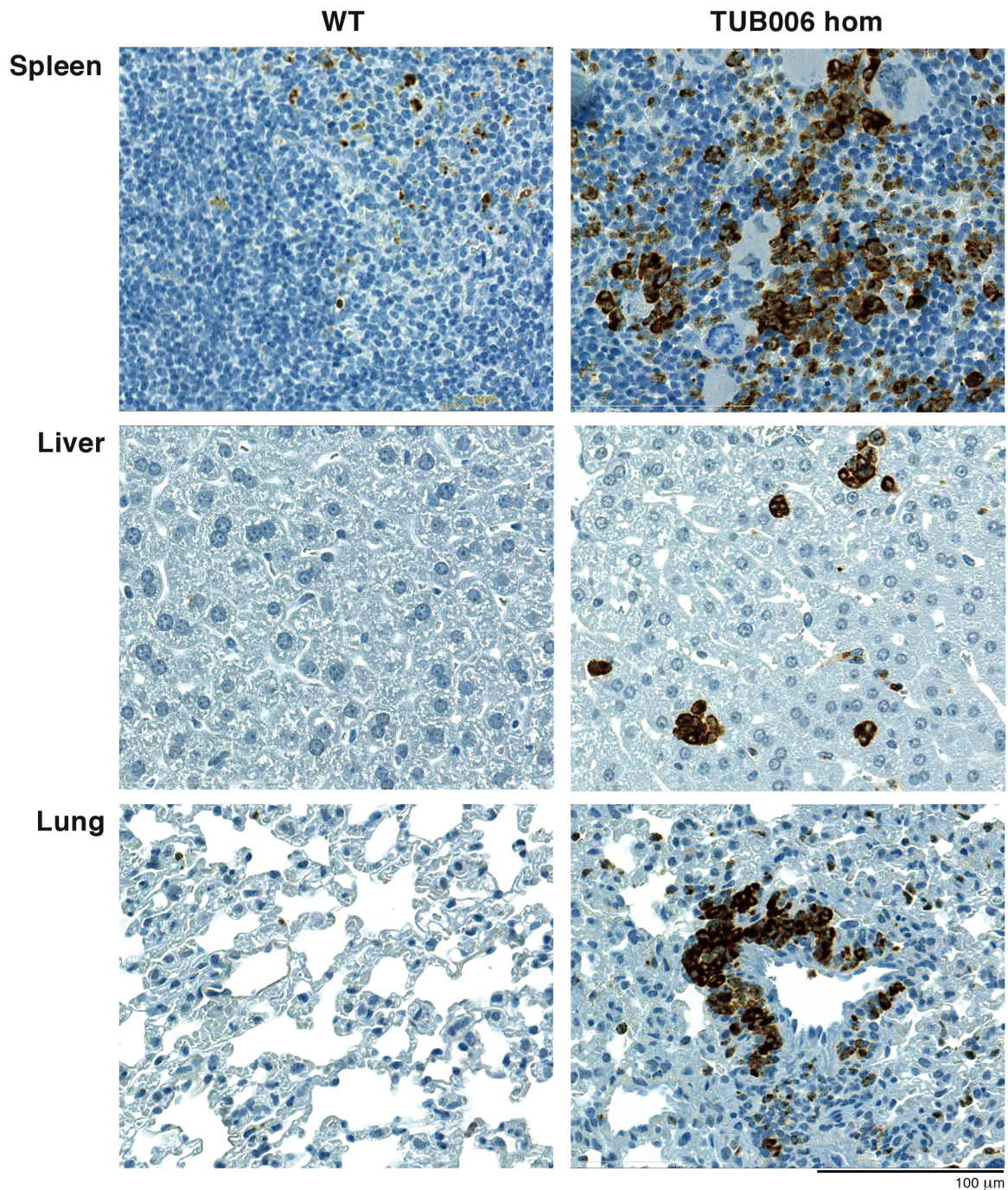


Figure 15: Myeloid infiltrates in spleen, liver and lung of homozygous TUB006 mutants point towards inflammation. Tissue sections of indicated organs were analyzed by immunohistology using visualization of neutrophil granulocytes via myeloperoxidase (MPO) staining. Sections from a representative eight-weeks old homozygous TUB006 mouse (hom) and wild type littermate (WT) are shown. MPO-positive cells appear brown.

5.2.3 Histopathological examination

To further characterize the phenotype of homozygous TUB006 mutants, six homozygous mice entered the Pathology Screen, one male and five females. They were around one month of age, weighting between 9 and 12 g. All organs of the animals were examined, displaying various pathological changes, summarized in Table 2.

Table 2: Summary of the histopathological examination of six homozygous TUB006 animals

	Patho-ID					
Organ	10.2205	11/525	11/958	11/961	11/1082	11/1083
Genital organs	Testicular atrophy	-		Not available	Not available	-
Lung	-	Infiltrates of granulocytes around blood vessles	Infiltrates of granulocytes around blood vessles, relaxed connective tissue around vessles with infiltrates	-	-	-
Liver	Increased extramedullary hematopoiesis, granulocytes in sinusoids	Increased extramedullary hematopoiesis, granulocytes in sinusoids	Increased extramedullary hematopoiesis, granulocytes in sinusoids	No extramedullary hematopoiesis, scattered granulocytes in sinusoids	Increased extramedullary hematopoiesis, granulocytes in sinusoids	Increased extramedullary hematopoiesis, granulocytes in sinusoids
Heart	-	-	Areas of old infarction	Small areas of calcification	Fibrosis and calcification in the heart	Cardiomyopathy, calcification
Kidney	-	-	Tubular atrophy	-	Slight tubular atrophy	Slight tubular atrophy
Spleen	Increase in granulocytes and megakaryocytes, no white pulp	Increase in granulocytes and megakaryocytes, no white pulp	Increase in granulocytes and megakaryocytes, no white pulp	Increase in granulocytes and megakaryocytes, no white pulp	Increase in granulocytes and megakaryocytes, no white pulp	Increase in granulocytes and megakaryocytes, no white pulp
Gut	Infiltrates of granulocytes	Infiltrates of granulocytes	Infiltrates of granulocytes	-	infiltrates of granulocytes	Nests of granulocytes

The pathology screen confirmed our previous findings of athymia as well as the extremely reduced body size of the homozygous animals as demonstrated by tibia length of 13 mm and a body weight of 8.6 g in comparison to 27.9 g for the wild type male mice. Granulocyte infiltrations were found in spleen, but also in liver, gut, and lung.

5.2.4 Dermatitis

The coat of homozygous TUB006 animals appeared roughened and showed foci of disrupted hair growth. This phenotype was progressive and in the further course developed to alopecia and incrustations, especially at neck, shoulders, abdomen and in some cases at extremities. At final stages, some animals developed ulcerous lesions.

For a deeper analysis of the skin abnormalities, dermatohistological methods were applied. Microscopic analysis of HE stained skin sections revealed increased hypodermal thickness, resembling murine models of systemic sclerosis (scleroderma; Pablos, Everett et al. 2004). Furthermore, lack of adipose tissue (lipodystrophy) was observed, as well as hyperparakeratosis, increased fibroblasts and blood vessels in the stratum corneum, epidermal hyperplasia, scarring alopecia and also massive infiltration of neutrophil granulocytes (Figure 16).

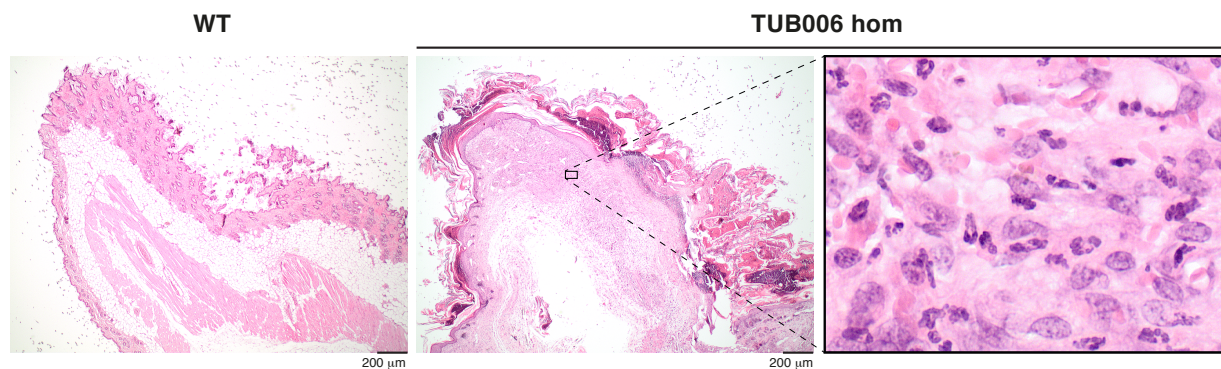


Figure 16: Histological analysis of skin sections. HE staining of a representative eight-weeks old wild type (WT) and homozygous TUB006 (hom) mouse. Homozygous sample shows abnormal thickening of the hypodermis, lack of the subcutaneous fat layer and scarring alopecia. Infiltrations of neutrophil granulocytes are shown at higher magnification in the right panel.

The skin phenotype observed in homozygous TUB006 mice may be a direct result of infection and/or chronic inflammation in the skin. Therefore, a closer look at the inflammatory milieu was of interest.

5.2.5 Inflammatory milieu in homozygous TUB006 mice

Proinflammatory cytokines such as IL-1 β , TNF- α and IL-6 are crucial mediators of inflammatory responses in various organs and tissues and therefore contribute to the pathogenesis of numerous (auto)inflammatory diseases: inflammatory bowel disease, rheumatoid and osteoarthritis, as well as inflammatory skin disorder, among others (Dinarello 2000; Gabay, Lamacchia et al. 2010; Croker, Lewis et al. 2011; Strober and Fuss 2011; Wojdasiewicz, Poniatowski et al. 2014).

Some of the pathological features found in TUB006 homozygotes, e.g. the massive granulocyte expansion and infiltration of neutrophils into tissues are probably governed by the cytokine milieu tending towards inflammation in these mice. Such inflammation induces granulocyte expansion, also known as “emergency granulopoiesis”, engages the total capacity of the bone marrow hematopoietic system and literally leaves no space for lymphopoiesis. The induction of this “emergency” system in TUB006 would explain that B cells, present at birth, disappear when granulocytes expand. In order to analyze the cytokine profile of TUB006 animals, plasma levels of cytokines IL-1 β , IL-6, IFN- γ , TNF- α , IL-4, IL-2, IL-5, chemokine (C-X-C motif) ligand 1 (CXCL1), IL-10, and IL-12 were determined.

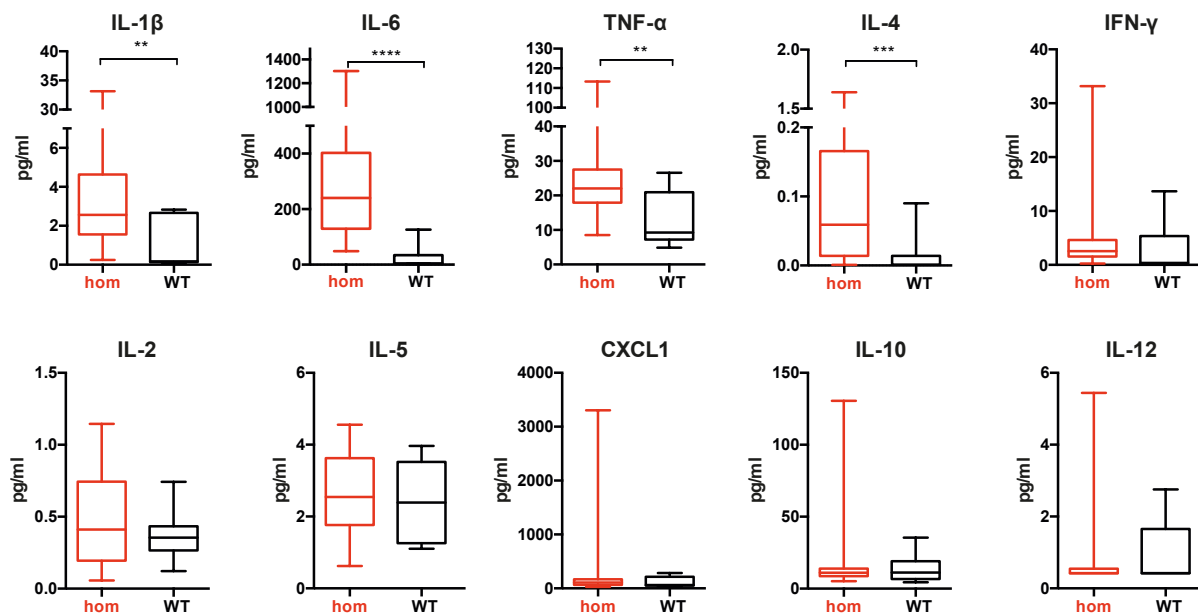


Figure 17: Cytokine profile in plasma of 32 homozygous TUB006 animals (hom) and wild type controls (WT).

Increased plasma levels of IL-1 β , IL-6 and TNF- α were observed in homozygous TUB006 mice. These proinflammatory cytokines point towards systemic inflammation and probably govern infiltration of granulocytes into tissues in TUB006. Interestingly, IL-4 levels were also increased.

5.2.6 Altered hematopoiesis in the bone marrow

The increased granulocyte numbers and lack of lymphocytes in TUB006 homozygotes could be a downstream effect caused by initial changes in the hematopoietic system. To determine whether defined steps during hematopoiesis are affected, multicolor flow cytometry panels for identification of hematopoietic stem cells and downstream

progenitor cells were established and relative proportions of the different developmental stages were assessed.

Stem cells antigen-1 (Sca-1, also known as Ly6a, lymphocyte antigen 6 complex, locus A) was one of the first identified markers expressed on the cell surface of stem and progenitor cells of the hematopoietic system. In combination with the tyrosine kinase c-Kit (alias CD117), Sca-1 is commonly used to characterize stem and progenitor cells. Both stem and early progenitors are lineage negative (Lin⁻). Stem cells are enriched in the Lin⁻ Sca-1⁺ cKit⁺ (LSK) fraction. Lineage progenitors are characterized by cKit expression in combination with other cell surface markers, such as signaling lymphocyte activation molecule (SLAM) CD150 or the IgG Fc γ Receptor III/II (Fc γ R or CD16/32). MEPs and GMPs are contained within the Lin⁻ Sca-1⁻ cKit⁺ compartment, GMPs being Fc γ R⁺ CD150⁻ CD34⁺, and MEPs being Fc γ R⁻ CD150⁺ CD34⁻ (Pronk, Rossi et al. 2007, Rieger, Smejkal et al. 2009)). CLPs are Lin⁻ Sca-1⁺ cKit^{intermediate} and 127⁺ (Kondo, Weissman et al. 1997).

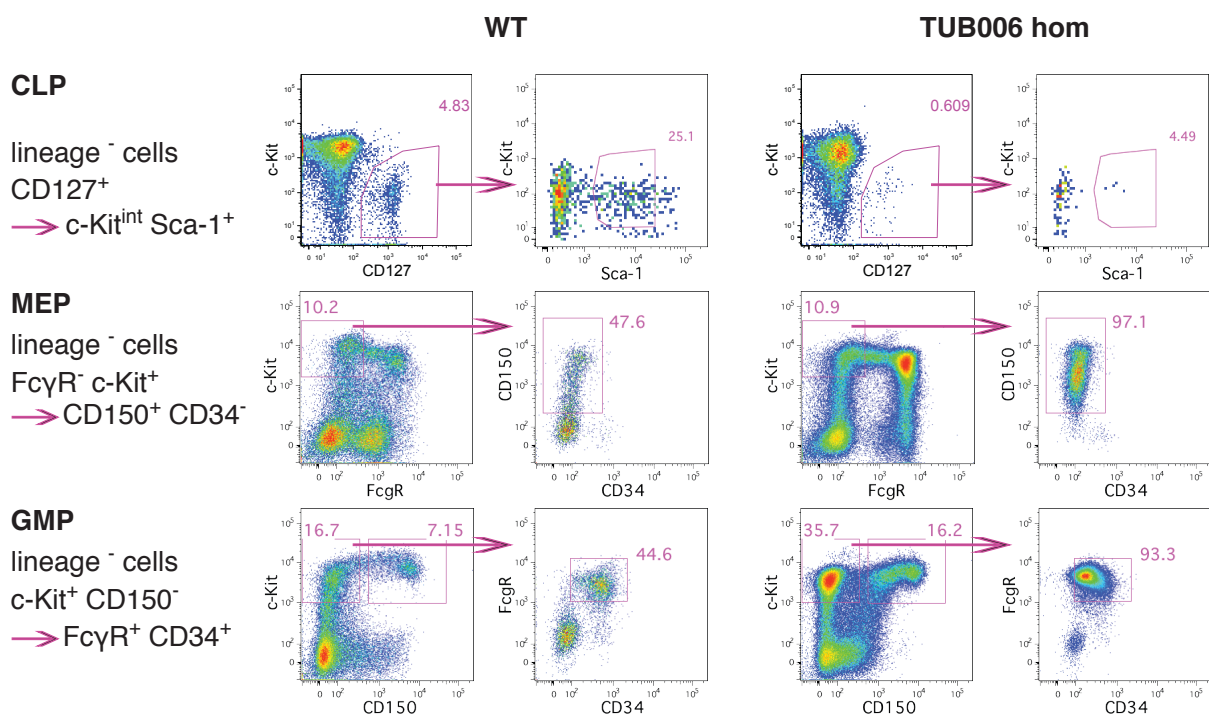


Figure 18: Alteration of hematopoietic precursors in the bone marrow. Flow cytometric analysis of common myeloid progenitors (CLP, top panel), megakaryocyte-erythrocyte progenitors (MEP, central panel), and granulocyte-macrophage progenitors (GMP, bottom panel) in the bone marrow from representative eight-weeks old homozygous (hom) TUB006 mouse and wild type (WT) control.

A flow cytometry panel was designed that allows identification of CLPs of the lymphoid branch, and MEPs and GMPs of the myeloid branch (for hematopoietic hierarchy refer to Figure 1). Detailed analysis of lymphoid and myeloid precursors in the bone marrow

revealed that the proportion of CLPs is essentially decreased in bone marrow from homozygous TUB006 animals, whereas GMPs and MEPs are largely increased (Figure 18).

Consequently, the hematopoietic stem cell compartment of eight-weeks old mice was analyzed, revealing intriguing findings. For flow cytometric identification of HSCs two alternative gating strategy were followed. The first classical approach aimed at identification of the LSK fraction. Since in homozygous mice no LSK fraction was detectable (Figure 19, top panel), the second strategy was applied. SLAM family markers CD48 and CD150 were used for identification of LT-HSCs, which are enriched within the CD150⁺ CD48⁻ fraction (Wilson, Laurenti et al. 2008). However, both approaches revealed similar results: The hematopoietic stem cells were drastically decreased in homozygous TUB006 mice (Figure 19).

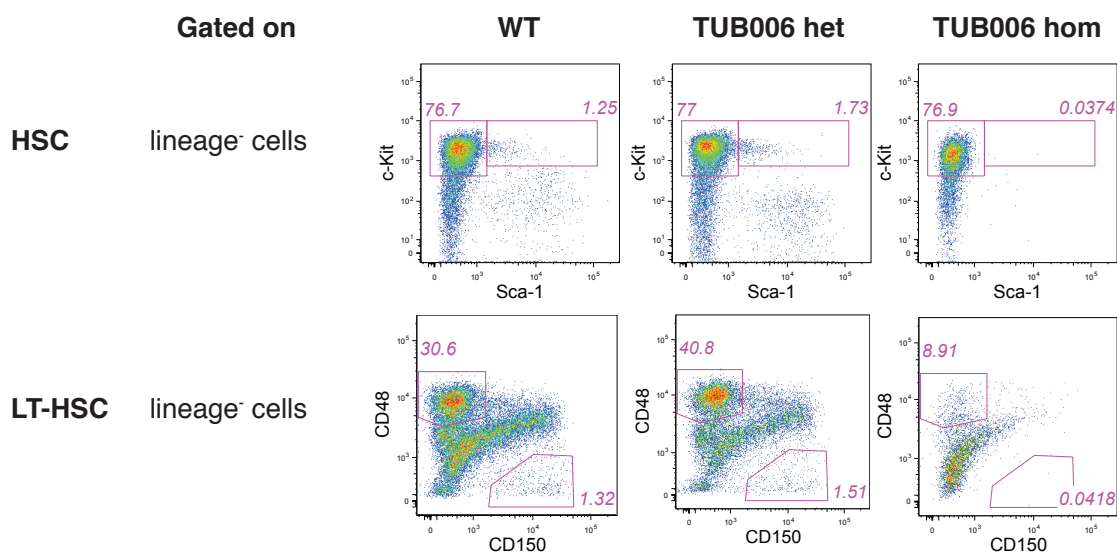


Figure 19: Identification of the hematopoietic stem cell (HSC) compartment in the bone marrow. Flow cytometric evaluation of lineage-negative Sca-1-positive c-Kit-positive cells (top panel) and lineage-negative CD150-positive CD48-negative cells (bottom panel) in eight-weeks old wild type (WT), heterozygous (het) and homozygous (hom) TUB006 mice.

Taken together, in homozygous TUB006 mice a hematopoietic defect was observed, with a virtual loss of the HSC compartment, strong decrease of the lymphoid precursors, and a massive increase in progenitors of the myeloid branch. The changes in the hematopoietic system most likely contribute to the downstream effects on lymphopoiesis and lymphatic tissue engraftment in the periphery. However, the phenotypic characterization of the hematopoietic precursors in the bone marrow does not answer the question whether this is a primary defect or is influenced by extrinsic factors.

5.3 Identification of the underlying genetic alteration

In an initial mapping attempt to identify the chromosomal localization of the underlying genetic mutation, heterozygous TUB006 animals were backcrossed twice with C57BL/6J mice and the resulting offspring interbred to produce homozygous TUB006 mutants with clearly detectable phenotype. DNA from 44 phenotypically homozygous TUB006 mutants was analyzed using 137 SNP markers (Klaften and Hrabě de Angelis 2005). For each marker analyzed, the logarithm of the odds (LOD)-score was determined. This coarse mapping revealed a linkage of the phenotype to five of eight SNPs located on chromosome 8 (LOD-Score > 3, Figure 20). The strongest linkage (LOD=16.7) could be detected with rs13479998, corresponding to a genomic region of 116.69 Mb (<http://www.ensembl.org>).

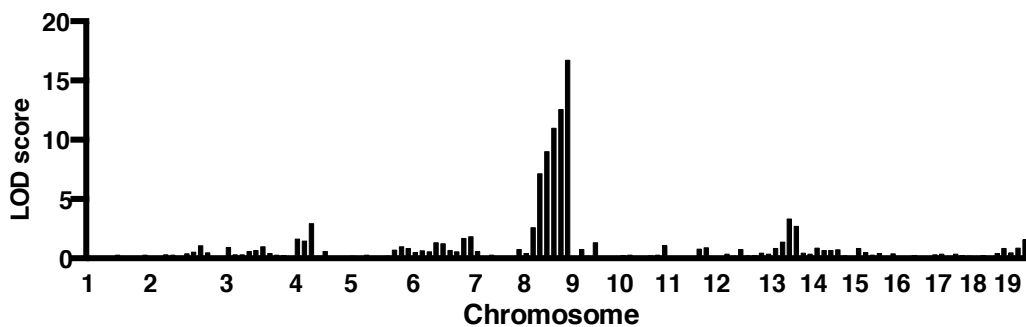


Figure 20: Genetic mapping of the TUB006 mutation by single nucleotide polymorphism (SNP) analysis between C57BL/6J and C3HeB/Fej strains.

The mapping approach still left a large candidate region. Comparison of the TUB006 phenotype with existing gene-targeted mice and human inherited disorders failed to reduce the number of candidate genes.

For many years, the major bottleneck in ENU mutagenesis projects was the identification of the causative mutation, which required time-consuming breeding and analytical efforts. That has recently changed with the development of Next-generation sequencing techniques, which represents the most efficient approach to identify the genetic mutation in ENU mutants. The vast majority of mutagen-induced mutations found to date is based on critical base pair changes in coding regions or splice sites. Therefore, sequencing can focus on these regions (exome sequencing, Fairfield, Gilbert et al. 2011, Hilton, Lewis et al. 2011, Sun, Mondal et al. 2012). In order to identify the causative mutation in TUB006, deep whole exome sequencing was performed using Illumina reversible termination technique (Zimprich, Benet-Pages et al. 2011). The false-positive rate inherent in this technique can be reduced by analyzing more than a single

mouse carrying the same mutation (Fairfield, Gilbert et al. 2011). Consequently, DNA from two affected animals (assuming their homozygous genotype) and one wild type littermate control was analyzed. The latter sample was included to rule out all variants between our C3HeB/FeJ wild type animals from the reference sequence, which was derived from another colony of C3HeB/FeJ animals. Strikingly, only one homozygous point mutation was present in both analyzed affected mice but not in the controls. Remarkably, this mutation was located exactly within the previously mapped candidate region on chromosome 8 (position of the mutation chr8:108459981).

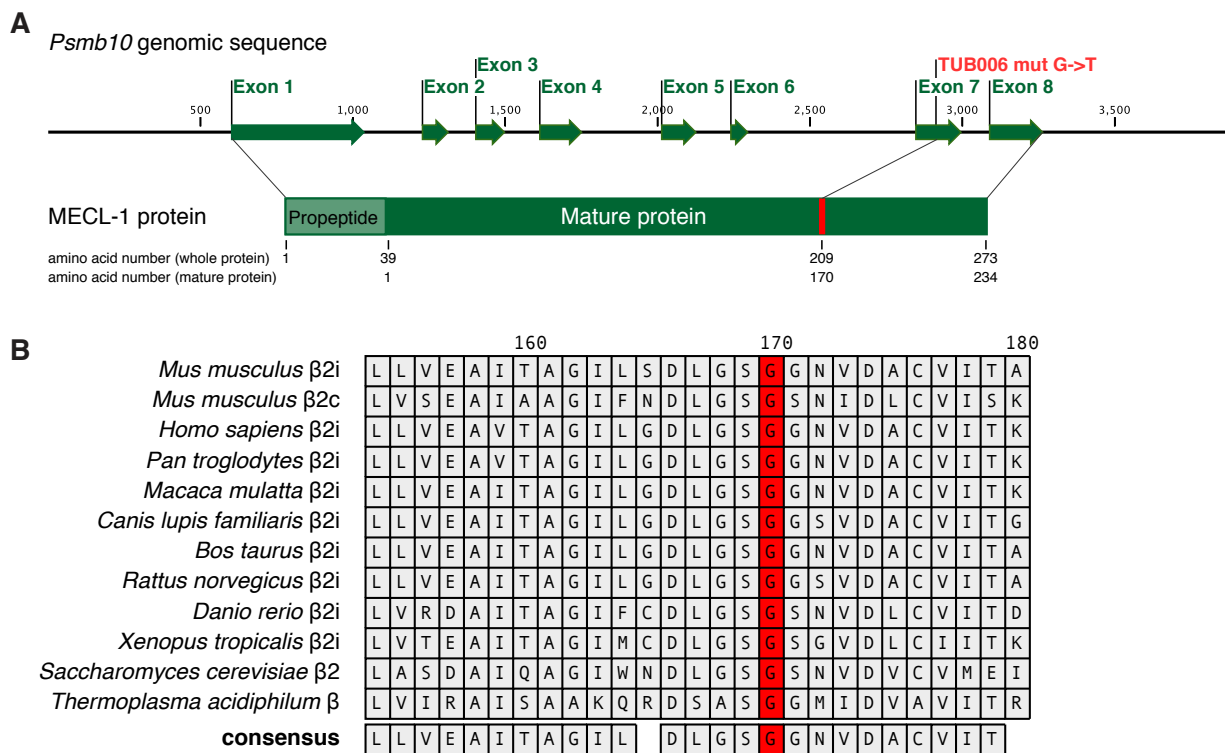


Figure 21: Location of the TUB006 mutation A) Genomic organization of the murine *Psmb10* gene. The TUB006 mutation (G->T transversion, depicted in red) is located in exon 7. The MECL-1 protein is generated in its inactive form containing the N-terminal propeptide of 39 amino acids. B) Multi-species amino acid sequence alignment of active β-subunits. Protein sequences are shown in the one-letter amino acid code. Residue numbers are assigned according to the sequence alignment to the β-subunit of the archaeon *Thermoplasma acidophilum*, as suggested by Huber et al., 2010.

The affected gene, proteasome subunit, beta type 10 (*Psmb10*, MGI: 1096380) encodes for MECL-1, a catalytic subunit of the immunoproteasome and thymoproteasome. The murine genomic sequence of the *Psmb10* gene spans 2.3 kb and contains eight exons (Figure 21 A; Cruz, Elenich et al. 1997). The identified point mutation is located in exon 7 of *Psmb10* and leads to an amino acid exchange from glycine to tryptophan at position 170 of the mature MECL-1 protein (Figure 21). Alignment of the protein sequence showed that glycine at position 170 is extremely conserved among species from the archaeon *Thermoplasma acidophilum*, through yeast, to vertebrates (Figure 21 B).

5.4 Establishment of genotyping protocols

Previously, the identification of heterozygous and homozygous TUB006 mutants had to be performed by visual inspection of the mice and/or by flow cytometric evaluation of peripheral blood leukocytes. However, to show that the phenotype correlates with the genotype, the establishment of genotyping methods is required. Furthermore, genotyping is needed for analysis of both embryos and young mice before onset of the visible phenotype. Identification of the mutation was the milestone in the project that facilitated establishment of genotyping protocols.

For fast and cost-efficient genotyping of heterozygous TUB006 mutants, heteroduplex analysis using LightScanner technology was utilized (Wittwer, Reed et al. 2003). The basis of this method is PCR, performed in the presence of the double-stranded DNA binding dye LCGreen. After amplification, the double-stranded PCR product undergoes continuous increase of temperature, and melting of the DNA strands releases the fluorescent LCGreen dye. The DNA melting and quantification of the fluorescence signal is performed in the LightScanner instrument.

In contrast to wild type and homozygous DNA, heterozygous TUB006 DNA contains two sequences, differing in a single nucleotide. The sequence alterations of the DNA strands lead to mismatched DNA hybrids called heteroduplexes. The melting temperature (t_m) of heteroduplexes is slightly lower than that of homoduplexes. The altered melting curves enable identification of heterozygotes by curve shape and/or position. In order to find the optimal genotyping conditions for the TUB006 mutation, different primer combinations were designed and tested. The melting temperature had to be adjusted in the PCR cyclers program by adding 2°C to the t_m initially calculated for primers, since addition of LCGreen dye increases the melting temperature of DNA. Best results were obtained with a short PCR product of 77 bp, amplified using the primer combination shown in Figure 22 A. Clearly separated heteroduplex products were observed that melted at lower temperatures than the homoduplex products (Figure 22 B, red curves).

Although the LightScanner genotyping showed excellent efficiency for identification of heterozygotes, distinguishing of wild types and homozygotes did unfortunately not perform well. To solve the problem of homozygote genotyping, classical Sanger sequencing of PCR products had to be applied (Sanger et al. 1977). The optimal primer

combination for PCR products suitable for Sanger sequencing and exemplary sequencing results are shown in Figure 22 A and C.

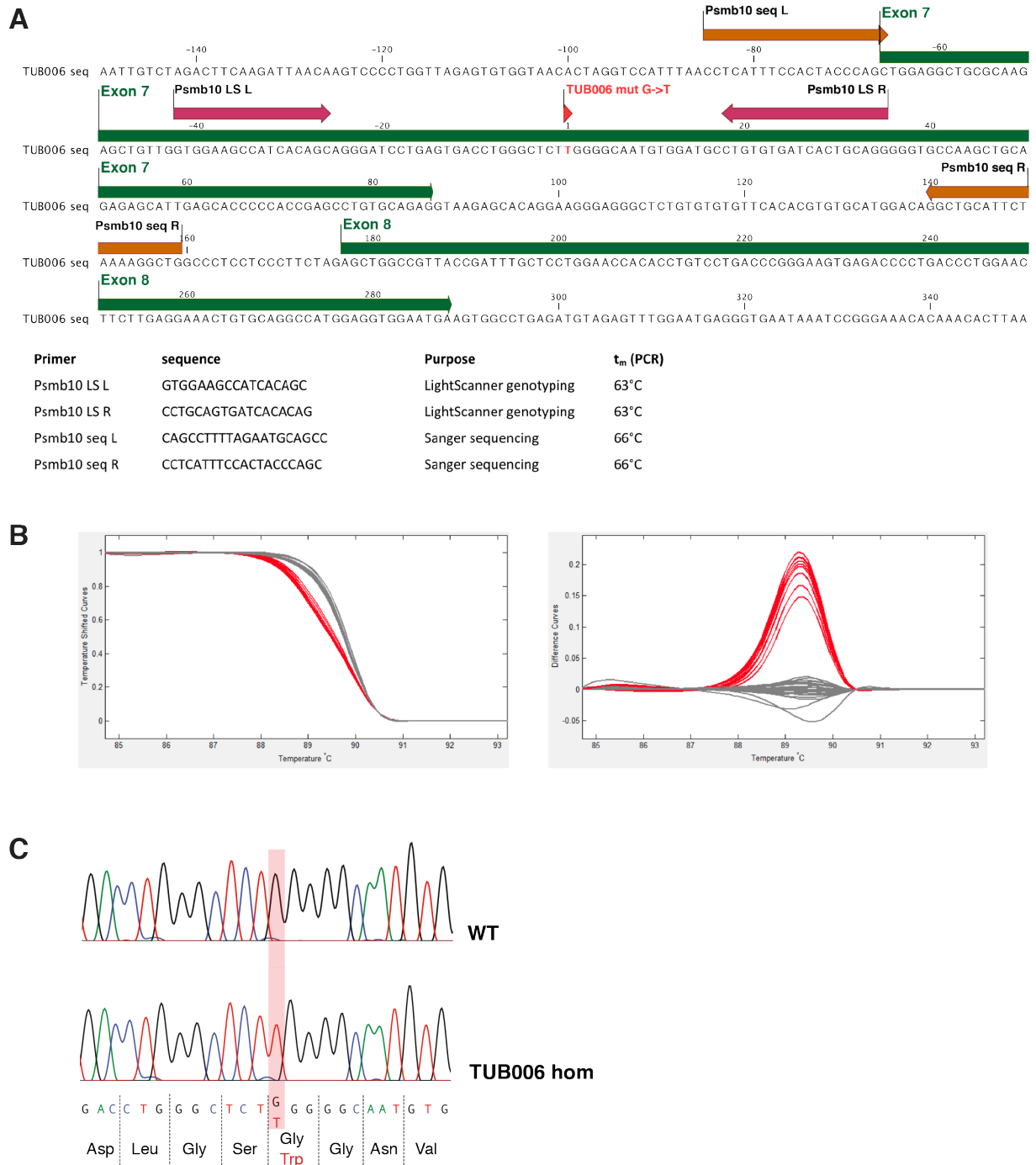


Figure 22: TUB006 genotyping. A) Genomic *Psmb10* sequence of a homozygous TUB006 mouse. Localization of the TUB006 mutation and the optimal primer combinations for genotyping are shown. B) Melting curve analysis via LightScanner software. Melting curves of DNA amplicates containing heteroduplexes (heterozygous samples) are depicted in red, grey curves show melting curves without heteroduplexes (wild type or homozygous samples). C) Sanger sequencing of representative wild type and homozygous TUB006 mutant.

5.5 T and NK cell deficiency is inborn, while B cell deficiency and granulocytosis develop later

The TUB006 phenotype may be based on deficient lymphocyte differentiation, enhanced susceptibility to opportunistic infection(s) and therefore may lead to an expansion of the granulocyte lineage. However, other lymphocyte-deficient mouse lines such as RAG1 KO and RAG IL-2 RG DKO do not exhibit increased granulocytic infiltrations, particularly not as drastically as observed in TUB006 homozygous mutants. Alternatively, it is possible that (auto-) inflammation and associated accumulation of granulocytes represent the primary TUB006 defect and cause the lack of the thymus and lymphocytes. With lymphocytes still detectable in newborn TUB006 homozygotes and increased numbers of granulocytes at this stage, granulocytosis in TUB006 homozygous mice might cause the lack of lymphocytes.

Establishment of genotyping protocols facilitated examination of younger mice before onset of the visible skin phenotype. In order to understand the development of the pathology in TUB006 mice, leukocyte subsets in peripheral blood and spleens from newborn TUB006 mice were analyzed by flow cytometry. T cells were profoundly reduced in peripheral blood and spleens from homozygous TUB006 neonates (Figure 23 A and B). NK cells were also drastically decreased in the periphery, whereas B cell and granulocyte frequencies were comparable to wild type levels (Figure 23 A and B). No differences in immunoglobulin levels between wild types, heterozygous, and homozygous neonates were observed (Figure 23 C).

These results demonstrate that the granulocytosis develops later than SCID. Since B cells are present in newborns, a lymphocyte progenitor defect at this age can be excluded (for analysis of lymphoid progenitors in the bone marrow from older mice refer to section 5.2.6).

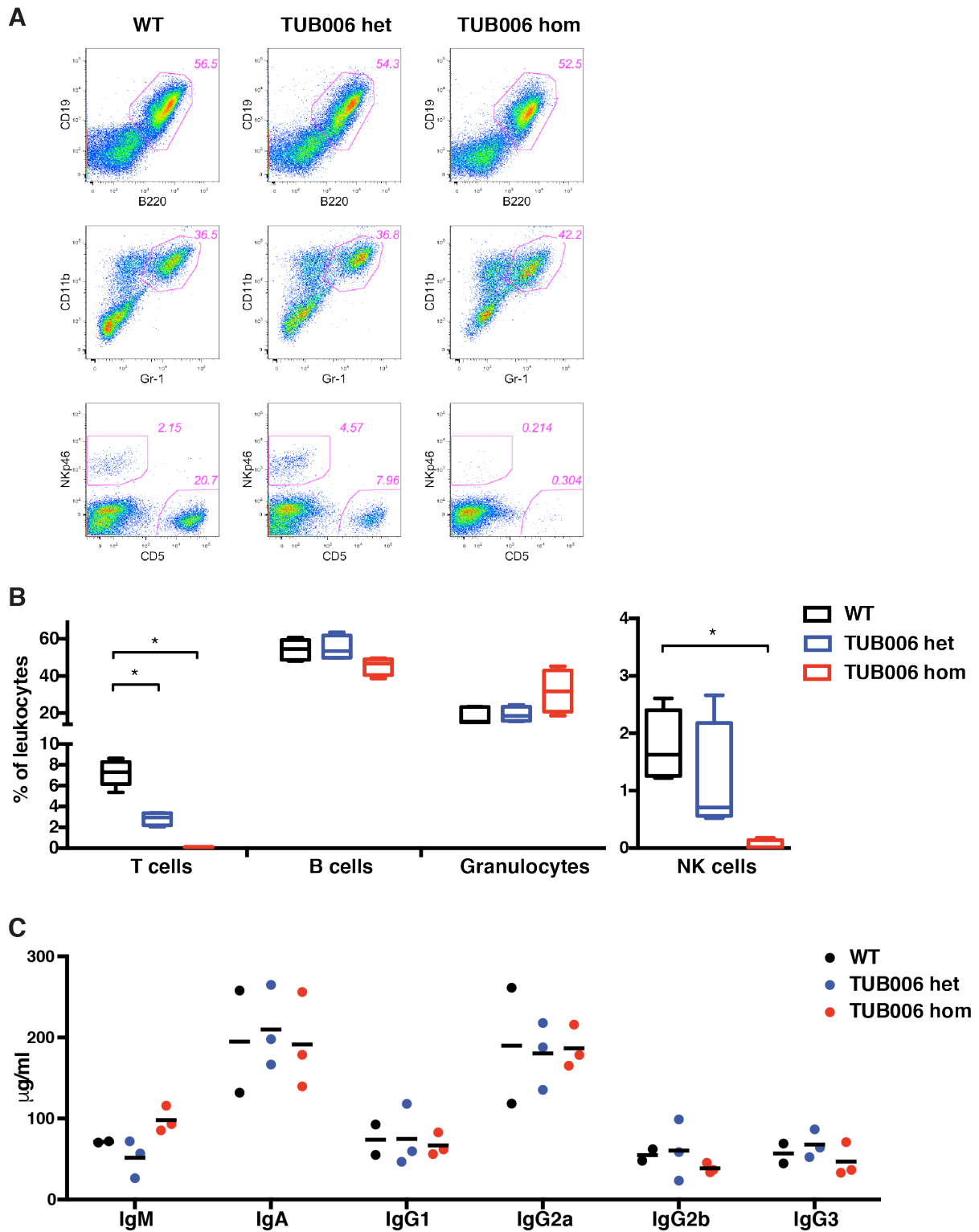


Figure 23: Phenotype of neonatal TUB006 mutants. Flow cytometric analysis of peripheral blood (A) and splenocytes (B) from 2-5 days old homozygous (hom), heterozygous (het) and wild type (WT) pups shown as representative dot plots (A) or box plots (B) of pooled data from 3 litters analyzed on 3 different days (n= 4-5 per group). Plasma concentration of antibody isotypes IgM, IgA, IgG1, IgG2a, IgG2b, IgG3 was measured in plasma obtained from two litters (2 and 5 days old, n= 2-3 per group).

5.6 Thymus is present but abnormal in newborn TUB006 homozygotes

As mentioned before, in mice with pronounced homozygous TUB006 phenotype (more than four weeks of age), the thymus was not detectable. In contrast to athymic adolescent homozygotes, vestigial thymi were present in newborn homozygotes. Although the thymi from heterozygous and particularly homozygous TUB006 mice were substantially smaller in size compared to wild type counterparts, a general thymus anlage defect can be excluded.

A detailed analysis of the medullary and cortical TECs in TUB006 thymi was performed by flow cytometry. Stromal cells are first gated for absence of the leukocyte marker CD45, then cTECs and mTECs can be distinguished by the cell surface expression of epithelial cell adhesion molecule (EpCam) and Ly-51. Obtained data indicate that cTECs were virtually absent in homozygous TUB006 thymi, whereas mTECs were readily detectable (Figure 24).

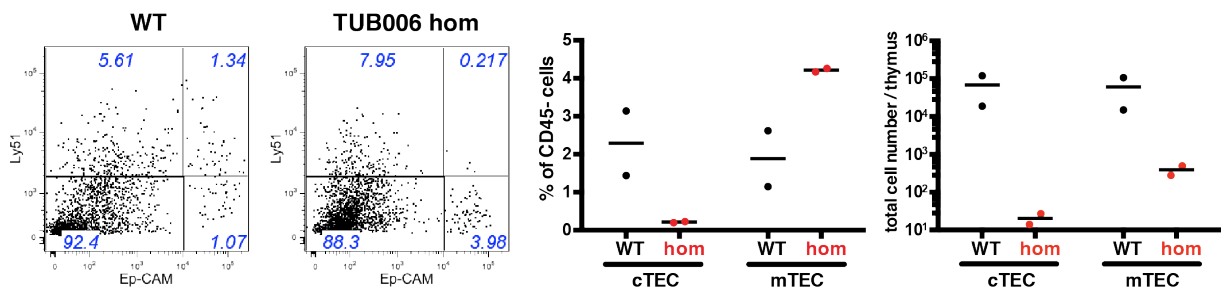


Figure 24: Thymic stroma defect in thymi from newborn TUB006 homozygotes. cTECs (EpCam⁺ Ly51⁻) and mTECs (EpCam⁺ Ly51⁺) from homozygous (hom) and wild type (WT) pups are shown as representative dot plots (left, plots are gated on living CD45-negative cells) or scatter plots (right, n=2, from one two days old litter). Dot plots (left) are gated on CD45⁻ cells; scatter plots (right) show percentages of CD45⁻ cells or total cell numbers per thymus.

The thymocyte differentiation was also examined by flow cytometry. TUB006 homozygous neonatal thymi revealed decreased frequencies of CD4SP and CD8SP thymocytes compared to the control littermates (Figure 25), suggesting a stop of the thymocyte development at the double positive (DP) stage.

Mice deficient for the thymoproteasome-specific subunit $\beta 5t$ showed impaired positive selection of CD8⁺ T cells, leading to a decrease of CD8SP thymocytes and CD8⁺ T cells in the periphery (Murata, Sasaki et al. 2007). In contrast to $\beta 5t$ -deficient mice, in thymi from TUB006 mice both CD4SP and CD8SP thymocytes are reduced, although the CD4 defect is more leaky (Figure 25). Therefore, it is unlikely that the thymic TUB006 phenotype resembles solely thymoproteasome deficiency. The question remains whether the observed defect is intrinsic to cells derived from the hematopoietic system,

e.g. maturing T cells expressing the immunoproteasome, or if the defect is caused by factors like thymus stroma cells, especially cTECs expressing the thymoproteasome. Transplantation of the bone marrow from homozygous TUB006 mice into wild type recipients would help to clarify this point.

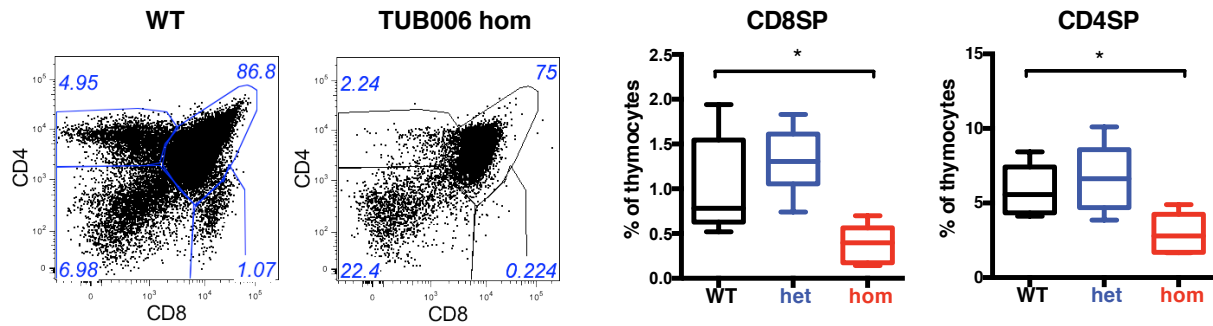


Figure 25: Impaired thymocyte maturation in homozygous TUB006 neonates. Thymocytes from 2-5 days old homozygous (hom), heterozygous (het) and wild type (WT) pups shown as representative dot plots (left, plots are gated on living CD45-positive thymocytes) or box plots of pooled data from 3 litters analyzed on 3 different days (right panels, n= 4-5 per group).

5.7 Bone marrow transplantation experiments

The observed SCID and/or autoinflammation of TUB006 mutants might be caused by a cell-intrinsic defect within the hematopoietic system. To address this question, bone marrow transplantation experiments are the appropriate method, as described for other mutant mouse lines at the German Mouse Clinic (Abe, Wechs et al. 2008). Bone marrow cells from either wild type or homozygous TUB006 mice were used to reconstitute either wild type or homozygous TUB006 recipients. Prior to intravenous administration of donor bone marrow cells, recipients were exposed to radiation in order to remove the endogenous hematopoiesis and clear the hematopoietic niches for donor-derived hematopoietic precursors.

The resulting homozygous TUB006 mutants that received wild type bone marrow cells will be henceforth designated as WT→TUB006 chimera. Chimeric mice generated by administration of TUB006 or wild type bone marrow to wild type recipients are termed TUB006→WT or WT→WT, respectively.

TUB006 bone marrow fails at reconstituting wild type recipients

If the TUB006 mutant phenotype was based on a hematopoietic cell-intrinsic defect, transfer of bone marrow cells derived from sick individuals into healthy recipients would transmit the disease to recipients. Pooled bone marrow cells derived from two eight-week-old homozygous TUB006 donors were transferred into wild type recipients (n=4) irradiated with two fractions of five Gy. As a control, wild type bone marrow was transplanted to wild type recipients (Figure 26 A). Surprisingly, the mutant bone marrow completely failed at reconstituting the wild type recipient. Numbers of leukocytes in circulation remained low and all recipients died within few weeks after transplantation (Figure 26 B). In contrast, WT→WT chimera showed hematopoietic reconstitution with CD45.2⁺ cells (Figure 26 C and D), proving that the newly produced leukocytes are derived from the transplanted donor bone marrow.

In summary, data from the first bone marrow transplantation study hint towards a hematopoietic defect in TUB006 mice, and is in line with the observation of extremely low HSC content in the bone marrow of homozygous TUB006 mice.

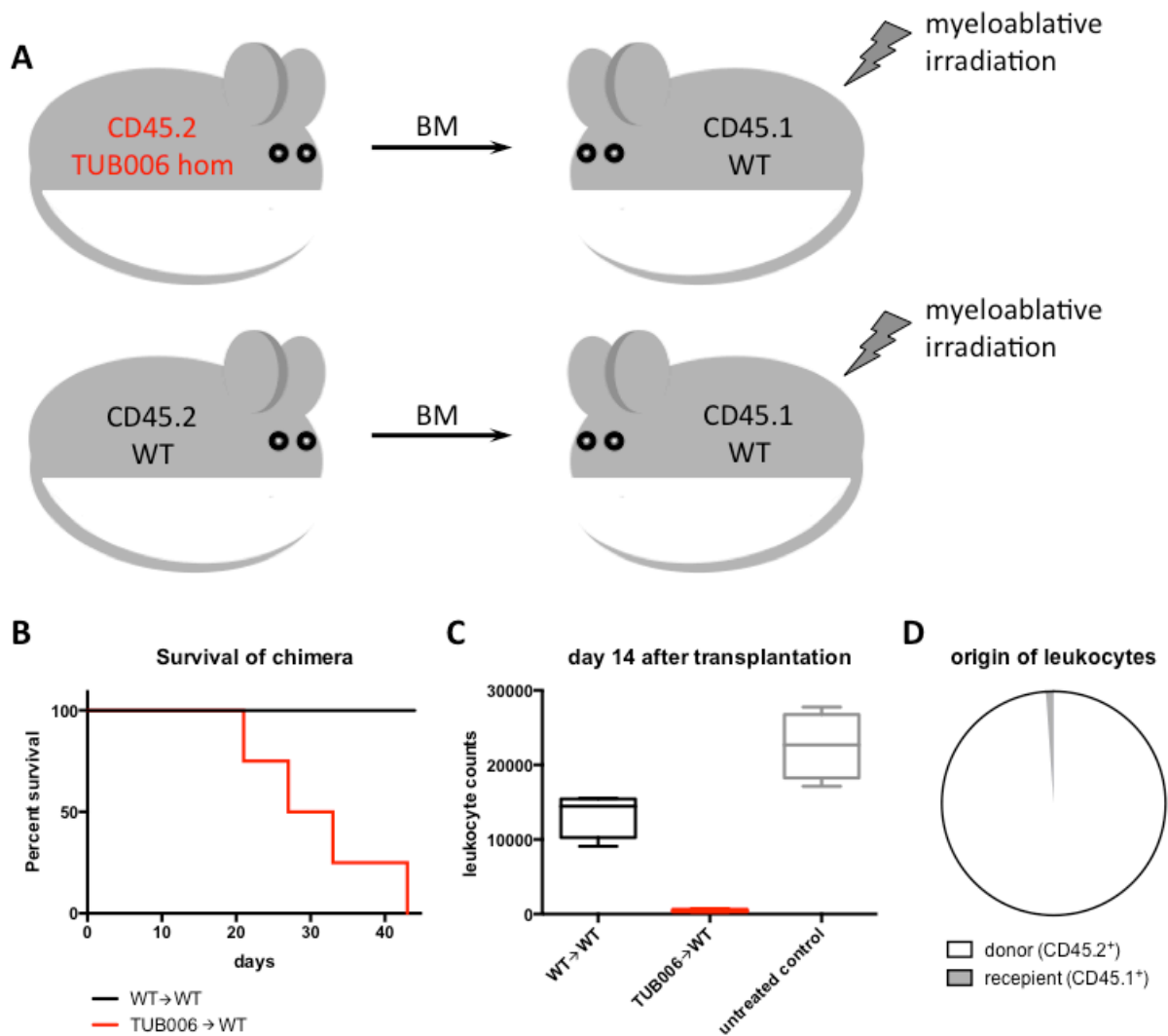


Figure 26: Bone marrow from homozygous TUB006 donors does not reconstitute wild type recipients. A) Experimental setup. B) Survival curve shows lethality of TUB006→WT chimeric mice. C) Leukocyte counts acquired by flow cytometry of peripheral blood from chimeric mice and untreated wild type controls shows reconstitution in WT→WT and failure in TUB006→WT chimera two weeks after transfer. D) Origin of leukocytes from the WT→WT chimera 14 days after bone marrow transplantation.

Inconsistent observations in WT→TUB006 bone marrow chimera

If the hematopoietic cell compartment solely was solely causing the disease, transfer of bone marrow cells from a healthy donor would reconstitute the recipient's leukocyte pool including B and NK cells. To evaluate the therapeutic effect, transfer of wild type bone marrow cells into irradiated homozygous TUB006 mutants was performed. As a control, wild type bone marrow was transferred into wild type recipients.

First pilot study

In the first pilot experimental setting the bone marrow transfer experiment was performed with TUB006 mice bred on the original genetic background C3HeB/FeJ. The

same irradiation dose (two fractions of five Gy) was used as for wild type recipients in the previously described TUB006→WT and WT→WT chimera.

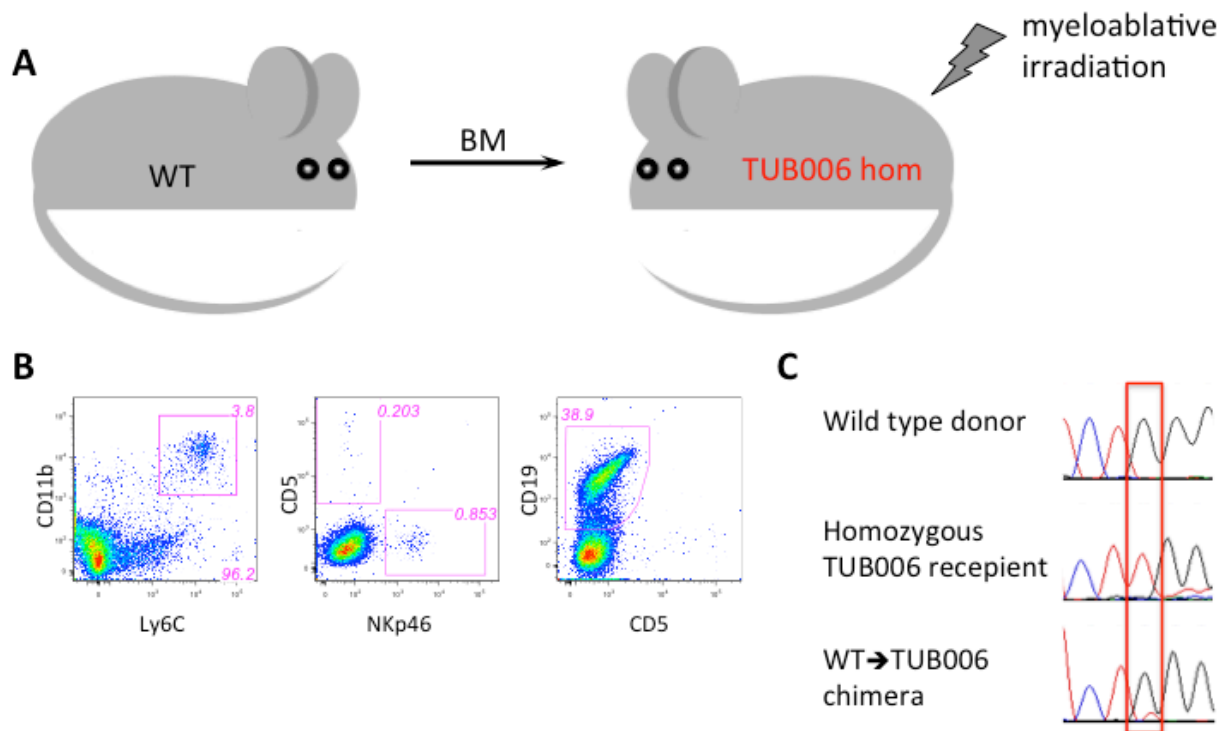


Figure 27: Wild type bone marrow cells give rise to B cells, NK cells and granulocytes in homozygous TUB006 hosts. A) Experimental setup. B) Flow cytometric analysis of peripheral blood leukocytes from WT→TUB006 bone marrow chimera two weeks after bone marrow transfer of wild type bone marrow into homozygous TUB006 recipients. The left dot plot shows the granulocyte gate (CD11b⁺ Gr-1⁺ cells), the central dot plot shows the T cell gate (CD5⁺ cells) and the NK cell gate (NKp46⁺ cells). The right dot plot shows the B cell gate (CD19⁺ cells). All plots are pregated on living leukocytes (CD45⁺ cells). C) Sanger sequencing of DNA isolated from blood leukocytes from a wild type donor, homozygous TUB006 recipient before bone marrow transplantation, and a representative WT→TUB006 bone marrow chimera two weeks after bone marrow transplantation. The TUB006 mutation locus is highlighted by the red rectangle. The black peak shows the nucleotide G (wild type sequence), the red peak shows the nucleotide T (homozygous sequence).

Blood samples from the resulting bone marrow chimera were analyzed one and two weeks after bone marrow transfer. Unfortunately, there is no available congenic strain at the C3HeB/FeJ background that would help to distinguish donor-derived and endogenous recipient-derived leukocytes. Nevertheless, to be able to evaluate the origin of blood cells in chimeric mice, DNA was extracted from peripheral blood leukocytes one and two weeks after bone marrow transfer. Sanger sequencing of the mutated *Psmb10* locus enables evaluation whether the leukocyte pool from chimeric mice contains mutated sequence (endogenous recipient's origin), wild type sequence (donor-derived cells), or both (mixed chimera).

Flow cytometric analysis of peripheral blood revealed that on day 14 in WT→TUB006 chimera, the B cell population is reconstituted to wild type levels (Figure 27 B).

Furthermore, at low frequencies also NK cells as well as granulocytes were present. However, the T cell compartment did not show reconstitution (Figure 27 B).

In order to exclude the possibility that the observed lymphopoiesis in the chimeric mice is a consequence of the irradiation itself, it was required to verify that leukocytes were derived from the transferred donor cells. Genetic analysis of DNA isolated from blood cells of the WT→TUB006 chimera clearly showed the black peak of the wild type sequence, with a tiny red peak of the mutant sequence (Figure 27 C), indicating that the vast majority of leukocytes originates from wild type donor bone marrow. It is unclear whether the small mutant signal is background or represents a small population of endogenous recipient-derived leukocytes. However, even with potential low numbers of endogenous leukocytes in the blood of chimeric mice, the data clearly demonstrate that reconstitution with wild type bone marrow enables development of lymphocytes. These results demonstrate that cell-exogenous factors required for B- and NK cell development are present and functional in homozygous TUB006 mice. T cells are not reconstituted most likely due to the absence of thymus in the homozygous recipients that is required for T cell development and maturation. In the timeframe of observation (two weeks) after bone marrow transfer there were no signs of granulocytosis.

Due to progression of morbidity in chimeric mice, a further follow-up of the experiment was unfortunately impossible. The mice had to be euthanized two weeks after irradiation. Considering the small body size of homozygous mutants, there is good reason to assume that the irradiation dose was too high.

Second pilot study

In the second experimental setup, the aim was to avoid the high lethality observed in homozygous TUB006 recipients of the first WT→TUB006 bone marrow transplantation experiment. In an attempt to reduce the harmful effect of the irradiation, a lower irradiation dose of two fractions of three Gy was applied (Figure 28 A). At the time of the second pilot study backcross of the TUB006 mouse line onto the BALB/c genetic background was accomplished. The congenic BALB/c strain was used to differentiate between cells from donor and recipient origin using isotyping of the leukocyte surface marker CD45 by flow cytometry.

Flow cytometric analysis of the peripheral blood gained from the generated WT→TUB006 bone marrow chimera showed that almost all detected leukocytes were

CD45.1⁺ indicating their origin from the donor bone marrow (Figure 28). Wild type bone marrow cells successfully engrafted the homozygous host.

Yet, leukocyte counts in the blood were rapidly increased in WT→TUB006 chimera to the levels of untreated homozygous TUB006 mice, substantially exceeding the leukocyte counts of the WT→WT control chimera as well as the untreated controls (Figure 28 C). Remarkably, the vast majority of cells found in the periphery turned out to be granulocytes (Figure 28 D), while the lymphocyte compartment did not show reconstitution (Figure 28 E and F). WT→TUB006 chimera generated in the second experimental setting developed SCID and granulocytosis within few weeks after transplantation. It indicates that the defect is based on extrinsic effects not inherent in the hematopoietic cells, forcing the wild type bone marrow to produce high numbers of granulocytes and repress lymphocyte production.

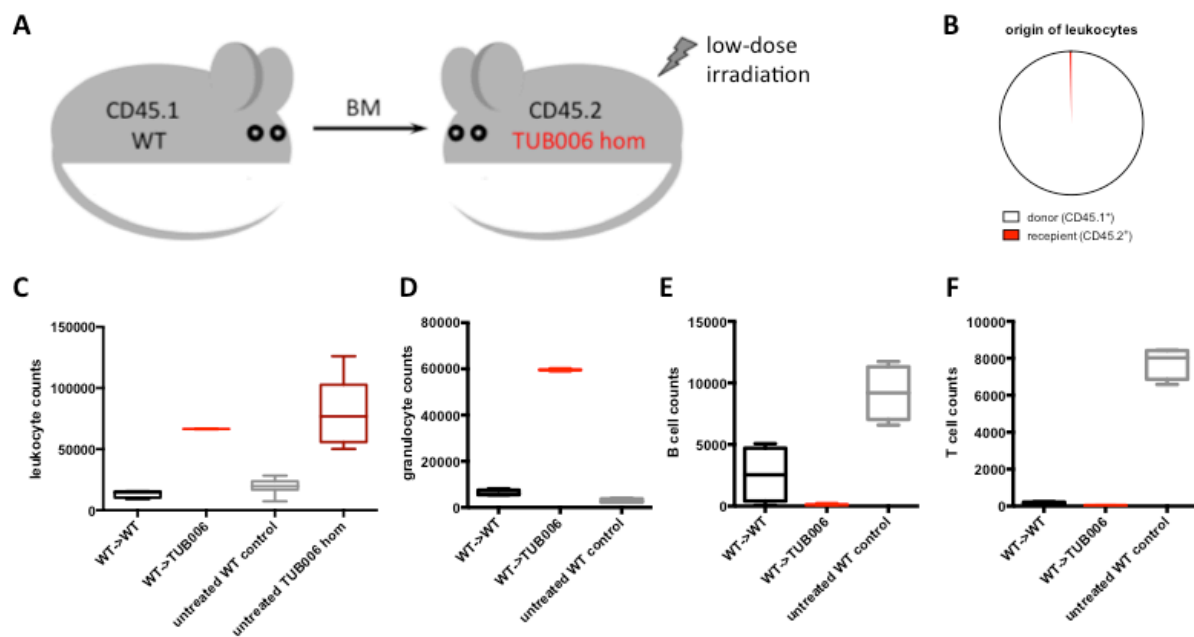


Figure 28: WT→TUB006 bone marrow chimera present granulocytosis. A) Experimental setup. B-F) Flow cytometric evaluation of peripheral blood leukocytes two weeks after bone marrow transfer. B) CD45 isotyping to distinguish donor-derived blood cells from endogenous recipient-derived leukocytes in WT→TUB006 chimera. C-F) leukocyte counts acquired from peripheral blood by flow cytometry: living leukocytes (C), granulocytes (D), B cells (E) and T cells (F).

Taken together, depending on the experimental setup, diametrically opposed results for the hematopoietic recovery were observed, showing that the TUB006 disease is complex and is caused by diverse interweaved factors. Wild type bone marrow can give rise to B and NK cells in TUB006 mice under some conditions, but under other circumstances is forced towards granulopoiesis by non-hematopoietic factors.

5.8 Impact of commensals on TUB006 phenotype

The TUB006 phenotype could be caused by enhanced susceptibility to opportunistic infection(s) leading to an expansion of the granulocyte lineage. It is possible that at least part of the detected phenotype is triggered by the presence of certain microorganisms. A thinkable scenario would be that hyperkeratosis and alopecia sensitize the skin of homozygous TUB006 mutants to skin damage, which allows bacteria to invade the dermis. Subsequently, inflammation provides activation of the complement system, release of cytokines from keratinocytes, expression of adhesion molecules on local blood vessels and extravasation of neutrophils. Not only the skin, also the gut might be a source of opportunistic pathogens, particularly considering the inborn severe T and NK cell deficiency in TUB006 homozygotes. The decline in B cells and simultaneous expansion of the granulocyte compartment might be a consequence of enhanced susceptibility to opportunistic infection(s).

To evaluate the impact of commensals on the pathogenesis, the TUB006 mutant phenotype was analyzed after transfer of the line into a germ-free environment. The results were intriguing: the disease developed identically under germ-free conditions. Germ-free heterozygous as well as homozygous TUB006 mice represented a phenocopy of mutants with a normal microflora (Figure 29), including homozygous lethality.

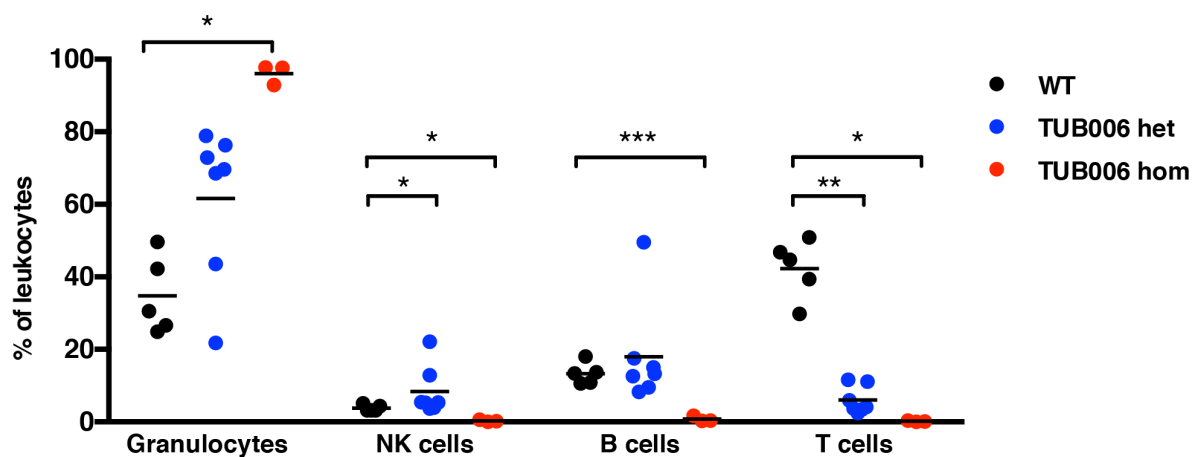


Figure 29: Persistence of the TUB006 phenotype under germ-free breeding conditions. Flow cytometric analysis of peripheral blood from wild type (WT), heterozygous (het) and homozygous (hom) TUB006 animals bred in a germ-free mouse facility.

This finding clearly demonstrates independence from microbiotic influence on the pathogenesis in TUB006, leading to the assumption that the inflammation in TUB006 can be triggered exclusively by sterile stimuli.

5.9 Validation of the mutation

Although our studies and the published information strongly suggest that the MECL-1^{G170W} mutation is causal for the observed TUB006 phenotype, involvement of further mutations cannot be fully excluded. In order to validate the mutation, tail DNA samples from more than 500 inbred mice were analyzed with a phenotype-genotype correlation of 100%.

The TUB006 mutant mouse line was initially bred on the genetic background of the C3HeB/FeJ inbred strain. To evaluate the influence of the genetic background on the TUB006 phenotype, and to further validate the link between the identified MECL-1 mutation and the TUB006 phenotype, two congenic strains of the TUB006 mouse line were generated. The causative mutation was thereby transferred to the inbred strains C57BL/6 und BALB/c.

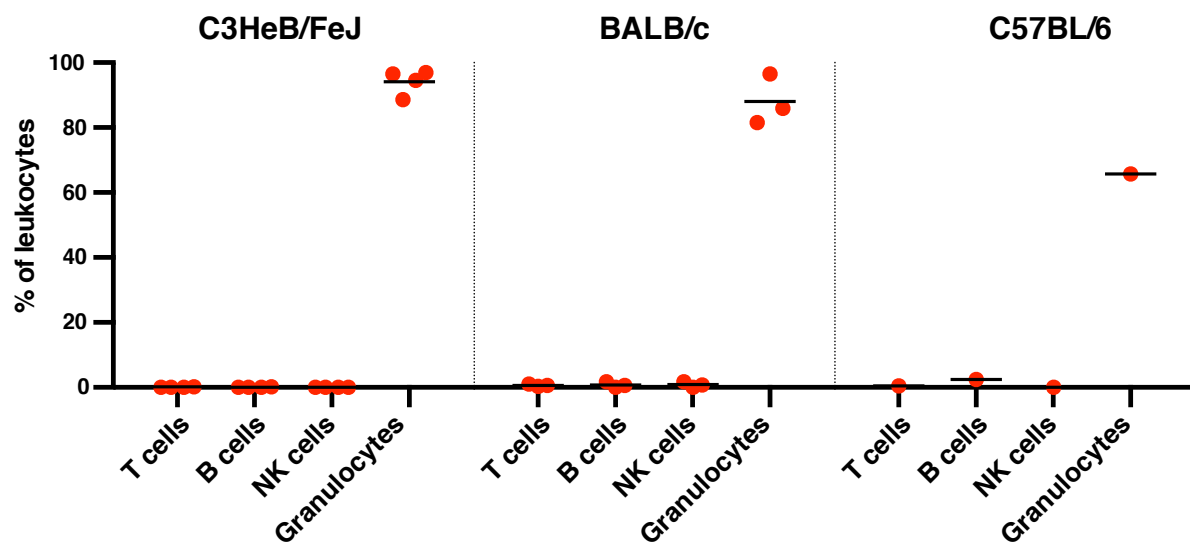


Figure 30: Phenotype of homozygous TUB006 mutants on different genetic backgrounds. Flow cytometric evaluation of peripheral blood leukocytes from homozygous TUB006 mutants bred on the indicated genetic backgrounds. All analyzed homozygotes presented SCID and granulocytosis.

Heterozygous TUB006 animals were crossed to wild type C57BL/6 or BALB/c mice, and the phenotype of the resulting offspring was analyzed. Mice showing the phenotype of reduced T cell frequencies were again crossed to C57BL/6 or BALB/c mice. The backcross generation N7 (C57BL/6) or N11 (BALB/c) was intercrossed to produce homozygous offspring. Analysis of homozygous offspring revealed strong phenotype persistence with symptoms identical to that of C3HeB/FeJ mice (Figure 30; the phenotype is described in detail in sections 5.2, 5.5 and 5.6), underscoring the causal relationship of the MECL-1^{G170W} mutation and the severe TUB006 phenotype.

Notably, TUB006 mutants bred on the BALB/c background have a prolonged life span when compared to C3HeB/FeJ or C57BL/6. The disease develops later and thymic tissue is detectable until the age of three weeks.

However, even after backcross for more than ten generations, there is still a significant probability of approx. 7% that a second closely linked mutation is contributing to the phenotype (Keays, Clark et al. 2006). To further validate the causative mutation and to analyze the gene dosage effect, TUB006 mice were crossed to MECL-1 knockout (MECL-1 KO) mice. The resulting offspring should be heterozygous for the knockout allele, 50% carrying one wild type allele (MECL-1^{+/-}) and 50% showing the hemizygous (MECL-1^{-/G170W}) genotype. Analysis of the hemizygous mice showed the key features of the homozygous (MECL-1^{G170W/G170W}) TUB006 phenotype, i.e. lack of T cells and NK cells (Figure 31). B cell- and granulocyte frequencies showed a high variance among hemizygous individuals, but nevertheless hemizygotes showed substantial lethality.

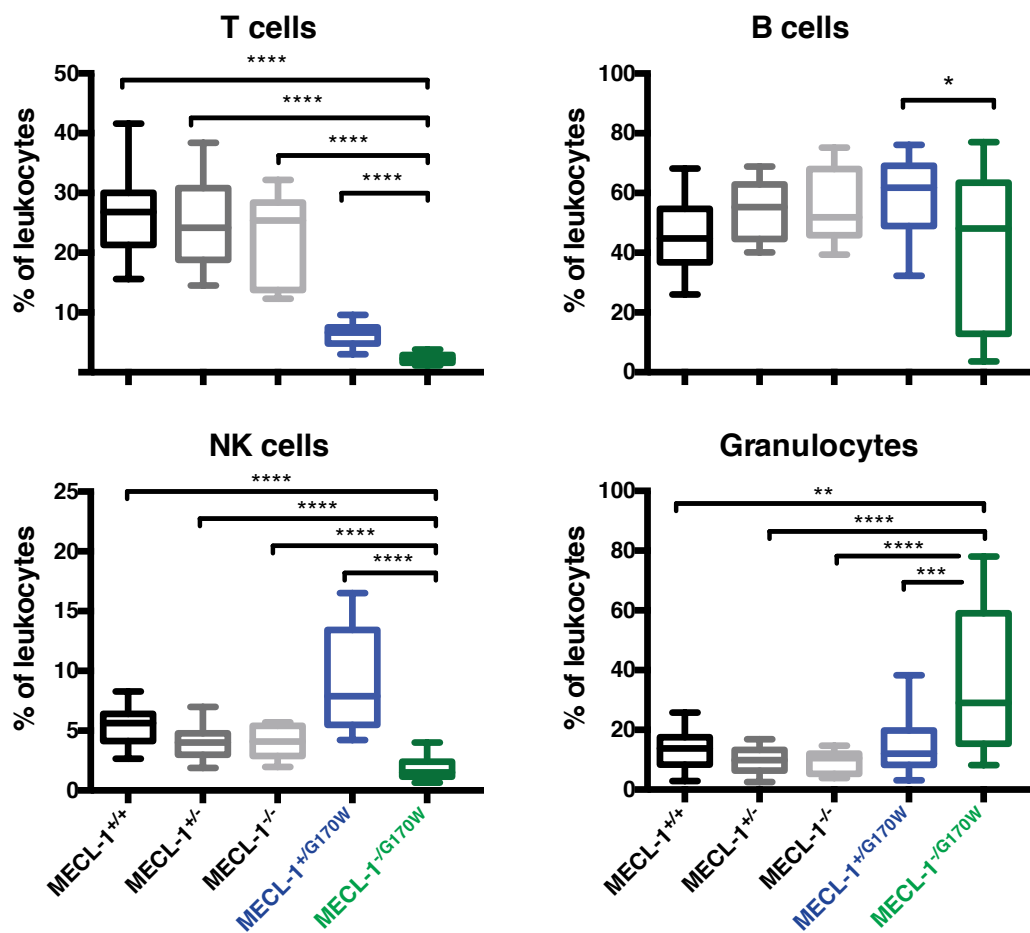


Figure 31: Validation of the mutation by phenotyping of the TUB006 × MECL-1 KO offspring. Comparison of the hemizygous (MECL-1^{-/G170W}) mice with wild type (MECL-1^{+/+}), heterozygous and homozygous MECL-1 knockout (MECL-1^{+/-} and MECL-1^{-/-}), and heterozygous TUB006 (MECL-1^{+/-}/G170W) mice. Flow cytometric evaluation of leukocyte frequencies in peripheral blood is shown.

Even though the phenotype of hemizygous mutants strongly underscores the causal relationship of the MECL-1^{G170W} mutation and the severe TUB006 phenotype, a formal proof requires either correcting the mutation by reinserting the wild type sequence or a de novo generation of the mutant. The recent development of the CRISPR-Cas9 technology has enabled new possibilities for gene editing in the oocyte. This system utilizes the adaptive bacterial defense tool, clustered regularly interspaced short palindromic repeats (CRISP) and CRISPR-associated protein 9 (Cas9) endonuclease that cleaves DNA at specific target positions. The specificity of the target is determined by guide-RNA, which can be designed to match the complementary genomic sequence of interest.

The gRNA of the “classical” CRISPR-Cas9 recognizes 20 bp of genomic sequence and allows Cas9 to induce double-strand DNA breaks. Due to a single recognition site and the ability of the guide-RNA to tolerate up to five mismatches, it is prone to bind to off-target sites. The novel CRISPR-Cas9 nickase strategy, however, minimizes off-target mutations by using paired nickases (Mali, Aach et al. 2013, Shen, Zhang et al. 2014). In this approach, two nickases are guided in a tail-to-tail orientation by two separate guide-RNAs (20 bp each) to adjacent target regions and induce two neighboring single-strand nicks on the opposite DNA strands, thus increasing specificity through doubling of target site length. After cleaving with either Cas9 or Cas9 nickase, the cleaved site is repaired by cellular repair mechanisms: non-homologous end joining (NHEJ) or homology-directed repair (HDR) in the presence of a recombination donor. Recently, this technique has been shown to be suitable for introduction of point mutations (Inui, Miyado et al. 2014).

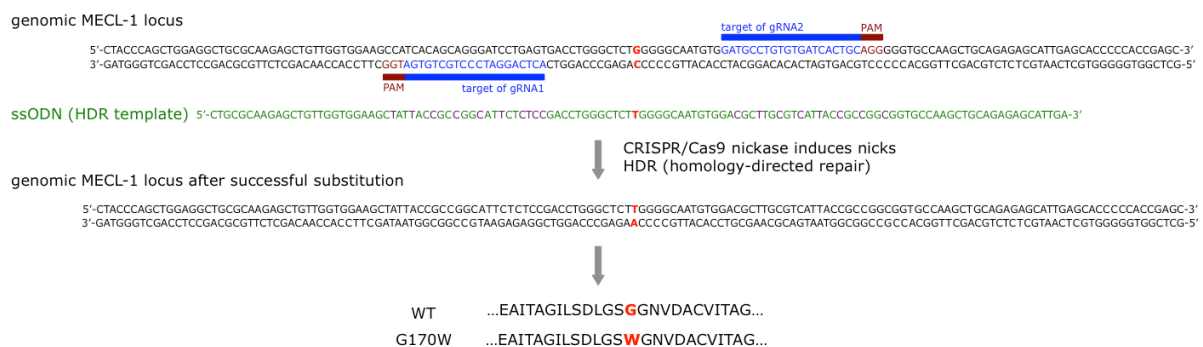


Figure 32: Mutational strategy of introduction of the G>T substitution in *Psmb10* using CRISPR/Cas9 technology. Schematic illustration shows the genomic mouse *Psmb10* locus encoding MECL-1, and locations of the guide-RNAs (gRNAs) and single-strand oligodeoxynucleotide (ssODN). Site of the mutation is indicated in red, the silent nucleotide exchanges in ssODN are indicated in purple.

The CRISPR-Cas9 nickase technology was used to specifically target the genomic MECL-1 locus in wild type C57BL/6 oocytes and recreate the TUB006 point mutation (Figure 32). Paired guide-RNAs for the TUB006 mutation locus were designed using a computational online-tool (<http://crispr.mit.edu/>). The Cas9 nickase as well as two gRNAs, each specific for one 20bp target sequence, were injected into the pronucleus of C57BL/6 oocytes. Additionally, a single-strand oligodeoxynucleotide (ssODN) was co-injected, containing the TUB006 mutation for HDR of the cleaved locus. This ssODN of 120 bp was modified by silent nucleotide exchanges to avoid recurrent cleavage. For design of the modifications, the codon usage bias was taken into account (Wada, Wada et al. 1992).

Unfortunately, at the time of finishing this PhD project, the generated offspring was not yet old enough for phenotypic analysis and genotyping.

5.10 Working hypothesis: MECL-1^{G170W} mutation causes proteasome assembly defect

In the case of coexistence of immuno-subunits and constitutive subunits, immuno-subunits are incorporated preferentially into nascent proteasomes (De, Jayarapu et al. 2003, Heink, Ludwig et al. 2005, Bai, Zhao et al. 2014). In gene-targeted MECL-1^{-/-} mice, MECL-1 is absent but can be compensated by its constitutive counterpart β 2c, leading to formation of functional proteasomes. In contrast to the knockout context, in TUB006 the mutated version MECL-1^{G170W} is expressed and presumably incorporated into proteasome precursors during the assembly process. Gly170 is located in a structurally highly conserved region of subunit β 2 at the interface of the two proteasome β -rings in both the murine proteasomes and yeast proteasome (Groll, Ditzel et al. 1997, Huber, Basler et al. 2012). Hence, its mutation to Trp was assumed to sterically hinder dimerization of two hemiproteasomes and to interfere with proteasome assembly. Protein structure modeling confirmed that the bulky MECL-1^{G170W} tryptophan side chain sterically clashed with amino acids of the β 6 subunit from the opposite proteasome ring (Figure 33). Consequently, the mutation G170W may preclude dimerization of hemiproteasomes and formation of enzymatically active proteasomes.

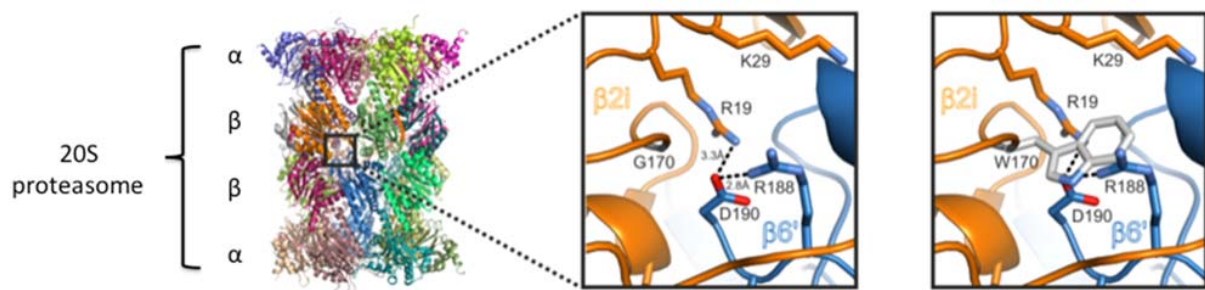


Figure 33: Basic structure of the 20S proteasome and structural modeling of the wild type and TUB006 immunoproteasome. The framed pictures show the interaction between MECL-1 (β 2i; orange) and β 6 (blue) subunit from the opposite β -ring. Left: wild type, right: TUB006.

In our working hypothesis based on protein modeling, the mutated MECL-1 retards the proteasome assembly. Since proteasomes are essential for all eukaryotic cells, we hypothesized that cells expressing MECL-1^{G170W} above a certain level might be defective in proteasome assembly and consequently nonviable.

5.11 Lethal effect of MECL-1^{G170W}-overexpression

According to the working hypothesis, overexpression of the mutated MECL-1 is expected to be lethal. In order to test this experimentally, a suitable retroviral vector was designed for transduction and expression of mutated MECL-1^{G170W} in primary splenocytes. To analyze the impact of MECL-1^{G170W}-overexpression in comparison to the wild type protein, coding sequences of wild type MECL-1 and MECL-1^{G170W} were cloned into the retroviral mP71 vector. For visualization and quantification of successfully transduced cells expressing the MECL-1 transgene, reporter constructs with fluorescent labeling of MECL-1 using GFP (green fluorescent protein) were generated. To ensure co-expression of MECL-1 and GFP, a cloning strategy was applied that produces a fusion gene under control of one promoter. The resulting bicistronic mRNA is translated to a protein that contains sequences of both, the protein of interest (MECL-1) and the reporter part (GFP). To assess whether the fusion of the reporter protein to MECL-1 affects the results, constructs containing two different linkers between MECL-1 and GFP were generated. In the first setting the P2A self-cleavage motif cleaves the protein chain, resulting in two separate proteins (Gao, Jack et al. 2012). In the second setting the self-cleavage ability of P2A was abrogated by a mutation, leading to expression of one single fused MECL-1 GFP protein. The design of the constructs is detailed in Figure 34 A.

The generated constructs were used to produce viral particles for transduction of primary wild type splenocytes. Due to the fact that retroviruses infect only proliferating cells, splenocytes were stimulated with agonistic anti-CD3 and anti-CD28 antibodies to induce T cell proliferation 24 hours prior to transduction. Following retroviral transduction, two parallel culture conditions for splenocytes were applied: either prolonged stimulation with anti-CD3 and anti-CD28 antibodies, or incubation with IL-2 and IL-15.

One day after transduction, initial transduction efficacies were assessed by flow cytometric evaluation of GFP producing cells. GFP expression was analyzed over time (24, 36, and 48 hours after transduction) as a surrogate marker for MECL-1^{WT} or MECL-1^{G170W} expressing cells. In addition, Annexin V staining was performed for identification of apoptotic cells 36 hours after transduction.

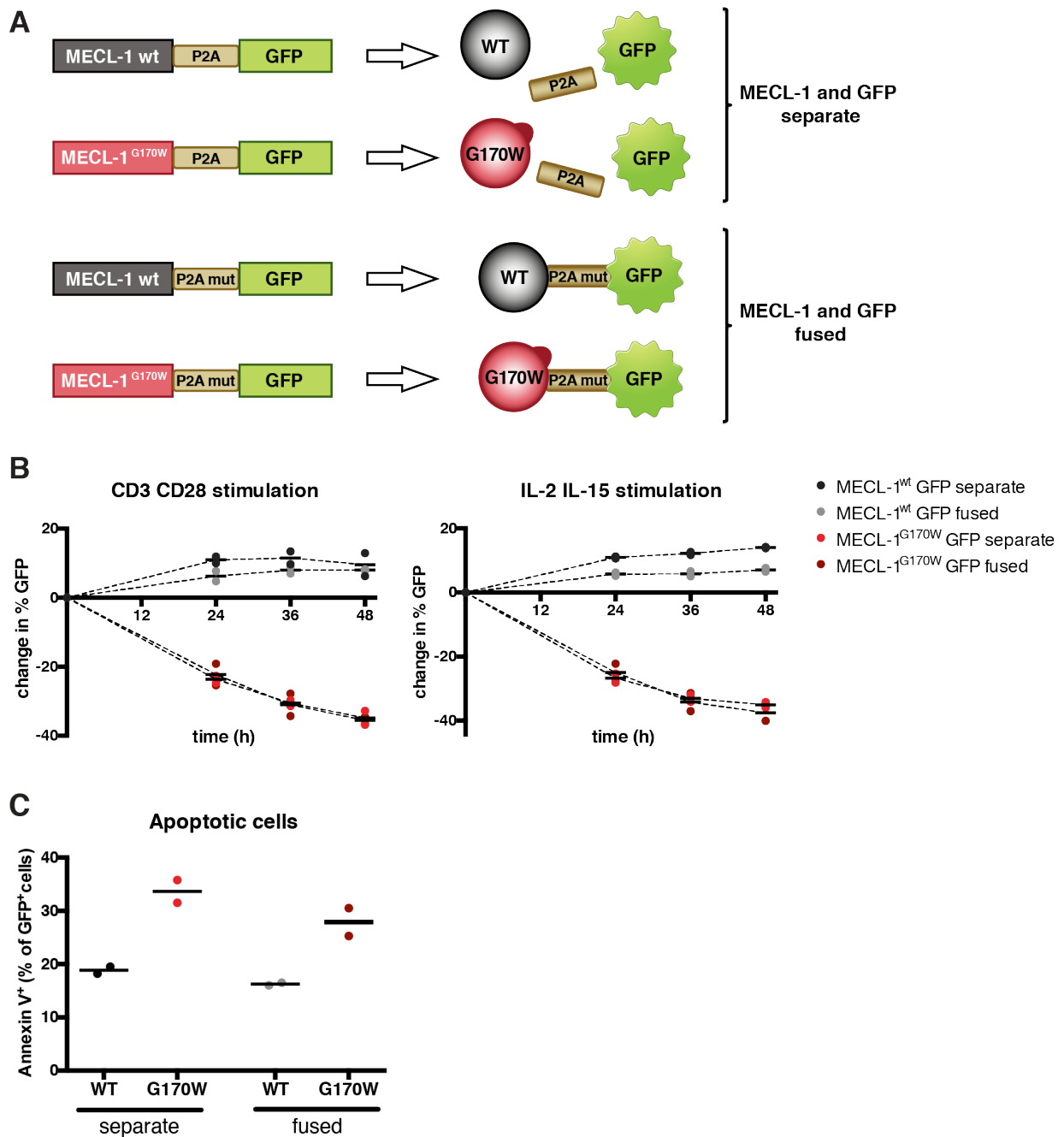


Figure 34: Overexpression of mutated MECL-1 causes cell death in murine splenocytes. A) Schematic illustration of the constructs used for transduction. B) Kinetics of the GFP signal detected in the splenocyte population after transduction. Plots show changes in GFP signal relative to transduction efficacy. After transduction, T cells were stimulated with anti-CD3 and anti-CD28 antibodies (left panel) or IL-2 and IL-15 (right panel). C) Apoptotic cells identified by Annexin V staining 36 hours after transduction are plotted as percentages of transduced (GFP⁺) cells. Data from one representative overexpression experiment are shown, in total the experiment was performed twice with similar results. In each experiment splenocytes were transduced with two different virus supernatants. Each point in the dot plots shows data from one separately transduced splenocyte sample.

The frequency of GFP⁺ cells decreased over time in cells transduced with MECL-1^{G170W} in both the fused and the separate MECL-1 GFP versions (Figure 34 B). This finding supports our hypothesis that MECL-1^{G170W} expression has lethal effects on cells. Since both fusion and co-expression constructs yielded very similar results, a difference in the stability of MECL-1 and MECL-1^{G170W} is unlikely to be responsible for the observed effects. Furthermore, there is no evidence for stimulus-dependent effects. Both, the TCR-

engaging CD3/CD28 and TCR-bypassing IL-2/IL15 stimulations lead to a similar decrease of MECL-1^{G170W}-expressing cells (Figure 34 B). Annexin V staining 36 hours post transduction revealed higher frequencies of apoptotic cells, showing an increase of programmed cell death in MECL-1^{G170W} expressing cells (Figure 34 C).

Taken together, these results clearly demonstrate lethal effects of MECL-1^{G170W} overexpression on murine splenocytes. Furthermore, MECL-1^{G170W} transduced T cells undergo rapid apoptosis independently of persistent TCR engagement.

5.12 Yeast mutagenesis and structural data

In spite of the phylogenetic distance between yeast and mammals, the principle cellular structures such as proteasomes are extremely conserved. This evolutionary conservation legitimates to introduce the TUB006 mutation into the yeast proteasome and analyze the impact of the amino acid exchange at molecular level. To prove the working hypothesis, we conducted yeast mutagenesis experiments. Noteworthy, yeast expresses only one proteasome type and any interruption of its assembly is lethal. Subunits of the yeast proteasome will be henceforth designated as γ - (yeast) subunits, e.g. $\gamma\beta 2$ for the $\beta 2$ subunit of the yeast proteasome.

For introduction of the TUB006 mutation into yeast cells, plasmid shuffling technique was applied (Figure 35). As basis for plasmid shuffling, yeast lacking the chromosomal $\gamma\beta 2$ -subunit was used, complemented with a removable URA3-marked plasmid pRS316 encoding wild type $\gamma\beta 2$ -subunit (Heinemeyer, Fischer et al. 1997). The TUB006 point mutation G170W was introduced into another plasmid encoding the $\gamma\beta 2$ subunit - the *LEU2*-plasmid pRS315. The basic yeast strain was then transformed with the constructed mutant plasmid pRS315-*PUP1*^{G170W}. Subsequently, transformants were selected on 5'FOA plates for removal of the URA3-marked plasmid encoding wild type $\gamma\beta 2$. As a result, the plasmid encoding wild type $\gamma\beta 2$ is removed and only the yeasts successfully transformed with the plasmid encoding mutant $\gamma\beta 2^{\text{G170W}}$ can survive. This plasmid shuffling experiment demonstrated that the $\gamma\beta 2^{\text{G170W}}$ mutant was not viable.

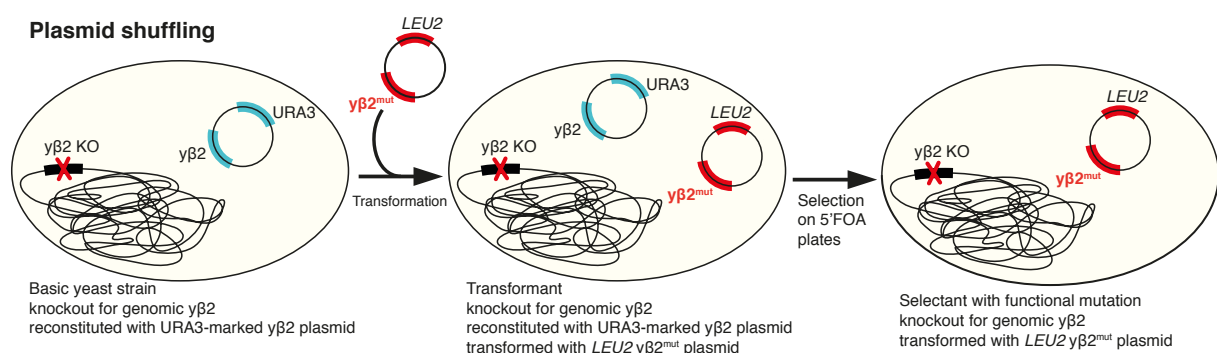


Figure 35: Schematic illustration of the plasmid shuffling technique in yeast. The basic $\gamma\beta 2$ -deficient yeast strain is rescued by wild type $\gamma\beta 2$ on the URA3-marked plasmid. Transformation with the *LEU2*-Plasmid encoding $\gamma\beta 2^{\text{G170A}}$ or $\gamma\beta 2^{\text{G170W}}$ ($\gamma\beta 2^{\text{mut}}$) and subsequent selective pressure against URA3 using 5'fluoro-orotic acid (5'FOA) results in survival of yeast cells containing only the $\gamma\beta 2^{\text{mut}}$ -encoding plasmid.

In parallel, the attenuated mutation G170A was introduced into the same position of construct pRS315. In contrast to the bulky tryptophan, alanine has a small amino acid residue and therefore would have less steric effects. Plasmid shuffling with the plasmid

encoding the $\gamma\beta 2^{G170A}$ mutation was also lethal to yeast. By happy chance, fusing a Protein A tag (ProA) to the C-terminus of the mutant $\gamma\beta 2^{G170A}$ subunit rescued the viability of the resulting $\gamma\beta 2^{G170A}$ -ProA mutant. Although $\gamma\beta 2^{G170A}$ -ProA yeasts showed a pronounced growth defect, its viability indicated successful incorporation of the mutant $\gamma\beta 2^{G170A}$ -ProA subunit into the yeast proteasome, at levels sufficient for some cells to survive. In contrast to the $\gamma\beta 2^{G170A}$ mutant, a C-terminal Protein A tag could not rescue $\gamma\beta 2^{G170W}$ yeasts, hinting towards additional negative effects of the bulky tryptophan residue on the proteasome biogenesis. Because expression of a proteolytically inactive $\gamma\beta 2$ does not affect the viability in yeast (Heinemeyer, Fischer et al. 1997, Groll, Heinemeyer et al. 1999), a general proteasome assembly defect was supposed to cause the lethality of $\gamma\beta 2^{G170A}$, $\gamma\beta 2^{G170W}$, and $\gamma\beta 2^{G170W}$ -ProA.

Next, proteasomes of the viable $\gamma\beta 2^{G170A}$ -ProA mutant yeast were purified by affinity chromatography and crystallized after removal of the Protein A tag. Structural data demonstrate the incorporation of the point mutation G170A and correct $\gamma\beta 2$ maturation by autolysis of the $\gamma\beta 2$ -propeptide. Using an isolation procedure based on activity assays to identify proteasome-containing fractions, only active proteasomes were purified. Therefore, assembly intermediates were not analyzed.

Overall, the structures of wild type and mutant $\gamma\beta 2$ -subunits were almost identical and therefore showed a good superimposition. The root-mean-square deviation (RMSD, the measure of the divergence of two aligned structures) between wild type and mutant structures was 0.3 Å, with the exception of the loop structure at the proximal part of the long C-terminal tail. The loop area (positions 192-197) was strongly distorted and less well defined in $\gamma\beta 2^{G170A}$ compared to the wild type $\gamma\beta 2$ -subunit (Figure 36 A). Detailed analysis of the site of mutation (Figure 36 B) revealed that exchange of glycine by alanine on position 170 would lead to steric conflicts between Ala170 and Arg19 from the same subunit $\gamma\beta 2$ (3.0 Å), and between Ala170 and the C-terminal amino acid Asp190 from subunit $\gamma\beta 6$ of the opposite β -ring (2.6 Å). To avoid steric clashes, the guanidine group of Arg19 and the carboxylate of Asp190 are shifted by up to 1.6 Å. These changes break the hydrogen bridges between the amino group of Arg19 and the carboxyl group of Asp190 (wild type: 3.1 Å; mutant: 5.1 Å) as well as the amino group of Arg19 and the C-terminus of subunit $\gamma\beta 6$ (wild type: 3.1 Å; mutant: 4.5 Å).

Furthermore, the mutation caused minor backbone distortions, which shortened the distance between the oxygen atom of Ser171 and carbon atom of Pro192 from 3.5 Å to

2.9 Å. This close contact flips Pro192 out of the hydrophobic pocket provided by Ile163, Trp164, Val173 and Leu190 of $\gamma\beta 2$ (Figure 36 B). The reorientation of Pro192 leads to a twist of the distal sequence Asn193-Glu196 outwards on the protein surface (Figure 36 B). The intra- and intersubunit contacts are destabilized by breaking of the hydrogen bridges between Asn193 and Ser171 (wild type: 3.0 Å; mutant: 9.6 Å) as well as Arg195 and Glu139 of $\gamma\beta 3$ (wild type: 2.7 Å; mutant: 11.7 Å).

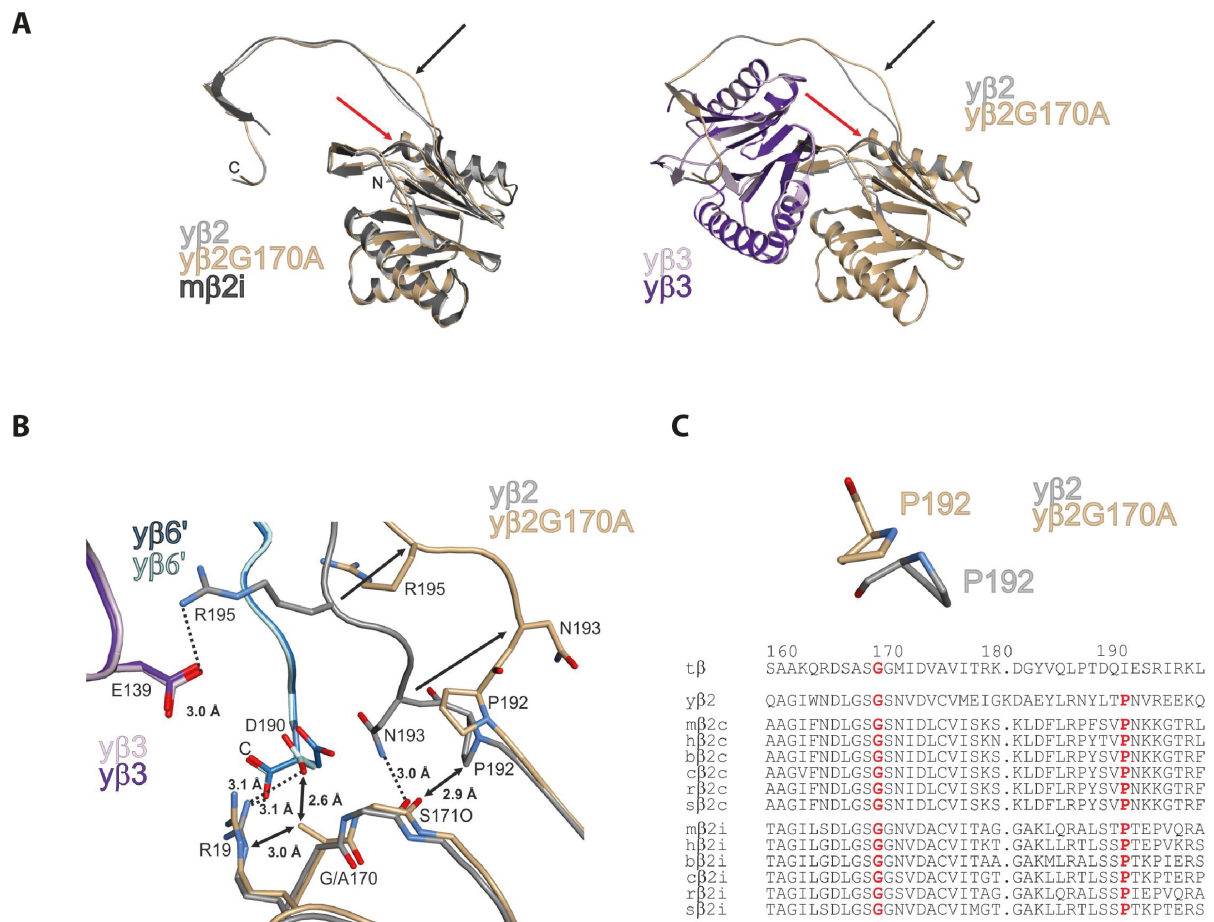


Figure 36: Crystal structure of the yeast $\beta 2^{G170A}$ intersubunit contacts. A) Illustration of the mutant yeast proteasome subunit $\gamma\beta 2^{G170A}$ (brown) superimposed onto the yeast wild type $\gamma\beta 2$ subunit (gray) and the mouse immunoproteasome subunit MECL-1 (black) is shown on the left panel. Association of the subunits $\gamma\beta 2$ and $\gamma\beta 3$ (purple) is shown on the right panel. Red arrows indicate the site of the G170A mutation and the black arrows mark the resulting conformational changes in the $\gamma\beta 2$ C-terminal tail. B) Site of mutation in subunit $\gamma\beta 2$ and the surrounding hydrogen-bonding network. Glycine exchange on position 170 leads to reorientation of residues 192-196 (black arrows). This results in breaking of hydrogen bonds (dotted lines) within $\gamma\beta 2$ and with/between the adjacent subunits $\gamma\beta 3$ of the same β -ring and $\gamma\beta 6$ of the opposite half proteasome, depicted in black. Black double arrows indicate steric clashes. C) Multi-species alignment of positions 160-200 of the $\beta 2$ unit. The strictly conserved proline on position 192 arranges the $\beta 2$ C-terminus for association with the neighboring $\beta 3$ subunit. In the mutant proteasome, turning of Pro192 changes the conformation of the $\beta 2$ C-terminus. Species abbreviations in sequence alignment: t: *Thermophilus acidophilum*; y: *Saccharomyces cerevisiae*; m: *Mus musculus*; h: *Homo sapiens*; b: *Bos taurus*; c: *Canis familiaris*; r: *Rattus norvegicus*; s: *Sus scrofa*; amino acid numbers are assigned according to the β -subunit of *T. acidophilum*.

The observed structural changes affect the orientation of the C-terminal tail of subunit $\gamma\beta 2^{G170A}$, which is essential for eukaryotic hemiproteasome assembly. Even though wild type and mutant $\gamma\beta 2$ -subunits structurally superimpose well, the strongly distorted loop structure Pro192-Glu197 has fatal effects on proteasome biogenesis. Structural data

suggest that the C-terminal appendage of $y\beta 2^{G170A}$ fails to properly associate with subunit $y\beta 3$ of the same β -ring. The extension of the C-terminal tail by the Protein A tag provides additional interaction surface and facilitates subunit interactions and hemiproteasome formation. Thus, the Protein A tag compensates for the deleterious conformational change in the $y\beta 2^{G170A}$ -appendage and enables survival of the mutant $y\beta 2^{G170A}$ yeasts.

The lethality of the mutant $y\beta 2^{G170W}$ cannot be rescued by extending of the C-terminal tail by Protein A tag, indicating that the bulky tryptophan residue leads to more severe steric impact.

6 Discussion

Primary immunodeficiencies (PID) comprise numerous diseases, key features of which are absence or malfunction of one or more components of the immune system (Al-Herz, Bousfiha et al. 2014). The genetic basis of these disorders is diverse, and a variety of underlying mutations have been identified in the past decades (Notarangelo 2010, Parvaneh, Casanova et al. 2013, Al-Herz, Bousfiha et al. 2014). However, there still are numerous patients suffering from PID with undefined etiology. Identification of the causative genetic alterations is pivotal for early diagnosis and development of therapeutic strategies. Furthermore, identification of novel genes that are involved in the pathogenesis as well as annotation of known genes to PID allows us to deepen our understanding of the immune system and its pathophysiology.

To study human genes and diseases, model organisms like yeast, fish, flies and foremost mice have been extensively used by researchers in academia and industry. The special role of mouse models has several reasons. First, humans and mice share a lot of molecular pathways, 99% of human genes are conserved in the mouse. Second, the mouse is a well-studied model and numerous techniques for modifying the mouse genome are well established. Third, the relatively fast breeding and small body size allow high-throughput and large-scale studies. Fourth, mouse models can be used for drug screening and evaluation of new therapies (Zambrowicz and Sands 2003).

However, increasing concerns arise about whether we need animal research in general and mouse models in particular. However, for highly complex networks such as the immune system, which crucially involves the cooperation of the bone marrow, thymus, the lymphatic and vascular systems, as well as peripheral organs and even microbiota, so far there is no conceivable experimental model that can mimic *in vivo* studies. For investigations of basic mechanisms of human PID, mouse research has been indispensable (Shultz and Sidman 1987, Joliat and Shultz 2001, Nelms and Goodnow 2001, Beutler, Jiang et al. 2006, Hoyne and Goodnow 2006, Rutschmann and Hoebe 2008). However, mouse models also bear limitations. In spite of a large number of similarities, there are several differences in the immune system of humans and mice (Mestas and Hughes 2004). For example, species-specific effects on neutrophils were reported, in particular regarding their numbers in blood and a diverging anti-microbial repertoire (Geering, Stoeckle et al. 2013). Lab mice also lack genetic variability, since

most experiments are made with inbred mouse strains that are virtually identical in their genomes. Furthermore, in contrast to humans, lab mice are housed in SPF environment, making mouse experiments easier to reproduce and control, but also less realistic as model system for humans. In addition, there are examples of drugs that were ineffective in humans although they worked well in animals. Even though lab mice are not always reliable as preclinical models, they have proven as an excellent model for humans in a huge number of scientific experiments. Mouse husbandry conditions can also shift the immune status of lab mice closer towards that of adult humans. Indeed, recent work proved this implication by housing SPF lab mice together with free-living mice and thereby exposing lab animals to common pathogens (Beura, Hamilton et al. 2016). Mouse research has also enabled great progress for therapies of a number of serious diseases, e.g. successful treatment of acute promyelocytic leukaemia that was previously mostly untreatable (Pandolfi, Stanley et al. 2015). Mice can also provide functional information on unknown genes that were found to be associated with human diseases by GWAS studies. Taken together, in spite of some limitations, mouse as a model organism has been proven invaluable for understanding the genetics and pathogenesis of PID.

Mice were also used in the large-scale mouse ENU mutagenesis approach (Hrabě de Angelis, Flaswinkel et al. 2000) that enabled this study. One of the mouse mutant lines identified within this screening approach has moved into the focus of this research project. The detailed characterization of the unique immunological phenotype was the first objective of this study. The main challenges, however, were the identification of the underlying mutation and gaining insights into the pathomechanism leading to the observed immunodeficiency.

6.1 Diverse aspects of T-lymphopenia and SCID in TUB006 mice

Abnormal leukocyte numbers in the periphery are associated with leukemia/lymphoma, immunodeficiency, and autoimmunity. Despite the importance of processes that regulate circulating leukocytes, details on the genetics and pathways involved remain to be elucidated.

Heterozygous mutants macroscopically develop normally, and except of T cell reduction show normal leukocyte numbers. In the *Listeria monocytogenes* infection model, there was no evidence for defects in the innate immune response, since during the first three

days infected mice showed good health conditions and comparable pathogen levels in spleen and liver on day three. The inflammatory response to *L.m.* involving neutrophil granulocytes, NK cells, and macrophages, which is crucial for early survival (Pamer 2004), was competent to control the infection in heterozygous mutants. However, beginning with day five a rapid progression of the disease was observed, leading to fatal susceptibility to the intracellular pathogen by day seven after infection. For complete bacterial clearance, *Listeria*-specific IFN- γ -producing CD8⁺ effector T cells are indispensable (Bancroft, Schreiber et al. 1987, Dalton, Pitts-Meek et al. 1993, Huang, Hendriks et al. 1993). The T cell response was impaired in heterozygous TUB006 mutants, antigen-specific CD8⁺ T cells were not detectable on day seven p.i., and peptide stimulation failed to induce IFN- γ production. These results demonstrate that the TUB006 phenotype in heterozygous mutants is numerically and functionally restricted to T cells.

This impaired T cell response in heterozygous TUB006 mutants was interesting, because the absence of immunoproteasome does not impair the responses against other epitopes that are made by constitutive proteasomes and mice lacking either LMP2, LMP7 or MECL-1 or both LMP7 and MECL-1, despite partially impaired CD8⁺ response, are capable of resolving infections with intracellular pathogens (Nussbaum, Rodriguez-Carreno et al. 2005, Sijts and Kloetzel 2011). Although differences in the generation of selected MHC I epitopes have been documented, the mice could readily cope with a whole array of viruses and bacteria including *Lymphocytic choriomeningitis virus* (LCMV), *Vaccinia virus* (VV) and *Listeria* with similar efficiency as wild types. To address the possibility that the failure of controlling the infection in TUB006 is due to the altered T cell repertoire, further research is required: it will be necessary to analyze the T cell repertoire in mutant mice, as well as the T cell response to recombinant *L.m.* strain expressing model antigens like ovalbumin (*L.m.*-ova) after completion of the TUB006-backcross onto the C57BL/6 background.

Upon TCR-independent stimulation with PMA and ionomycin, T cells from infected heterozygous TUB006 mutants were able to produce IFN- γ . Although the frequency of IFN- γ producing CD8⁺ cells was significantly lower compared to wild type splenocytes, the general capability of producing IFN- γ rules out a complete T cell deficiency. The T cell response and cytokine production was analyzed in mice that survived until day 7 p.i., thus a lethal effect of high-level IFN- γ production in mutants and subsequent

survival of cytokine low-producers would lead to biased observations. However, diminished INF- γ production after PMA and ionomycin treatment was also observed previously by Rockwell et al. in LMP7 MECL-1 double-knockout splenocytes. Although the exact mechanism and function of this regulation is yet unresolved, the immunoproteasome plays a role in mRNA expression of some cytokines, particularly INF- γ (Rockwell, Monaco et al. 2012). TUB006 might be an appropriate model to study the functional and mechanistic questions of the cytokine regulation by the immunoproteasome in T cells.

The TUB006 T cell defect is most likely composed of multiple closely linked layers. First, there is evidence that the immunoproteasome is constitutively expressed in T cells and seems to have a pivotal but not yet understood T cell-intrinsic function (Zaiss, de Graaf et al. 2008, Moebius, van den Broek et al. 2010). Second, T cell maturation in the thymus is probably affected by the mutated thymoproteasome in TUB006 mice, leading to an altered T cell receptor repertoire. Third, the proteasome/immunoproteasome machinery supplies peptides for antigen presentation in the context of MHC I, and is therefore essential for CD8⁺ T cell survival and activation in an extrinsic manner. Further studies of the TUB006 mouse model might help to unpuzzle in some part this complex interplay and elucidate the thymoproteasome impact on T cell maturation, as well as intrinsic and extrinsic roles of the immunoproteasome in T cell survival and function.

Even though it is known that MECL-1 is constitutively expressed in T cells (*Immunological Genome Project*, <http://www.immgen.org>), the functional and mechanistic task of MECL-1 in T cells still remains to be elucidated. MECL-1 is part of both the immunoproteasome and the thymoproteasome. An increased CD4⁺ to CD8⁺ T cell ratio was observed in heterozygous TUB006 mutants, and even more pronounced in homozygotes. Similarly, the increased CD4/CD8 T cell ratio was observed in MECL-1^{-/-} mice (Basler, Moebius et al. 2006), and in mice deficient for the thymoproteasome-specific subunit $\beta 5t$ (Murata, Sasaki et al. 2007). The thymoproteasome is responsible for peptide production for positive selection during T cell maturation (Xing, Jameson et al. 2013), hence the CD4/CD8 ratio of MECL1^{-/-} mice may be influenced by the altered positive selection in the thymus. On the other hand, the increased CD4/CD8 ratio remains after transplantation of MECL1^{-/-} bone marrow into wild type recipients, where MECL-1 deficient T cell progenitors undergo normal maturation and differentiation in

the wild type thymic environment (Zaiss, de Graaf et al. 2008). Thus, the underlying regulatory mechanism of changes in the CD4⁺ to CD8⁺ T cell ratio is (at least in part) thymus-independent and seems to be intrinsic to peripheral T cells. The phenomenon of MECL-1 as T cell intrinsic factor was also demonstrated by Moebius et al., who reported a loss of adoptively transferred MECL-1^{-/-} T cells into infected hosts. This loss was not due to graft rejection, but rather to a T cell intrinsic functional requirement for MECL-1 (Moebius, van den Broek et al. 2010). Taken together, it seems that the requirement for immunoproteasomes for the expansion and survival of T cells is critical under certain circumstances.

The special requirement of MECL-1 in T cells is supported by the selective gene dosage effect on T lymphocytes TUB006 mice: the significant reduction of T cells in heterozygous mice and a virtual T cell loss in homozygous mice. T cells might be the most susceptible cell type, because in this cell population the most alterations are combined: like the intrinsic cell defect combined with the developmental alteration in the thymus. The thymoproteasome produces peptides for MHC I and is therefore required for positive selection of CD8⁺, but not MHC II-restricted CD4⁺ T cells. In thymoproteasome-deficient mice exclusively the positive selection of CD8⁺ T cells is affected, thereby reducing CD8SP thymocytes and CD8⁺ T cells in the periphery, but not CD4SP thymocytes or CD4⁺ T cells (Murata, Sasaki et al. 2007, Xing, Jameson et al. 2013). In contrast, homozygous TUB006 mice additionally show CD4SP thymocyte and CD4⁺ T cell deficiency, which cannot be explained solely by defective thymoproteasome but indicate that the developmental step from the DP to SP stage that accompanies positive selection is profoundly hampered in both MHC I- and MHC II-restricted T cells. This might result from the complete lack of the thymoproteasome-expressing cTECs in TUB006 homozygotes. This is supported by the finding that transient cTEC depletion leads to impaired development of both CD4⁺ and CD8⁺ T cells (Rode and Boehm 2012). A recently published study helps to determine the respective and potentially compounded roles of the immunoproteasome and thymoproteasome deficiency. A spontaneous mutation in the gene encoding the thymoproteasome-specific subunit $\beta 5t$ leads to reduction of CD4SP and CD8SP thymocytes, as well as naïve T cells in the periphery. Both, CD4⁺ and CD8⁺ T cells were affected, but the CD8⁺ T cell defect was more severe, very similar to the heterozygous TUB006 phenotype. The lymphopenia is a consequence of substantial loss of cTECs and thymic tissue in these TN mutant mice (Nitta, Muro et al.

2015). Likewise, TN and homozygous TUB006 mutants show atrophic thymus and substantial loss of cTECs. The thymoproteasome is found exclusively in cTECs (Murata, Sasaki et al. 2007, Tomaru, Ishizu et al. 2009, Xing, Jameson et al. 2013), while mTECs contain immuno- and constitutive proteasome (Nil, Firat et al. 2004). Therefore, the thymus defect in TUB006 mice was more pronounced in cTECs, while significantly more mTECs were viable.

Maturation from DP to SP thymocytes is crucial for T cells to acquire capacity of self – non-self discrimination, to be steadily replenished to the naïve T cell pool in the periphery and to ensure the functionality of the T cell repertoire. The maturation is governed by interaction of TCRs with self-peptides in association with MHC molecules in the thymus. Lack of cTECs has an impact on positive selection of both CD4SP and CD8SP thymocytes. Correlating the degree of cTEC reduction with the consequences for CD8⁺ and CD4⁺ T cell development could shed further light on the physiological function of this particular cell type. The process of T cell development and repertoire formation has been studied for decades, but the physiological and pathological importance of positive selection is still controversial. When transferred into wild type recipients, thymi from newborn homozygous TUB006 mice could provide an important tool for understanding the complex T cell maturation process in more detail. In this system, wild type T cells progenitors would undergo maturation and selection within the mutant defective thymic stroma, which is characterized by a selective loss of cTECs.

Homozygous TUB006 mice develop SCID including lack of all major types of lymphocytes: T, B and NK cells. Since other cell types such as NK- and B-cells are unaffected by cTEC depletion, additional factors are assumed to cause SCID in TUB006 mice. At neonatal age, homozygotes show inborn deficiency in T and NK cells, but normal B cell frequencies. T- and NK-lineages have in common their requirement for MHC I encounter during maturation and developmental signals through IL-7 and IL-15. However, mice deficient for MHC I surface expression have a functionally impaired but numerically normal NK cell compartment (Orr and Lanier 2010), thus it is unlikely that alterations in MHC I expression are causative for the NK cell deficiency in TUB006 mice. NK cells are known to be sensitive to proteasome malfunction as they undergo apoptosis upon treatment with proteasome inhibitors (Wang, Ottosson et al. 2009, Feng, Holmlund et al. 2014). Furthermore, bortezomib down-regulates the expression of NKp46 on the cell surface of non-apoptotic NK cells (Wang, Ottosson et al. 2009). It could be

hypothesized that the absence of a functional proteasome could lead to the disappearance of NK cells in TUB006. In case reports of Nakaja-Nishimura syndrome – one of the ALDD syndromes – NK defects were described. In contrast to TUB006, NK cells in these patients were numerically normal, but showed reduced activity (Tanaka, Miyatani et al. 1993).

The differences in the neonatal B and T cells could also be based on their differential regulation of basal immuno-subunit expression. Whereas the constitutive IFN signaling is sufficient for B cells, the expression in T cells depends on two mechanisms: IFN-dependent signal transducer and activator of transcription 1 (STAT1) activation as well as IFN-independent IL-7 dependent STAT1 activation (Lee, Gimeno et al. 1999). The regulation in NK cells is not yet dissolved.

T cell homeostasis is governed by TCR-MHC interactions and IL-7 stimulation. These signals, ensuring T cell survival under steady-state conditions, lead to compensatory T cell proliferation in lymphopenic environment (Takada and Jameson 2009). It was shown that this process is associated with autoimmunity (King, Ilic et al. 2004). The phenotype of T cells derived by peripheral homeostatic proliferation is skewed towards a memory-like phenotype (Goldrath, Bogatzki et al. 2000). The same T cell phenotype is observed in thymoproteasome-deficient mice (Nitta, Murata et al. 2010) and in TUB006 mutants and presumably reflects the reduced thymic output and typical changes during thymus-independent homeostatic T cell proliferation in lymphopenic mice (Goldrath, Bogatzki et al. 2000). To test whether T cell-intrinsic factors or factors provided by non-T cells affect CD8⁺ T cell activation, differentiation and maintenance in TUB006 mice, adoptive T cell transfer experiments should be performed: analysis of T cell survival after transfer of wild type T cells into homozygous and heterozygous TUB006 mutants as well as the vice versa approach to transfer mutant TUB006 T cells into lymphopenic RAG1 deficient hosts.

6.2 Granulocytosis and inflammation in TUB006 mice

In addition to SCID, homozygous TUB006 mutants exhibit granulocytosis and autoinflammation of the skin and several organs, leading to early lethality. In most of the analyzed organs granulocyte infiltrations were observed, except of the brain. This might be due to the fact that leukocyte extravasation to the brain adopts a special mechanism (Carvalho-Tavares, Hickey et al. 2000).

Resolution of inflammation is crucial for the host. Under conditions where complete healing does not occur, as in the setting of chronic infection or prolonged exposure to injurious agents, the inflammatory response remains unresolved and can be detrimental to the host. Macrophages and neutrophils persist and continue to secrete inflammatory cytokines, ROS, proteases and growth factors that lead to inappropriate tissue destruction, as well as fibroblast proliferation, aberrant collagen accumulation and scarring or fibrosis. The complex developmental and functional relationships within the immune system, as well as the influence of pathological changes have complicated elucidating of the underlying pathomechanisms in homozygous TUB006 mice.

The pathological findings of severely increased granulocytes may be associated to chronic myeloid leukemia (CML). Increased frequency of granulocytes in peripheral blood and infiltrations of granulocytes in lung, liver, spleen, gut and skin are indications of CML. The myeloproliferative disease is characterized by the abnormal proliferation and accumulation of mature and maturing myeloid cells, and enlargement of the spleen due to infiltration of the red pulp. Moreover, recently SNPs in human *Psmb10* have been linked to increased risk for CML (Bruzzoni-Giovanelli, Gonzalez et al. 2015). On the contrary, athymic phenotype and SCID contradict the hypothesis of CML as underlying disorder. Furthermore, the bone marrow transfer experiment showed that the granulocytosis in homozygous TUB006 host can also occur with donor-derived bone marrow, ruling out CML as a pathomechanism in TUB006 mice.

Accelerated granulocyte production in response to infection or sterile stimuli is known as emergency granulopoiesis. Emergency granulopoiesis is characterized by blood leukocytosis, neutrophilia, and the appearance of hypersegmented immature neutrophil precursor cells in the peripheral blood (known as left-shift), which are only present in the bone marrow during physiological steady-state conditions (Manz and Boettcher 2014). These symptoms closely resemble the observations in homozygous TUB006 mice. Compared to the steady-state maintenance, the neutrophil production and egress from the bone marrow switches to a differential regulation during emergency response, involving IL-1 signaling (Hirai, Zhang et al. 2006, Cain, Snowden et al. 2011).

The granulocyte expansion temporally correlates with the B cell loss in TUB006 mice. B cell and granulocyte frequencies are negatively correlated (Ueda, Kondo et al. 2005). Emergency granulopoiesis is accompanied by decreased lymphocyte production (Manz and Boettcher 2014). Therefore, expansion of the granulocyte lineage may lead to the B

cell deficiency in TUB006 mice. Indeed, in the bone marrow from eight weeks-old TUB006 animals a strong reduction of lymphoid precursors was observed, and simultaneous increase of the myeloid progenitors. This finding demonstrates that the TUB006 defect appears early during hematopoiesis.

The emergency granulopoiesis can occur in response to different stimuli, such as infections or sterile stimuli. The lack of adaptive immune system in TUB006 mice implies enhanced susceptibility to opportunistic infections. To evaluate the influence of microbiota onto the pathogenesis in TUB006 mice, we transferred the mouse line into a germ-free mouse facility. Interestingly, the phenotype of germ-free heterozygous as well as homozygous TUB006 mice developed identically to that of SPF-mice. Although the influence of reactivation of endogenous retrovirus cannot be excluded (Yu, Lubben et al. 2012), the persistence of the TUB006 phenotype under germ-free conditions points towards independence from microbiotic triggers and suggests sterile inflammation.

Similar to microbially induced inflammation, sterile inflammation is marked by fever, increased production of hepatic acute phase proteins, recruitment of neutrophils and macrophages to the site of inflammation and the production of proinflammatory cytokines, particularly TNF- α , IL-6 and IL-1 β (Chen and Nunez 2010, Joosten, Netea et al. 2013). One of the most potent triggers of sterile inflammation is cell death (Rock, Latz et al. 2010). Sterile inflammation induced by cell death was shown to be dependent on the Nlrp3 inflammasome and IL-1 (Chen and Nunez 2010). Mice deficient for the IL-1 receptor mice have a significant reduction of neutrophil recruitment to cell death-induced sterile inflammation (Chen, Kono et al. 2007). The neutrophil attraction to sites of skin necrosis is also governed by IL-1 β (Sadik, Kim et al. 2011). In homozygous TUB006 mice, the plasma levels of proinflammatory cytokines IL-1 β , IL-6 and TNF- α were increased. IL-1 β acts as a key player in many chronic diseases, e.g. diabetes, atherosclerosis, osteoarthritis and cancer (Dinarello 2011, Wojdasiewicz, Poniatowski et al. 2014). This cytokine induces inflammatory responses in various organs and tissues and is therefore one of the most potent proinflammatory cytokines (Dinarello 1984). IL-1 β and TNF- α show synergistic effects by activating of the same group of intracellular signaling pathways and increasing inflammation (Wojdasiewicz, Poniatowski et al. 2014). Both cytokines stimulate upregulation of IL-6. IL-1 β and IL-6 deficient mice fail to develop a systemic inflammatory response to sterile stimuli (Fattori, Cappelletti et al. 1994, Kopf, Baumann et al. 1994, Zheng, Fletcher et al. 1995). IL-1 β deficiency leads to

failure of IL-6 induction (Fantuzzi, Ku et al. 1997). IL-1 β can be produced by monocytes, macrophages, DCs, B- and NK cells, as well as by neutrophils in mice with skin inflammation. However, the cellular sources of cytokines in TUB006 are unknown. To rescue the TUB006 phenotype, a therapeutic treatment with antibodies neutralizing IL-1 β would be a promising approach, as well as crossing of the TUB006 mouse line with IL-1 or IL-1 receptor knockout mice.

In immunoproteasome-associated ALDD syndrome, a non-typical pattern of inflammatory cytokines was described, distinct from the cytokine signature observed in TUB006. Increased IL-6 and in some cases IFN- γ levels were observed in sera (Agarwal, Xing et al. 2010, Arima, Kinoshita et al. 2011, Liu, Ramot et al. 2012) and skin (Kitamura, Maekawa et al. 2011) of these patients, notably without elevation of IL-1 and TNF- α (Agarwal, Xing et al. 2010).

Interestingly, besides the proinflammatory cytokines, also IL-4 levels were abnormally high in homozygous TUB006 mutants. IL-4 possesses anti-inflammatory qualities and suppresses production of inflammatory cytokines such as IL-12, IL-6 and TNF- α (Sriram, Xu et al. 2014). Most likely, upregulation of IL-4 is a compensatory mechanism to neutralize the harmful inflammation as described in patients with rheumatoid arthritis (Rivas, Mozo et al. 1995).

6.3 Hematopoietic defect

Phenotypically, no HSC in bone marrow from homozygous TUB006 mice were observed. However, to exclude that low frequencies not detectable by flow cytometry are still present, functional HSC assays are necessary. The most important assay to assess HSC function is the capability of an HSC to reconstitute the bone marrow of lethally irradiated hosts. In this assay, wild type recipient mice are irradiated with a dose lethal for the hematopoietic cells of the recipient mouse. Then, the recipient mouse is transplanted with bone marrow cells from a homozygous TUB006 donor mouse. One single HSC would be able to rescue the host by giving life-long multi-lineage engraftment, showing both the capability of these cell to self-renew as well as to differentiate into all hematopoietic lineages (Osawa, Hanada et al. 1996, Ema, Sudo et al. 2005). In contrast, if HSCs were absent or non-functional in TUB006 bone marrow, the reconstitution of the system would not be possible. The latter variant was observed in the TUB006 \rightarrow WT bone marrow chimera. The TUB006 bone marrow failed at

reconstituting the host, showing a clear defect in the bone marrow from homozygous TUB006 mice at the donor age of eight weeks, in line with the undetectable stem cells in TUB006 mice. However, neutrophils were present in homozygous mice, and B cells were present in newborns, assuming functionality of HSCs at least until a certain age.

HSC are spatially located in highly organized microenvironmental niches at the endosteum of the bone. In response to stress or injury, HSC can be released into the blood stream, a process called HSC mobilization. This system is also used in human patients for stem cell collection from peripheral blood prior to stem cell transplantation (Lemoli and D'Addio 2008). Increased release of leukocytes and HSC from the bone marrow is also part of the immune system response to inflammation. Thereby, the granulocyte colony-stimulating factor (G-CSF) that stimulates the bone marrow to produce granulocytes and stem cells acts as one of the main mobilizing factors. The mobilization of stem cells in response to severe chronic inflammation is a supposable explanation for lack of HSC in the bone marrow from homozygous TUB006 mice.

Due to the failure of TUB006 bone marrow to engraft wild type hosts, the question is still to be answered whether transfer of the mutant bone marrow can transmit the TUB006 disease. To assess this issue, as well as to evaluate the functionality of HSCs, the TUB006→WT bone marrow transfer experiment should be repeated with younger homozygous TUB006 donors.

The vice versa bone marrow transfer of wild type bone marrow into homozygous TUB006 recipients showed quite contradicting results depending on the experimental conditions. In one setting, recovery of B cells, as well as low frequencies of granulocytes and NK cells were observed two weeks after bone marrow transfer. The T cell compartment did not show reconstitution, most likely due to the absence of thymus in homozygous recipients. However, this experiment shows that the TUB006 defect is intrinsic to the hematopoietic system and can be rescued by transfer of wild type bone marrow.

On the other hand, the second approach to generate WT→TUB006 chimera presented granulocytosis and SCID two weeks after transplantation, showing that wild type bone marrow can be forced towards granulopoiesis in response to extrinsic cues. In both experiments, the vast majority of leukocytes originated from the transferred donor bone marrow. There were three differences between the experiments. First, the genetic

background of the mouse line was C3HeB/FeJ or BALB/c, respectively. Second, the age of the recipients varied between five weeks in the first setting and more than eleven weeks in the second setting. Third, the irradiation dose was reduced in the second experiment (two fractions of three Gy instead of five Gy per fraction) in an attempt to avoid the rapid lethality observed in the first experiment. The lower irradiation dose might be not sufficient to eliminate all recipient-derived leukocytes, although the peripheral blood leukocytes showed expression of the donor CD45 isotype two weeks after bone marrow transfer. Which of these differences was crucial for the pleiotropic hematopoietic effects, remains to be elucidated. However, the results clearly demonstrate complexity of the TUB006 phenotype comprising defects on different levels. Both intrinsic and extrinsic factors play crucial roles in the pathogenesis of the immunodeficiency in the TUB006 mutant line. To clarify these opposing effects, further bone marrow transfer studies will be needed.

6.4 Analysis of the cell-specific roles in the pathogenesis of TUB006 by generation of conditional knock in mouse model

Engineering of a conditional MECL-1^{G170W} point mutation knock in mouse will allow inducible cell type- or tissue-restricted expression of MECL-1^{G170W}. This conditional MECL-1^{G170W} knock in mouse model will be useful to conclusively assess the contribution of different cell types to the pathogenesis in TUB006 mice.

Targeting of the endogenous MECL-1 locus ascertains that endogenous promotor and other regulatory sequences enable gene expression levels and patterns of MECL-1^{G170W} identical to that of wild type MECL-1. The strategy was developed to insert a mutated duplication of exon 7 on the complementary strand upstream of the endogenous exon 7. The sequence containing both, wild type and mutated exons 7, is floxed, i.e. flanked by antidromic *loxP* sites as depicted in Figure 37. This gene targeting strategy allows normal expression of the endogenous wild type MECL-1 until induction of the mutant MECL-1 via Cre-mediated recombination, since the mutant exon lies in opposite transcriptional orientation within an intron. Cre expression and subsequent recombination leads to the inversion of the floxed sequence, thereby inducing expression of mutated MECL-1 and simultaneously, inactivation of the wild type allele.

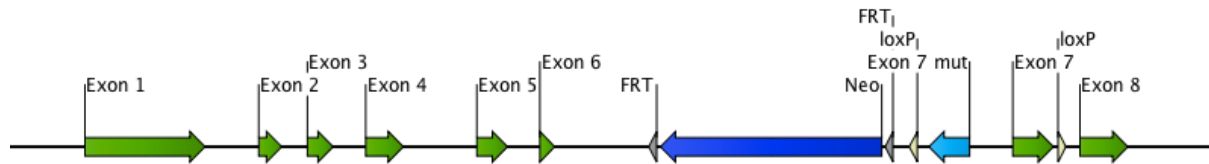


Figure 37: Schematic illustration of the construction of the conditional knock in mouse mutant. The genomic sequence of *Psmb10* contains eight exons, the TUB006 mutation is located in exon 7. The mutational strategy is shown for creating mice in which a point mutant allele replaces the wild type allele by expression of Cre recombinase. Mutant (light blue) and wild type (green) exons 7 are flanked by *loxP* sites (beige).

In order to insert the mutated exon 7 duplicate together with the *loxP* sites and neomycin resistance (Neo) cassette, homologous recombination in embryonic stem (ES) cells can be utilized. In case of inefficient recombination of the complete targeting sequence including the distal downstream *loxP* site, transfection can be repeated, with co-transfection of a supplementary Cas9 and gRNA expression vector. Assisted targeting strategy using Cas9 nuclease to induce a DNA break within the targeting region (e.g. insertion site of the downstream *loxP* element) was shown to enhance recombination efficiency significantly. Successfully recombined ES cells are selected by adding neomycin to the culture media, and thereafter the Neo cassette is removed by FLP-mediated recombination in vivo. Selected ES clones are injected into blastocytes to produce chimeric mice. Following germ-line transmission, the resulting heterozygous mice will be intercrossed to produce homozygous offspring. Subsequently, the floxed mouse line can be crossed to different mouse lines expressing Cre recombinase globally or under control of cell type-restricted promoters, e.g. CD19 (B cells), CD4 (T cells), *Csf1r* (macrophages), *KRT14* (keratinocytes) etc. To minimize effects on development of the analyzed cell type, as well as to circumvent the early lethal phenotype, tamoxifen-inducible Cre lines can be used.

6.5 Molecular impact of the MECL-1^{G170W} mutation

To understand the pathogenesis in TUB006, a closer look into the proteasome biology is required. Besides the three known mammalian proteasome types, mixed-type proteasomes incorporating the subunits LMP2, β 2c and LMP7 or β 1c, β 2c and LMP7 were identified (De, Jayarapu et al. 2003, Guillaume, Chapiro et al. 2010), indicating that the lack of certain subunits can be compensated by the incorporation of a redundant subunit. For instance, LMP2 can be replaced by β 2c, and LMP7 by β 5c (Nandi, Jiang et al. 1996, Stohwasser, Kuckelkorn et al. 1996). In MECL-1 deficient mice the corresponding constitutive subunit β 2c fills in for MECL-1 and thus, proteasome assembly proceeds

leading to either constitutive proteasomes or mixed types containing the subunits LMP2, β 2c, LMP7 or β 2c, β 1c, LMP7 (De, Jayarapu et al. 2003). Furthermore, mice lacking all three immuno-subunits can still assemble constitutive proteasomes containing β 2c, β 1c, and β 5c. In β 5t-deficient mice, cTECs compensatively assemble LMP2, MECL-1, and LMP7-containing immunoproteasomes, and in β 5t LMP7 double deficient mice β 1c β 2c β 5c-containing constitutive proteasomes (Xing, Jameson et al. 2013). In conclusion, a eukaryotic cell is viable if it is able to produce any kind of functional proteasome. Regarding the compensatory flexibility, lack of pronounced immunodeficiencies in mice lacking one or a combination of non-constitutive proteasomal subunits is plausible. The differences in proteasomal compositions lead to significant alteration of CD8⁺ T cell number and repertoire, but overall the resulting phenotypes are modest and the gene-targeted mice are healthy (Fehling, Swat et al. 1994, Basler, Moebius et al. 2006, Murata, Sasaki et al. 2007, Kincaid, Che et al. 2012). In contrast, the strong immune phenotype of the TUB006 mutant mice differs from the knockout counterparts, implying a non-compensable defect.

The principle proteasome structure as well as assembly pathway is strongly conserved among species, from the yeast proteasome to the mammalian proteasome subtypes (Marques, Palanimurugan et al. 2009, Huber, Basler et al. 2012). Proteasome assembly starts with the formation of the α -ring, followed by association of the β subunits. The subunits β 7 and β 2 carry C-terminal tails that are pivotal for interactions with other β -subunits. The C-tail of subunit β 2 is crucial for the incorporation of the β 3 subunit (Ramos, Marques et al. 2004, Hirano, Kaneko et al. 2008). This tail-mediated β 2- β 3 interaction is essential for the stability of the proteasome precursor and continuing of the assembly line (Li, Kusmierczyk et al. 2007). Since defects of the proteasome biogenesis are lethal, the C-tail of β 2 is essential for cell survival.

To elucidate molecular aspects of the TUB006 mutation G170W, we introduced the G170W and the attenuated G170A mutations into the analogous β 2 subunit of the yeast proteasome. Mutagenesis experiments in yeast revealed that the γ β 2-mutations G170W and G170A were lethal. Lethal effects indicate defective proteasome assembly, since inactivation of proteolytic activity does not affect yeast viability (Heinemeyer, Fischer et al. 1997, Groll, Heinemeyer et al. 1999). Auspiciously, fusion of the yeast β 2-C-terminus to a Protein A tag rescued the mutant G170A and enabled crystallographic analysis of its proteasome. Structural data showed rearrangements in a loop region of the C-terminal

appendage of $\gamma\beta 2^{G170A}$. Without the Protein A tag, displacement of the $\gamma\beta 2$ tail disturbs $\beta 3$ association and hence disrupts the proteasome assembly pathway. The Protein A tag fused to subunit $\gamma\beta 2$ extends the C-terminal tail of $\gamma\beta 2$ and stabilizes the $\gamma\beta 2$ - $\gamma\beta 3$ interaction, thereby supporting hemiproteasome formation. Overcoming the proteasome assembly failure by stabilizing the $\gamma\beta 2$ - $\gamma\beta 3$ interactions enables survival of the yeast cells. In contrast, the mutation G170W cannot be rescued by fusion of the Protein A tag, implying that additional effects lead to proteasome maturation failure. Tryptophan with its aromatic residue is the largest amino acid, its molecular size by far exceeds the second smallest amino acid alanine. Even if Protein A tag fusion rescued the $\gamma\beta 2$ - $\gamma\beta 3$ interaction, the bulky tryptophan would probably sterically hinder the final association of two hemiproteasomes.

Regarding these molecular insights into the proteasome assembly defect, the severe immunodeficiency of TUB006 mutants can be explained by the following model. In cells co-expressing constitutive and immuno-subunits, cooperative assembly preferentially leads to the formation of homogenous immunoproteasomes (Bai, Zhao et al. 2014). In particular, MECL-1 is preferentially incorporated into nascent proteasomes (De, Jayarapu et al. 2003). Initial MECL-1 association requires LMP2, and LMP7 is incorporated preferentially into MECL-1 and LMP2 containing proteasome precursors (Groettrup, Standera et al. 1997, Griffin, Nandi et al. 1998). In TUB006, MECL-1^{G170W} together with LMP2 might be assembled into precursor complexes, but docking of subunit $\beta 3$ adjacent to MECL-1^{G170W} is impaired due to the structural changes of the C-terminus of MECL-1^{G170W}. Proteasome intermediates composed of a heptameric α -ring, MECL-1^{G170W}, and LMP2 accumulate. In conclusion, all cells expressing MECL-1^{G170W} fail to assemble functional proteasomes and succumb. A very similar mutation on the same position 170 in the thymoproteasome-specific subunit $\beta 5i$ was recently reported to be lethal for cTECs. Interestingly, like $\beta 2$ subunits, the subunit $\beta 5t$ is also endowed with a C-terminal tail, which is absent in the subunits $\beta 5c$ and $\beta 5i$ (Murata, Sasaki et al. 2007). The mutant $\beta 5t^{G170R}$ subunit induces accumulation of thymoproteasome precursor complexes leading to cell death in cTECs (Nitta, Muro et al. 2015).

According to our model, the expression of MECL-1^{G170W} and its preferential incorporation into proteasomes leads to defective immunoproteasome as well as thymoproteasome assembly and manifests in selective cell death of MECL-1^{G170W} expressing cells and eventually immunodeficiency. In support of this model, mutation of

G170W in subunit $\beta 2$ of the yeast proteasome is lethal. Moreover, retroviral overexpression of MECL-1^{G170W} in wild type splenocytes confirmed the lethal effect on murine cells. Comparison of the observed phenotype in homozygous TUB006 mice with online database of the *Immunological Genome Project* (<http://www.immgen.org/>) demonstrates that cell types with a high constitutive expression of MECL-1 are absent, e.g. cTECs and CD4SP and SD8SP thymocytes in the thymus, and T cells and NK cells in the periphery. Cell death is a potent trigger of sterile inflammation marked by neutrophil recruitment (Chen and Nunez 2010). Thus, this model also explains the granulocytosis and neutrophil infiltration into tissues observed in homozygous TUB006 mutants.

In human LMP7-associated syndromes, an underlying immunoproteasome assembly defect was suggested. Presumably, the assembly defect governed by LMP7 mutations is more flexible than that caused by MECL-1^{G170W} and can be partly compensated by formation of constitutive or mixed proteasomes. The incorporation of $\beta 2$ ($\beta 2c$ or MECL-1) during the proteasome biogenesis is the initial step of the beta-ring assembly, while LMP7 is the latest incorporated catalytic subunit. The function of $\beta 2c$ /MECL-1 exchange is still elusive, because in contrast to the $\beta 1c$ /LMP2 and $\beta 5c$ /LMP7 pairs, the exchange of $\beta 2c$ with MECL-1 does not lead to a change of neither proteolytic activity nor substrate specificity (Huber, Basler et al. 2012). Thus, our data point towards a key initiator role of MECL-1 in the formation of non-constitutive proteasomes. Apparently, expression of the mutant version of the MECL-1 protein in TUB006 results in phenotypic properties distinct from its knockout counterpart, demonstrating the power of phenotype-driven “forward genetics” approach to identify a broader range of gene functions by creating not only loss-of-function mutants but also gain-of-function, hypo-/hypermorphs or dominant-negative mutations not discovered with the “reverse” gene-driven approach (Justice, Noveroske et al. 1999, Nelms and Goodnow 2001, Cook, Vinuesa et al. 2006).

6.6 Human relevance

The identification of causative mutations in mice with immunodeficiencies/clinical phenotypes can lead to the discovery of novel human disease genes. *Listeria monocytogenes* is a pathogen that is relevant for human disease. Immunocompromised individuals are susceptible to infection with *L.m.*; in severe cases *Listeria* can cause

sepsis and meningitis. This work indicates that heterozygous TUB006 mutants present a selective deficiency in adaptive T cell immunity and are highly susceptible to *L.m.* The high homology of the murine and human MECL-1 and the severe infection susceptibility phenotype in heterozygous TUB006 mice indicate for the first time that MECL-1 mutations are relevant for human disease and suggest including MECL-1 as a candidate gene for screening in human individuals with primary immunodeficiency of unknown etiology. Rare homozygous carriers would develop a severe disease, and there is the possibility that homozygous MECL-1 mutation would be lethal in humans. Nevertheless, heterozygous MECL-1 mutations would appear with a higher incidence and lead to lymphopenia and probably chronic infections.

So far, in heterozygous TUB006 mice a selective T cell defect was observed. In order to further concretize the assumed symptoms in the human setting in several clinical areas, a broader phenotyping in the GMC (Gailus-Durner, Fuchs et al. 2005) is intended. Besides the Immunology Screen, where the TUB006 mutant was identified, the GMC phenotyping pipeline includes analysis of behaviour, bone and cartilage development, neurology, clinical chemistry, eye development, allergy, steroid metabolism, energy metabolism, lung function, vision and pain perception, molecular phenotyping, cardiovascular analyses and pathology (<http://www.mouseclinic.de>). The comprehensive phenotyping will help to understand the holistic effects of the TUB006 mutation, and finally support our search for human individuals with MECL-1 mutations.

The symptoms of the human LMP7-associated ALDD syndrome match in some part the homozygous TUB006 phenotype, e.g. granulocyte infiltration into the skin, autoinflammation and lipodystrophy (Garg, Hernandez et al. 2010, Arima, Kinoshita et al. 2011, Kitamura, Maekawa et al. 2011, Liu, Ramot et al. 2012). However, none of the patients described so far in case studies presented with SCID. The divergent disease symptoms can be referred to three facts. First, the development of SCID in TUB006 animals might be explained by the fact that in contrast to ALDD-associated immunosubunit LMP7, MECL-1 is not only incorporated into the immunoproteasome, but is also part of the thymoproteasome. Second, species-specific differences in the immune system might also lead to observed differences between humans and mice (Mestas and Hughes 2004). Third, the genetic variability of human patients contrasts the mouse research using inbred strains that are in theory genetically identical organisms. However, TUB006 mice bred on different genetic backgrounds shows that genetic variability in

fact influences the phenotype of TUB006 mice. Although the key features of the disease are identical, the severity differs. BALB/c mutants display doubled life span compared to C57BL/6 and C3HeB/FeJ, and later onset of the disease. The strain-dependent susceptibility may be ascribed to the complexity of IFN- γ regulation. IFN- γ secretion is significantly higher in C57BL/6 and C3HeB/FeJ mice compared to BALB/c (Schroder, Hertzog et al. 2004). Thorough literature research did not reveal any available mouse model for the proteasome-associated human syndromes. In spite of the differences between ALDD and TUB006 symptoms, most of the symptoms are identical. Furthermore, it is generally accepted that there is no single perfect mouse model for each disease. Instead, different models are usually used to study different aspects of a given disease. Taken together, TUB006 is the first mouse model for ALDD and might provide important insights for future therapy development.

The primary task of proteasomes to degrade proteins yields different effects on the immune system, such as the selective degradation of regulatory proteins or production of peptides for MHC I presentation. For this reason, proteasomes have become attractive drug targets for treatment of cancer or autoimmune disorders. Tumor cells have accelerated cell cycle and metabolism, requiring high turnover rates of proteins. This often leads to increased levels of proteasomes in transformed cells, rendering them highly sensitive to proteasome inhibition. Proteasome inhibitors have been explored in clinical trials as therapeutic compounds for treatment of solid tumors and hematological malignancies. For example, the proteasome inhibitor bortezomib has been approved for the treatment of multiple myeloma (Borissenko and Groll 2007). In certain diseases, the pathogenesis depends on elevated immunoproteasome levels (Lee and Kim 2011). Mostly, these diseases are associated with inflammation and increased cytokine levels, e.g. inflammatory bowel disease and Crohn's disease (Fitzpatrick, Small et al. 2007, Lee and Kim 2011). Thus, selective immunoproteasome inhibitors have also become attractive candidates as therapeutic compounds and proven their effectiveness in autoimmune disorders (Muchamuel, Basler et al. 2009, Basler, Dajee et al. 2010). These results together with the crystal structure analysis of the immunoproteasome (Huber, Basler et al. 2012), has significantly stimulated proteasome research in academia and industry. The results obtained in this study dealing with a hitherto undescribed immunological defect based on a single point mutation in the immuno- and thymoproteasome further underscore the significance of the proteasome research. The

novel mouse model of primary immunodeficiency and its relevance for understanding basic aspects of proteasome assembly might have a lot of implications.

7 References

- Abe, K., S. Wechs, S. Kalaydjiev, T. J. Franz, D. H. Busch, H. Fuchs, D. Soewarto, H. Behrendt, S. Wagner, T. Jakob and M. Hrabě de Angelis (2008). "Novel lymphocyte-independent mechanisms to initiate inflammatory arthritis via bone marrow-derived cells of Ali18 mutant mice." *Rheumatology* **47**(3): 292-300.
- Agarwal, A. K., C. Xing, G. N. DeMartino, D. Mizrachi, M. D. Hernandez, A. B. Sousa, L. Martinez de Villarreal, H. G. dos Santos and A. Garg (2010). "PSMB8 encoding the beta5i proteasome subunit is mutated in joint contractures, muscle atrophy, microcytic anemia, and panniculitis-induced lipodystrophy syndrome." *Am J Hum Genet* **87**(6): 866-872.
- Akashi, K., D. Traver, T. Miyamoto and I. L. Weissman (2000). "A clonogenic common myeloid progenitor that gives rise to all myeloid lineages." *Nature* **404**(6774): 193-197.
- Aki, M., N. Shimbara, M. Takashina, K. Akiyama, S. Kagawa, T. Tamura, N. Tanahashi, T. Yoshimura, K. Tanaka and A. Ichihara (1994). "Interferon-gamma induces different subunit organizations and functional diversity of proteasomes." *J Biochem* **115**(2): 257-269.
- Al-Herz, W., A. Bousfiha, J. L. Casanova, T. Chatila, M. E. Conley, C. Cunningham-Rundles, A. Etzioni, J. L. Franco, H. B. Gaspar, S. M. Holland, C. Klein, S. Nonoyama, H. D. Ochs, E. Oksenhendler, C. Picard, J. M. Puck, K. Sullivan and M. L. Tang (2014). "Primary immunodeficiency diseases: an update on the classification from the international union of immunological societies expert committee for primary immunodeficiency." *Front Immunol* **5**: 162.
- Anderson, G. and Y. Takahama (2012). "Thymic epithelial cells: working class heroes for T cell development and repertoire selection." *Trends Immunol* **33**(6): 256-263.
- Apostolou, I., A. Sarukhan, L. Klein and H. von Boehmer (2002). "Origin of regulatory T cells with known specificity for antigen." *Nat Immunol* **3**(8): 756-763.
- Arbones, M. L., D. C. Ord, K. Ley, H. Ratech, C. Maynard-Curry, G. Otten, D. J. Capon and T. F. Tedder (1994). "Lymphocyte homing and leukocyte rolling and migration are impaired in L-selectin-deficient mice." *Immunity* **1**(4): 247-260.
- Arima, K., A. Kinoshita, H. Mishima, N. Kanazawa, T. Kaneko, T. Mizushima, K. Ichinose, H. Nakamura, A. Tsujino, A. Kawakami, M. Matsunaka, S. Kasagi, S. Kawano, S. Kumagai, K. Ohmura, T. Mimori, M. Hirano, S. Ueno, K. Tanaka, M. Tanaka, I. Toyoshima, H. Sugino, A. Yamakawa, K. Tanaka, N. Niikawa, F. Furukawa, S. Murata, K. Eguchi, H. Ida and K. Yoshiura (2011). "Proteasome assembly defect due to a proteasome subunit beta type 8 (PSMB8) mutation causes the autoinflammatory disorder, Nakajo-Nishimura syndrome." *Proc Natl Acad Sci U S A* **108**(36): 14914-14919.
- Auffray, C., D. Fogg, M. Garfa, G. Elain, O. Join-Lambert, S. Kayal, S. Sarnacki, A. Cumano, G. Lauvau and F. Geissmann (2007). "Monitoring of blood vessels and tissues by a population of monocytes with patrolling behavior." *Science* **317**(5838): 666-670.

- Auffray, C., M. H. Sieweke and F. Geissmann (2009). "Blood monocytes: development, heterogeneity, and relationship with dendritic cells." *Annu Rev Immunol* **27**: 669-692.
- Azzam, H. S., A. Grinberg, K. Lui, H. Shen, E. W. Shores and P. E. Love (1998). "CD5 expression is developmentally regulated by T cell receptor (TCR) signals and TCR avidity." *J Exp Med* **188**(12): 2301-2311.
- Badovinac, V. P. and J. T. Harty (2002). "CD8(+) T-cell homeostasis after infection: setting the 'curve'." *Microbes Infect* **4**(4): 441-447.
- Bai, M., X. Zhao, K. Sahara, Y. Ohte, Y. Hirano, T. Kaneko, H. Yashiroda and S. Murata (2014). "Assembly mechanisms of specialized core particles of the proteasome." *Biomolecules* **4**(3): 662-677.
- Bancroft, G. J., R. D. Schreiber, G. C. Bosma, M. J. Bosma and E. R. Unanue (1987). "A T cell-independent mechanism of macrophage activation by interferon-gamma." *J Immunol* **139**(4): 1104-1107.
- Barbaric, I., S. Wells, A. Russ and T. N. Dear (2007). "Spectrum of ENU-induced mutations in phenotype-driven and gene-driven screens in the mouse." *Environ Mol Mutagen* **48**(2): 124-142.
- Basler, M., M. Dajee, C. Moll, M. Groettrup and C. J. Kirk (2010). "Prevention of experimental colitis by a selective inhibitor of the immunoproteasome." *J Immunol* **185**(1): 634-641.
- Basler, M., J. Moebius, L. Elenich, M. Groettrup and J. J. Monaco (2006). "An altered T cell repertoire in MECL-1-deficient mice." *J Immunol* **176**(11): 6665-6672.
- Beura, L. K., S. E. Hamilton, K. Bi, J. M. Schenkel, O. A. Odumade, K. A. Casey, E. A. Thompson, K. A. Fraser, P. C. Rosato, A. Filali-Mouhim, R. P. Sekaly, M. K. Jenkins, V. Vezys, W. N. Haining, S. C. Jameson and D. Masopust (2016). "Normalizing the environment recapitulates adult human immune traits in laboratory mice." *Nature* **532**(7600): 512-516.
- Beutler, B., Z. Jiang, P. Georgel, K. Crozat, B. Croker, S. Rutschmann, X. Du and K. Hoebe (2006). "Genetic analysis of host resistance: Toll-like receptor signaling and immunity at large." *Annu Rev Immunol* **24**: 353-389.
- Bishop, D. K. and D. J. Hinrichs (1987). "Adoptive transfer of immunity to *Listeria monocytogenes*. The influence of in vitro stimulation on lymphocyte subset requirements." *J Immunol* **139**(6): 2005-2009.
- Bochtler, M., L. Ditzel, M. Groll and R. Huber (1997). "Crystal structure of heat shock locus V (HslV) from *Escherichia coli*." *Proc Natl Acad Sci U S A* **94**(12): 6070-6074.
- Borissenko, L. and M. Groll (2007). "20S proteasome and its inhibitors: crystallographic knowledge for drug development." *Chem Rev* **107**(3): 687-717.
- Bossi, G., C. Trambas, S. Booth, R. Clark, J. Stinchcombe and G. M. Griffiths (2002). "The secretory synapse: the secrets of a serial killer." *Immunol Rev* **189**: 152-160.
- Bratton, D. L. and P. M. Henson (2011). "Neutrophil clearance: when the party is over, clean-up begins." *Trends Immunol* **32**(8): 350-357.
- Bruzzoni-Giovanelli, H., J. R. Gonzalez, F. Sigaux, B. O. Villoutreix, J. M. Cayuela, J. Guilhot, C. Preudhomme, F. Guilhot, J. L. Poyet and P. Rouselot (2015). "Genetic

- polymorphisms associated with increased risk of developing chronic myelogenous leukemia." Oncotarget **6**(34): 36269-36277.
- Busch, D. H. and E. G. Pamer (1999). "T lymphocyte dynamics during *Listeria monocytogenes* infection." Immunol Lett **65**(1-2): 93-98.
- Busch, D. H., I. M. Pilip, S. Vijh and E. G. Pamer (1998). "Coordinate regulation of complex T cell populations responding to bacterial infection." Immunity **8**(3): 353-362.
- Busch, D. H., S. Vijh and E. G. Pamer (2001). "Animal model for infection with *Listeria monocytogenes*." Curr Protoc Immunol **Chapter 19**: Unit 19 19.
- Cain, D. W., P. B. Snowden, G. D. Sempowski and G. Kelsoe (2011). "Inflammation triggers emergency granulopoiesis through a density-dependent feedback mechanism." PLoS One **6**(5): e19957.
- Carlyle, J. R., A. Mesci, B. Ljutic, S. Belanger, L. H. Tai, E. Rousselle, A. D. Troke, M. F. Proteau and A. P. Makrigiannis (2006). "Molecular and genetic basis for strain-dependent NK1.1 alloreactivity of mouse NK cells." J Immunol **176**(12): 7511-7524.
- Carvalho-Tavares, J., M. J. Hickey, J. Hutchison, J. Michaud, I. T. Sutcliffe and P. Kubes (2000). "A role for platelets and endothelial selectins in tumor necrosis factor-alpha-induced leukocyte recruitment in the brain microvasculature." Circ Res **87**(12): 1141-1148.
- Catalina, M. D., M. C. Carroll, H. Arizpe, A. Takashima, P. Estess and M. H. Siegelman (1996). "The route of antigen entry determines the requirement for L-selectin during immune responses." J Exp Med **184**(6): 2341-2351.
- Cesta, M. F. (2006). "Normal structure, function, and histology of the spleen." Toxicol Pathol **34**(5): 455-465.
- Cheers, C., I. F. McKenzie, H. Pavlov, C. Waid and J. York (1978). "Resistance and susceptibility of mice to bacterial infection: course of listeriosis in resistant or susceptible mice." Infect Immun **19**(3): 763-770.
- Chen, C. J., H. Kono, D. Golenbock, G. Reed, S. Akira and K. L. Rock (2007). "Identification of a key pathway required for the sterile inflammatory response triggered by dying cells." Nat Med **13**(7): 851-856.
- Chen, G. Y. and G. Nunez (2010). "Sterile inflammation: sensing and reacting to damage." Nat Rev Immunol **10**(12): 826-837.
- Chen, P. and M. Hochstrasser (1996). "Autocatalytic subunit processing couples active site formation in the 20S proteasome to completion of assembly." Cell **86**(6): 961-972.
- Chen, W., W. Jin, N. Hardegen, K. J. Lei, L. Li, N. Marinos, G. McGrady and S. M. Wahl (2003). "Conversion of peripheral CD4+CD25- naive T cells to CD4+CD25+ regulatory T cells by TGF-beta induction of transcription factor Foxp3." J Exp Med **198**(12): 1875-1886.
- Chiossone, L., J. Chaix, N. Fuseri, C. Roth, E. Vivier and T. Walzer (2009). "Maturation of mouse NK cells is a 4-stage developmental program." Blood **113**(22): 5488-5496.
- Come, C., A. Cvrljevic, M. M. Khan, I. Treise, T. Adler, J. A. Aguilar-Pimentel, B. Au-Yeung, E. Sittig, T. D. Laajala, Y. Chen, S. Oeder, J. Calzada-Wack, M. Horsch, T. Aittokallio, D. H. Busch, M. W. Ollert, F. Neff, J. Beckers, V. Gailus-Durner, H. Fuchs, M. Hrabě

- de Angelis, Z. Chen, R. Lahesmaa and J. Westermarck (2016). "CIP2A Promotes T-Cell Activation and Immune Response to *Listeria monocytogenes* Infection." PLoS One **11**(4): e0152996.
- Cook, M. C., C. G. Vinuesa and C. C. Goodnow (2006). "ENU-mutagenesis: insight into immune function and pathology." Curr Opin Immunol **18**(5): 627-633.
- Cruz, M., L. A. Elenich, T. A. Smolarek, A. G. Menon and J. J. Monaco (1997). "DNA sequence, chromosomal localization, and tissue expression of the mouse proteasome subunit Imp10 (Psm10) gene." Genomics **45**(3): 618-622.
- Dahlmann, B., T. Ruppert, L. Kuehn, S. Merforth and P. M. Kloetzel (2000). "Different proteasome subtypes in a single tissue exhibit different enzymatic properties." J Mol Biol **303**(5): 643-653.
- Dahlqvist, J., J. Klar, N. Tiwari, J. Schuster, H. Torma, J. Badhai, R. Pujol, M. A. van Steensel, T. Brinkhuizen, L. Gijezen, A. Chaves, G. Tadini, A. Vahlquist and N. Dahl (2010). "A single-nucleotide deletion in the POMP 5' UTR causes a transcriptional switch and altered epidermal proteasome distribution in KLICK genodermatosis." Am J Hum Genet **86**(4): 596-603.
- Dalton, D. K., S. Pitts-Meek, S. Keshav, I. S. Figari, A. Bradley and T. A. Stewart (1993). "Multiple defects of immune cell function in mice with disrupted interferon-gamma genes." Science **259**(5102): 1739-1742.
- De, M., K. Jayarapu, L. Elenich, J. J. Monaco, R. A. Colbert and T. A. Griffin (2003). "Beta 2 subunit propeptides influence cooperative proteasome assembly." J Biol Chem **278**(8): 6153-6159.
- DeGrendele, H. C., P. Estess and M. H. Siegelman (1997). "Requirement for CD44 in activated T cell extravasation into an inflammatory site." Science **278**(5338): 672-675.
- Dinarello, C. A. (1984). "Interleukin-1 and the pathogenesis of the acute-phase response." N Engl J Med **311**(22): 1413-1418.
- Dinarello, C. A. (2011). "A clinical perspective of IL-1beta as the gatekeeper of inflammation." Eur J Immunol **41**(5): 1203-1217.
- Ditzel, L., R. Huber, K. Mann, W. Heinemeyer, D. H. Wolf and M. Groll (1998). "Conformational constraints for protein self-cleavage in the proteasome." J Mol Biol **279**(5): 1187-1191.
- Ema, H., K. Sudo, J. Seita, A. Matsubara, Y. Morita, M. Osawa, K. Takatsu, S. Takaki and H. Nakauchi (2005). "Quantification of self-renewal capacity in single hematopoietic stem cells from normal and Lnk-deficient mice." Dev Cell **8**(6): 907-914.
- Epelman, S., K. J. Lavine and G. J. Randolph (2014). "Origin and functions of tissue macrophages." Immunity **41**(1): 21-35.
- Fagarasan, S., N. Watanabe and T. Honjo (2000). "Generation, expansion, migration and activation of mouse B1 cells." Immunol Rev **176**: 205-215.
- Fairfield, H., G. J. Gilbert, M. Barter, R. R. Corrigan, M. Curtain, Y. Ding, M. D'Ascenzo, D. J. Gerhardt, C. He, W. Huang, T. Richmond, L. Rowe, F. J. Probst, D. E. Bergstrom, S. A. Murray, C. Bult, J. Richardson, B. T. Kile, I. Gut, J. Hager, S. Sigurdsson, E. Mauceli, F. Di Palma, K. Lindblad-Toh, M. L. Cunningham, T. C. Cox, M. J. Justice, M. S. Spector, S. W. Lowe, T. Albert, L. R. Donahue, J. Jeddloh, J. Shendure and L. G.

- Reinholdt (2011). "Mutation discovery in mice by whole exome sequencing." Genome Biol **12**(9): R86.
- Fantuzzi, G., G. Ku, M. W. Harding, D. J. Livingston, J. D. Sipe, K. Kuida, R. A. Flavell and C. A. Dinarello (1997). "Response to local inflammation of IL-1 beta-converting enzyme- deficient mice." J Immunol **158**(4): 1818-1824.
- Fattori, E., M. Cappelletti, P. Costa, C. Sellitto, L. Cantoni, M. Carelli, R. Faggioni, G. Fantuzzi, P. Ghezzi and V. Poli (1994). "Defective inflammatory response in interleukin 6-deficient mice." J Exp Med **180**(4): 1243-1250.
- Fay, N. S., E. C. Larson and J. M. Jameson (2016). "Chronic Inflammation and gammadelta T Cells." Front Immunol **7**: 210.
- Fehling, H. J., W. Swat, C. Laplace, R. Kuhn, K. Rajewsky, U. Muller and H. von Boehmer (1994). "MHC class I expression in mice lacking the proteasome subunit LMP-7." Science **265**(5176): 1234-1237.
- Feng, X., T. Holmlund, C. Zheng and B. Fadeel (2014). "Proapoptotic effects of the novel proteasome inhibitor b-AP15 on multiple myeloma cells and natural killer cells." Exp Hematol **42**(3): 172-182.
- Finley, D. (2009). "Recognition and processing of ubiquitin-protein conjugates by the proteasome." Annu Rev Biochem **78**: 477-513.
- Fitzpatrick, L. R., J. S. Small, L. S. Poritz, K. J. McKenna and W. A. Koltun (2007). "Enhanced intestinal expression of the proteasome subunit low molecular mass polypeptide 2 in patients with inflammatory bowel disease." Dis Colon Rectum **50**(3): 337-348; discussion 348-350.
- Flaswinkel, H., F. Alessandrini, B. Rathkolb, T. Decker, E. Kremmer, A. Servatius, T. Jakob, D. Soewarto, S. Marschall, C. Fella, H. Behrendt, J. Ring, E. Wolf, R. Balling, M. Hrabě de Angelis and K. Pfeffer (2000). "Identification of immunological relevant phenotypes in ENU mutagenized mice." Mamm Genome **11**(7): 526-527.
- Fuchs, H., V. Gailus-Durner, S. Neschen, T. Adler, L. C. Afonso, J. A. Aguilar-Pimentel, L. Becker, A. Bohla, J. Calzada-Wack, C. Cohrs, A. Dewert, B. Fridrich, L. Garrett, L. Glasl, A. Gotz, W. Hans, S. M. Holter, M. Horsch, A. Hurt, E. Janas, D. Janik, M. Kahle, M. Kistler, T. Klein-Rodewald, C. Lengger, T. Ludwig, H. Maier, S. Marschall, K. Micklich, G. Moller, B. Naton, C. Prehn, O. Puk, I. Racz, M. Rass, B. Rathkolb, J. Rozman, M. Scheerer, E. Schiller, A. Schrewe, R. Steinkamp, C. Stoger, M. Sun, W. Szymczak, I. Treise, I. L. Vargas Panesso, A. M. Vernaleken, M. Willershauser, A. Wolff-Muscate, R. Zeh, J. Adamski, J. Beckers, R. Bekeredjian, D. H. Busch, O. Eickelberg, J. Favor, J. Graw, H. Hofler, C. Hoschen, H. Katus, M. Klingenspor, T. Klopstock, F. Neff, M. Ollert, H. Schulz, T. Stoger, E. Wolf, W. Wurst, A. O. Yildirim, A. Zimmer and M. Hrabě de Angelis (2012). "Innovations in phenotyping of mouse models in the German Mouse Clinic." Mamm Genome **23**(9-10): 611-622.
- Gailus-Durner, V., H. Fuchs, L. Becker, I. Bolle, M. Brielmeier, J. Calzada-Wack, R. Elvert, N. Ehrhardt, C. Dalke, T. J. Franz, E. Grundner-Culemann, S. Hammelbacher, S. M. Holter, G. Holzlwimmer, M. Horsch, A. Javaheri, S. V. Kalaydjiev, M. Klempt, E. Kling, S. Kunder, C. Lengger, T. Lisse, T. Mijalski, B. Naton, V. Pedersen, C. Prehn, G. Przemeczek, I. Racz, C. Reinhard, P. Reitmeir, I. Schneider, A. Schrewe, R. Steinkamp, C. Zybill, J. Adamski, J. Beckers, H. Behrendt, J. Favor, J. Graw, G. Heldmaier, H. Hofler, B. Ivandic, H. Katus, P. Kirchhof, M. Klingenspor, T. Klopstock, A. Lengeling, W. Muller, F. Ohl, M. Ollert, L. Quintanilla-Martinez, J. Schmidt, H. Schulz, E. Wolf,

- W. Wurst, A. Zimmer, D. H. Busch and M. H. de Angelis (2005). "Introducing the German Mouse Clinic: open access platform for standardized phenotyping." Nat Methods **2**(6): 403-404.
- Galandrini, R., E. Galluzzo, N. Albi, C. E. Grossi and A. Velardi (1994). "Hyaluronate is costimulatory for human T cell effector functions and binds to CD44 on activated T cells." J Immunol **153**(1): 21-31.
- Gallastegui, N. and M. Groll (2010). "The 26S proteasome: assembly and function of a destructive machine." Trends Biochem Sci **35**(11): 634-642.
- Gao, S. Y., M. M. Jack and C. O'Neill (2012). "Towards optimising the production of and expression from polycistronic vectors in embryonic stem cells." PLoS One **7**(11): e48668.
- Garg, A., M. D. Hernandez, A. B. Sousa, L. Subramanyam, L. Martinez de Villarreal, H. G. dos Santos and O. Barboza (2010). "An autosomal recessive syndrome of joint contractures, muscular atrophy, microcytic anemia, and panniculitis-associated lipodystrophy." J Clin Endocrinol Metab **95**(9): E58-63.
- Geering, B., C. Stoeckle, S. Conus and H. U. Simon (2013). "Living and dying for inflammation: neutrophils, eosinophils, basophils." Trends Immunol **34**(8): 398-409.
- Geisberger, R., M. Lamers and G. Achatz (2006). "The riddle of the dual expression of IgM and IgD." Immunology **118**(4): 429-437.
- Geissmann, F., S. Jung and D. R. Littman (2003). "Blood monocytes consist of two principal subsets with distinct migratory properties." Immunity **19**(1): 71-82.
- Germain, R. N. (1994). "MHC-dependent antigen processing and peptide presentation: providing ligands for T lymphocyte activation." Cell **76**(2): 287-299.
- Germain, R. N. (2002). "T-cell development and the CD4-CD8 lineage decision." Nat Rev Immunol **2**(5): 309-322.
- Godfrey, D. I., K. J. Hammond, L. D. Poulton, M. J. Smyth and A. G. Baxter (2000). "NKT cells: facts, functions and fallacies." Immunol Today **21**(11): 573-583.
- Goldrath, A. W. and M. J. Bevan (1999). "Low-affinity ligands for the TCR drive proliferation of mature CD8+ T cells in lymphopenic hosts." Immunity **11**(2): 183-190.
- Goldrath, A. W., L. Y. Bogatzki and M. J. Bevan (2000). "Naive T cells transiently acquire a memory-like phenotype during homeostasis-driven proliferation." J Exp Med **192**(4): 557-564.
- Gomes, A. V. (2013). "Genetics of proteasome diseases." Scientifica **2013**: 637629.
- Gordon, S. M., J. Chaix, L. J. Rupp, J. Wu, S. Madera, J. C. Sun, T. Lindsten and S. L. Reiner (2012). "The transcription factors T-bet and Eomes control key checkpoints of natural killer cell maturation." Immunity **36**(1): 55-67.
- Griffin, T. A., D. Nandi, M. Cruz, H. J. Fehling, L. V. Kaer, J. J. Monaco and R. A. Colbert (1998). "Immunoproteasome assembly: cooperative incorporation of interferon gamma (IFN-gamma)-inducible subunits." J Exp Med **187**(1): 97-104.
- Groettrup, M., C. J. Kirk and M. Basler (2010). "Proteasomes in immune cells: more than peptide producers?" Nat Rev Immunol **10**(1): 73-78.

- Groettrup, M., R. Kraft, S. Kostka, S. Standera, R. Stohwasser and P. M. Kloetzel (1996). "A third interferon-gamma-induced subunit exchange in the 20S proteasome." Eur J Immunol **26**(4): 863-869.
- Groettrup, M., S. Standera, R. Stohwasser and P. M. Kloetzel (1997). "The subunits MECL-1 and LMP2 are mutually required for incorporation into the 20S proteasome." Proc Natl Acad Sci U S A **94**(17): 8970-8975.
- Grogan, J. L., M. Mohrs, B. Harmon, D. A. Lacy, J. W. Sedat and R. M. Locksley (2001). "Early transcription and silencing of cytokine genes underlie polarization of T helper cell subsets." Immunity **14**(3): 205-215.
- Groll, M., L. Ditzel, J. Lowe, D. Stock, M. Bochtler, H. D. Bartunik and R. Huber (1997). "Structure of 20S proteasome from yeast at 2.4 Å resolution." Nature **386**(6624): 463-471.
- Groll, M., W. Heinemeyer, S. Jager, T. Ullrich, M. Bochtler, D. H. Wolf and R. Huber (1999). "The catalytic sites of 20S proteasomes and their role in subunit maturation: a mutational and crystallographic study." Proc Natl Acad Sci U S A **96**(20): 10976-10983.
- Guillaume, B., J. Chapiro, V. Stroobant, D. Colau, B. Van Holle, G. Parvizi, M. P. Bousquet-Dubouch, I. Theate, N. Parmentier and B. J. Van den Eynde (2010). "Two abundant proteasome subtypes that uniquely process some antigens presented by HLA class I molecules." Proc Natl Acad Sci U S A **107**(43): 18599-18604.
- Gumley, T. P., I. F. McKenzie and M. S. Sandrin (1995). "Tissue expression, structure and function of the murine Ly-6 family of molecules." Immunol Cell Biol **73**(4): 277-296.
- Haluszczak, C., A. D. Akue, S. E. Hamilton, L. D. Johnson, L. Pujanauski, L. Teodorovic, S. C. Jameson and R. M. Kedl (2009). "The antigen-specific CD8⁺ T cell repertoire in unimmunized mice includes memory phenotype cells bearing markers of homeostatic expansion." J Exp Med **206**(2): 435-448.
- Hanninen, A., M. Maksimow, C. Alam, D. J. Morgan and S. Jalkanen (2011). "Ly6C supports preferential homing of central memory CD8⁺ T cells into lymph nodes." Eur J Immunol **41**(3): 634-644.
- Hayakawa, K., R. R. Hardy, D. R. Parks and L. A. Herzenberg (1983). "The "Ly-1 B" cell subpopulation in normal immunodeficient, and autoimmune mice." J Exp Med **157**(1): 202-218.
- Heinemeyer, W., M. Fischer, T. Krimmer, U. Stachon and D. H. Wolf (1997). "The active sites of the eukaryotic 20 S proteasome and their involvement in subunit precursor processing." J Biol Chem **272**(40): 25200-25209.
- Heink, S., D. Ludwig, P. M. Kloetzel and E. Kruger (2005). "IFN-gamma-induced immune adaptation of the proteasome system is an accelerated and transient response." Proc Natl Acad Sci U S A **102**(26): 9241-9246.
- Henderson, R. B., J. A. Hobbs, M. Mathies and N. Hogg (2003). "Rapid recruitment of inflammatory monocytes is independent of neutrophil migration." Blood **102**(1): 328-335.
- Hershko, A., A. Ciechanover and A. Varshavsky (2000). "Basic Medical Research Award. The ubiquitin system." Nat Med **6**(10): 1073-1081.

- Hilton, J. M., M. A. Lewis, M. Grati, N. Ingham, S. Pearson, R. A. Laskowski, D. J. Adams and K. P. Steel (2011). "Exome sequencing identifies a missense mutation in *Isl1* associated with low penetrance otitis media in dearisch mice." Genome Biol **12**(9): R90.
- Hirai, H., P. Zhang, T. Dayaram, C. J. Hetherington, S. Mizuno, J. Imanishi, K. Akashi and D. G. Tenen (2006). "C/EBPbeta is required for 'emergency' granulopoiesis." Nat Immunol **7**(7): 732-739.
- Hirano, Y., T. Kaneko, K. Okamoto, M. Bai, H. Yashiroda, K. Furuyama, K. Kato, K. Tanaka and S. Murata (2008). "Dissecting beta-ring assembly pathway of the mammalian 20S proteasome." EMBO J **27**(16): 2204-2213.
- Hori, S., T. Nomura and S. Sakaguchi (2003). "Control of regulatory T cell development by the transcription factor Foxp3." Science **299**(5609): 1057-1061.
- Hoyne, G. F. and C. C. Goodnow (2006). "The use of genomewide ENU mutagenesis screens to unravel complex mammalian traits: identifying genes that regulate organ-specific and systemic autoimmunity." Immunol Rev **210**: 27-39.
- Hrabě de Angelis, M. H., H. Flaswinkel, H. Fuchs, B. Rathkolb, D. Soewarto, S. Marschall, S. Heffner, W. Pargent, K. Wuensch, M. Jung, A. Reis, T. Richter, F. Alessandrini, T. Jakob, E. Fuchs, H. Kolb, E. Kremmer, K. Schaeble, B. Rollinski, A. Roscher, C. Peters, T. Meitinger, T. Strom, T. Steckler, F. Holsboer, T. Klopstock, F. Gekeler, C. Schindewolf, T. Jung, K. Avraham, H. Behrendt, J. Ring, A. Zimmer, K. Schughart, K. Pfeffer, E. Wolf and R. Balling (2000). "Genome-wide, large-scale production of mutant mice by ENU mutagenesis." Nat Genet **25**(4): 444-447.
- Huang, S., W. Hendriks, A. Althage, S. Hemmi, H. Bluethmann, R. Kamijo, J. Vilcek, R. M. Zinkernagel and M. Aguet (1993). "Immune response in mice that lack the interferon-gamma receptor." Science **259**(5102): 1742-1745.
- Huber, E. M., M. Basler, R. Schwab, W. Heinemeyer, C. J. Kirk, M. Groettrup and M. Groll (2012). "Immuno- and constitutive proteasome crystal structures reveal differences in substrate and inhibitor specificity." Cell **148**(4): 727-738.
- Huster, K. M., V. Busch, M. Schiemann, K. Linkemann, K. M. Kerksiek, H. Wagner and D. H. Busch (2004). "Selective expression of IL-7 receptor on memory T cells identifies early CD40L-dependent generation of distinct CD8+ memory T cell subsets." Proc Natl Acad Sci U S A **101**(15): 5610-5615.
- Inui, M., M. Miyado, M. Igarashi, M. Tamano, A. Kubo, S. Yamashita, H. Asahara, M. Fukami and S. Takada (2014). "Rapid generation of mouse models with defined point mutations by the CRISPR/Cas9 system." Sci Rep **4**: 5396.
- Jaakkola, I., M. Merinen, S. Jalkanen and A. Hanninen (2003). "Ly6C induces clustering of LFA-1 (CD11a/CD18) and is involved in subtype-specific adhesion of CD8 T cells." J Immunol **170**(3): 1283-1290.
- Jager, S., M. Groll, R. Huber, D. H. Wolf and W. Heinemeyer (1999). "Proteasome beta-type subunits: unequal roles of propeptides in core particle maturation and a hierarchy of active site function." J Mol Biol **291**(4): 997-1013.
- Joliat, M. J. and L. D. Shultz (2001). "The molecular bases of spontaneous immunological mutations in the mouse and their homologous human diseases." Clin Immunol **101**(2): 113-129.

- Joosten, L. A., M. G. Netea and C. A. Dinarello (2013). "Interleukin-1beta in innate inflammation, autophagy and immunity." *Semin Immunol* **25**(6): 416-424.
- Justice, M. J., J. K. Noveroske, J. S. Weber, B. Zheng and A. Bradley (1999). "Mouse ENU mutagenesis." *Hum Mol Genet* **8**(10): 1955-1963.
- Karasuyama, H., K. Obata, T. Wada, Y. Tsujimura and K. Mukai (2011). "Newly appreciated roles for basophils in allergy and protective immunity." *Allergy* **66**(9): 1133-1141.
- Karlhofer, F. M. and W. M. Yokoyama (1991). "Stimulation of murine natural killer (NK) cells by a monoclonal antibody specific for the NK1.1 antigen. IL-2-activated NK cells possess additional specific stimulation pathways." *J Immunol* **146**(10): 3662-3673.
- Keays, D. A., T. G. Clark and J. Flint (2006). "Estimating the number of coding mutations in genotypic- and phenotypic-driven N-ethyl-N-nitrosourea (ENU) screens." *Mamm Genome* **17**(3): 230-238.
- Kincaid, E. Z., J. W. Che, I. York, H. Escobar, E. Reyes-Vargas, J. C. Delgado, R. M. Welsh, M. L. Karow, A. J. Murphy, D. M. Valenzuela, G. D. Yancopoulos and K. L. Rock (2012). "Mice completely lacking immunoproteasomes show major changes in antigen presentation." *Nat Immunol* **13**(2): 129-135.
- King, C., A. Ilic, K. Koelsch and N. Sarvetnick (2004). "Homeostatic expansion of T cells during immune insufficiency generates autoimmunity." *Cell* **117**(2): 265-277.
- Kish-Trier, E. and C. P. Hill (2013). "Structural biology of the proteasome." *Annu Rev Biophys* **42**: 29-49.
- Kitamura, A., Y. Maekawa, H. Uehara, K. Izumi, I. Kawachi, M. Nishizawa, Y. Toyoshima, H. Takahashi, D. M. Standley, K. Tanaka, J. Hamazaki, S. Murata, K. Obara, I. Toyoshima and K. Yasutomo (2011). "A mutation in the immunoproteasome subunit PSMB8 causes autoinflammation and lipodystrophy in humans." *J Clin Invest* **121**(10): 4150-4160.
- Klaften, M. and M. Hrabě de Angelis (2005). "ARTS: a web-based tool for the set-up of high-throughput genome-wide mapping panels for the SNP genotyping of mouse mutants." *Nucleic Acids Res* **33**(Web Server issue): W496-500.
- Klare, N., M. Seeger, K. Janek, P. R. Jungblut and B. Dahlmann (2007). "Intermediate-type 20 S proteasomes in HeLa cells: "asymmetric" subunit composition, diversity and adaptation." *J Mol Biol* **373**(1): 1-10.
- Klymiuk, I., L. Kenner, T. Adler, D. H. Busch, A. Boersma, M. Irmeler, B. Fridrich, V. Gailus-Durner, H. Fuchs, N. Leitner, M. Muller, R. Kuhn, M. Schleder, I. Treise, M. H. de Angelis and J. Beckers (2012). "In vivo functional requirement of the mouse Ifitm1 gene for germ cell development, interferon mediated immune response and somitogenesis." *PLoS One* **7**(10): e44609.
- Knop, M., K. Siegers, G. Pereira, W. Zachariae, B. Winsor, K. Nasmyth and E. Schiebel (1999). "Epitope tagging of yeast genes using a PCR-based strategy: more tags and improved practical routines." *Yeast* **15**(10B): 963-972.
- Kondo, M., I. L. Weissman and K. Akashi (1997). "Identification of clonogenic common lymphoid progenitors in mouse bone marrow." *Cell* **91**(5): 661-672.

- Kopf, M., H. Baumann, G. Freer, M. Freudenberg, M. Lamers, T. Kishimoto, R. Zinkernagel, H. Bluethmann and G. Kohler (1994). "Impaired immune and acute-phase responses in interleukin-6-deficient mice." *Nature* **368**(6469): 339-342.
- Korner, H., T. H. Winkler, J. D. Sedgwick, M. Rollinghoff, A. Basten and M. C. Cook (2001). "Recirculating and marginal zone B cell populations can be established and maintained independently of primary and secondary follicles." *Immunol Cell Biol* **79**(1): 54-61.
- Kronenberg, M. (2005). "Toward an understanding of NKT cell biology: progress and paradoxes." *Annu Rev Immunol* **23**: 877-900.
- Kunjappu, M. J. and M. Hochstrasser (2014). "Assembly of the 20S proteasome." *Biochim Biophys Acta* **1843**(1): 2-12.
- Lagasse, E. and I. L. Weissman (1996). "Flow cytometric identification of murine neutrophils and monocytes." *J Immunol Methods* **197**(1-2): 139-150.
- Laufer, T. M., J. DeKoning, J. S. Markowitz, D. Lo and L. H. Glimcher (1996). "Unopposed positive selection and autoreactivity in mice expressing class II MHC only on thymic cortex." *Nature* **383**(6595): 81-85.
- Lee, C. K., R. Gimeno and D. E. Levy (1999). "Differential regulation of constitutive major histocompatibility complex class I expression in T and B lymphocytes." *J Exp Med* **190**(10): 1451-1464.
- Lee, W. and K. B. Kim (2011). "The immunoproteasome: an emerging therapeutic target." *Curr Top Med Chem* **11**(23): 2923-2930.
- Lemischka, I. R. and K. A. Moore (2003). "Stem cells: interactive niches." *Nature* **425**(6960): 778-779.
- Lemoli, R. M. and A. D'Addio (2008). "Hematopoietic stem cell mobilization." *Haematologica* **93**(3): 321-324.
- Lennon-Dumenil, A. M., A. H. Bakker, P. Wolf-Bryant, H. L. Ploegh and C. Lagaudriere-Gesbert (2002). "A closer look at proteolysis and MHC-class-II-restricted antigen presentation." *Curr Opin Immunol* **14**(1): 15-21.
- Li, X., A. R. Kusmierczyk, P. Wong, A. Emili and M. Hochstrasser (2007). "beta-Subunit appendages promote 20S proteasome assembly by overcoming an Ump1-dependent checkpoint." *The EMBO journal* **26**(9): 2339-2349.
- Liu, Y., Y. Ramot, A. Torrelo, A. S. Paller, N. Si, S. Babay, P. W. Kim, A. Sheikh, C. C. Lee, Y. Chen, A. Vera, X. Zhang, R. Goldbach-Mansky and A. Zlotogorski (2012). "Mutations in proteasome subunit beta type 8 cause chronic atypical neutrophilic dermatosis with lipodystrophy and elevated temperature with evidence of genetic and phenotypic heterogeneity." *Arthritis Rheum* **64**(3): 895-907.
- Livak, F., M. Tourigny, D. G. Schatz and H. T. Petrie (1999). "Characterization of TCR gene rearrangements during adult murine T cell development." *J Immunol* **162**(5): 2575-2580.
- Lutz, C., B. Ledermann, M. H. Kosco-Vilbois, A. F. Ochsenbein, R. M. Zinkernagel, G. Kohler and F. Brombacher (1998). "IgD can largely substitute for loss of IgM function in B cells." *Nature* **393**(6687): 797-801.
- Lynch, R. M., S. Naswa, G. L. Rogers, Jr., S. A. Kania, S. Das, E. J. Chesler, A. M. Saxton, M. A. Langston and B. H. Voy (2010). "Identifying genetic loci and spleen gene

- coexpression networks underlying immunophenotypes in BXD recombinant inbred mice." *Physiol Genomics* **41**(3): 244-253.
- Majetschak, M., M. Perez, L. T. Sorell, J. Lam, M. E. Maldonado and R. W. Hoffman (2008). "Circulating 20S proteasome levels in patients with mixed connective tissue disease and systemic lupus erythematosus." *Clin Vaccine Immunol* **15**(9): 1489-1493.
- Malek, T. R. and I. Castro (2010). "Interleukin-2 receptor signaling: at the interface between tolerance and immunity." *Immunity* **33**(2): 153-165.
- Mali, P., J. Aach, P. B. Stranges, K. M. Esvelt, M. Moosburner, S. Kosuri, L. Yang and G. M. Church (2013). "CAS9 transcriptional activators for target specificity screening and paired nickases for cooperative genome engineering." *Nat Biotechnol* **31**(9): 833-838.
- Manz, M. G. and S. Boettcher (2014). "Emergency granulopoiesis." *Nat Rev Immunol* **14**(5): 302-314.
- Marques, A. J., R. Palanimurugan, A. C. Matias, P. C. Ramos and R. J. Dohmen (2009). "Catalytic mechanism and assembly of the proteasome." *Chem Rev* **109**(4): 1509-1536.
- Martina, M. N., S. Noel, A. Saxena, H. Rabb and A. R. Hamad (2015). "Double negative (DN) alphabeta T cells: misperception and overdue recognition." *Immunol Cell Biol* **93**(3): 305-310.
- Masopust, D., V. Vezys, E. J. Usherwood, L. S. Cauley, S. Olson, A. L. Marzo, R. L. Ward, D. L. Woodland and L. Lefrancois (2004). "Activated primary and memory CD8 T cells migrate to nonlymphoid tissues regardless of site of activation or tissue of origin." *J Immunol* **172**(8): 4875-4882.
- McDonald, B., K. Pittman, G. B. Menezes, S. A. Hirota, I. Slaba, C. C. Waterhouse, P. L. Beck, D. A. Muruve and P. Kubers (2010). "Intravascular danger signals guide neutrophils to sites of sterile inflammation." *Science* **330**(6002): 362-366.
- McHeyzer-Williams, L. J. and M. G. McHeyzer-Williams (2004). "Developmentally distinct Th cells control plasma cell production in vivo." *Immunity* **20**(2): 231-242.
- McHeyzer-Williams, L. J. and M. G. McHeyzer-Williams (2005). "Antigen-specific memory B cell development." *Annu Rev Immunol* **23**: 487-513.
- Mestas, J. and C. C. Hughes (2004). "Of mice and not men: differences between mouse and human immunology." *J Immunol* **172**(5): 2731-2738.
- Metzker, M. L. (2010). "Sequencing technologies - the next generation." *Nat Rev Genet* **11**(1): 31-46.
- Moebius, J., M. van den Broek, M. Groettrup and M. Basler (2010). "Immunoproteasomes are essential for survival and expansion of T cells in virus-infected mice." *Eur J Immunol* **40**(12): 3439-3449.
- Mombaerts, P., J. Iacomini, R. S. Johnson, K. Herrup, S. Tonegawa and V. E. Papaioannou (1992). "RAG-1-deficient mice have no mature B and T lymphocytes." *Cell* **68**(5): 869-877.
- Morrison, S. J., A. M. Wandycz, H. D. Hemmati, D. E. Wright and I. L. Weissman (1997). "Identification of a lineage of multipotent hematopoietic progenitors." *Development* **124**(10): 1929-1939.

- Morrison, S. J. and I. L. Weissman (1994). "The long-term repopulating subset of hematopoietic stem cells is deterministic and isolatable by phenotype." *Immunity* **1**(8): 661-673.
- Muchamuel, T., M. Basler, M. A. Aujay, E. Suzuki, K. W. Kalim, C. Lauer, C. Sylvain, E. R. Ring, J. Shields, J. Jiang, P. Shwonek, F. Parlatti, S. D. Demo, M. K. Bennett, C. J. Kirk and M. Groettrup (2009). "A selective inhibitor of the immunoproteasome subunit LMP7 blocks cytokine production and attenuates progression of experimental arthritis." *Nat Med* **15**(7): 781-787.
- Mukai, K., K. Matsuoka, C. Taya, H. Suzuki, H. Yokozeki, K. Nishioka, K. Hirokawa, M. Etori, M. Yamashita, T. Kubota, Y. Minegishi, H. Yonekawa and H. Karasuyama (2005). "Basophils play a critical role in the development of IgE-mediated chronic allergic inflammation independently of T cells and mast cells." *Immunity* **23**(2): 191-202.
- Murali-Krishna, K., L. L. Lau, S. Sambhara, F. Lemonnier, J. Altman and R. Ahmed (1999). "Persistence of memory CD8 T cells in MHC class I-deficient mice." *Science* **286**(5443): 1377-1381.
- Murata, S., K. Sasaki, T. Kishimoto, S. Niwa, H. Hayashi, Y. Takahama and K. Tanaka (2007). "Regulation of CD8+ T cell development by thymus-specific proteasomes." *Science* **316**(5829): 1349-1353.
- Murata, S., Y. Takahama and K. Tanaka (2008). "Thymoproteasome: probable role in generating positively selecting peptides." *Curr Opin Immunol* **20**(2): 192-196.
- Murata, S., H. Yashiroda and K. Tanaka (2009). "Molecular mechanisms of proteasome assembly." *Nat Rev Mol Cell Biol* **10**(2): 104-115.
- Murphy, K. M. and S. L. Reiner (2002). "The lineage decisions of helper T cells." *Nat Rev Immunol* **2**(12): 933-944.
- Nandi, D., H. Jiang and J. J. Monaco (1996). "Identification of MECL-1 (LMP-10) as the third IFN-gamma-inducible proteasome subunit." *J Immunol* **156**(7): 2361-2364.
- Nandi, D., E. Woodward, D. B. Ginsburg and J. J. Monaco (1997). "Intermediates in the formation of mouse 20S proteasomes: implications for the assembly of precursor beta subunits." *EMBO J* **16**(17): 5363-5375.
- Nathan, C. (2006). "Neutrophils and immunity: challenges and opportunities." *Nat Rev Immunol* **6**(3): 173-182.
- Nehls, M., B. Kyewski, M. Messerle, R. Waldschutz, K. Schuddekopf, A. J. Smith and T. Boehm (1996). "Two genetically separable steps in the differentiation of thymic epithelium." *Science* **272**(5263): 886-889.
- Nelms, K. A. and C. C. Goodnow (2001). "Genome-wide ENU mutagenesis to reveal immune regulators." *Immunity* **15**(3): 409-418.
- Nil, A., E. Firat, V. Sobek, K. Eichmann and G. Niedermann (2004). "Expression of housekeeping and immunoproteasome subunit genes is differentially regulated in positively and negatively selecting thymic stroma subsets." *Eur J Immunol* **34**(10): 2681-2689.
- Nitta, T., S. Murata, K. Sasaki, H. Fujii, A. M. Ripen, N. Ishimaru, S. Koyasu, K. Tanaka and Y. Takahama (2010). "Thymoproteasome shapes immunocompetent repertoire of CD8+ T cells." *Immunity* **32**(1): 29-40.

- Nitta, T., R. Muro, Y. Shimizu, S. Nitta, H. Oda, Y. Ohte, M. Goto, R. Yanobu-Takanashi, T. Narita, H. Takayanagi, H. Yasuda, T. Okamura, S. Murata and H. Suzuki (2015). "The thymic cortical epithelium determines the TCR repertoire of IL-17-producing gammadeltaT cells." *EMBO Rep* **16**(5): 638-653.
- Notarangelo, L. D. (2010). "Primary immunodeficiencies." *J Allergy Clin Immunol* **125**(2 Suppl 2): S182-194.
- Nussbaum, A. K., M. P. Rodriguez-Carreno, N. Benning, J. Botten and J. L. Whitton (2005). "Immunoproteasome-deficient mice mount largely normal CD8+ T cell responses to lymphocytic choriomeningitis virus infection and DNA vaccination." *J Immunol* **175**(2): 1153-1160.
- Ohnmacht, C. and D. Voehringer (2009). "Basophil effector function and homeostasis during helminth infection." *Blood* **113**(12): 2816-2825.
- Orr, M. T. and L. L. Lanier (2010). "Natural killer cell education and tolerance." *Cell* **142**(6): 847-856.
- Osawa, M., K. Hanada, H. Hamada and H. Nakauchi (1996). "Long-term lymphohematopoietic reconstitution by a single CD34-low/negative hematopoietic stem cell." *Science* **273**(5272): 242-245.
- Pablos, J. L., E. T. Everett and J. S. Norris (2004). "The tight skin mouse: an animal model of systemic sclerosis." *Clin Exp Rheumatol* **22**(3 Suppl 33): S81-85.
- Pacholczyk, R., H. Ignatowicz, P. Kraj and L. Ignatowicz (2006). "Origin and T cell receptor diversity of Foxp3+CD4+CD25+ T cells." *Immunity* **25**(2): 249-259.
- Pamer, E. and P. Cresswell (1998). "Mechanisms of MHC class I-restricted antigen processing." *Annu Rev Immunol* **16**: 323-358.
- Pamer, E. G. (2004). "Immune responses to *Listeria monocytogenes*." *Nat Rev Immunol* **4**(10): 812-823.
- Pamer, E. G., A. J. Sijts, M. S. Villanueva, D. H. Busch and S. Vijn (1997). "MHC class I antigen processing of *Listeria monocytogenes* proteins: implications for dominant and subdominant CTL responses." *Immunol Rev* **158**: 129-136.
- Pandolfi, A., R. F. Stanley, Y. Yu, B. Bartholdy, G. Pendurti, K. Gritsman, J. Boulwood, J. Chernoff, A. Verma and U. Steidl (2015). "PAK1 is a therapeutic target in acute myeloid leukemia and myelodysplastic syndrome." *Blood* **126**(9): 1118-1127.
- Parvaneh, N., J. L. Casanova, L. D. Notarangelo and M. E. Conley (2013). "Primary immunodeficiencies: a rapidly evolving story." *J Allergy Clin Immunol* **131**(2): 314-323.
- Perry, J. S., C. W. Lio, A. L. Kau, K. Nutsch, Z. Yang, J. I. Gordon, K. M. Murphy and C. S. Hsieh (2014). "Distinct contributions of Aire and antigen-presenting-cell subsets to the generation of self-tolerance in the thymus." *Immunity* **41**(3): 414-426.
- Perry, S. S., L. J. Pierce, W. B. Slayton and G. J. Spangrude (2003). "Characterization of thymic progenitors in adult mouse bone marrow." *J Immunol* **170**(4): 1877-1886.
- Petkova, S. B., R. Yuan, S. W. Tsaih, W. Schott, D. C. Roopenian and B. Paigen (2008). "Genetic influence on immune phenotype revealed strain-specific variations in peripheral blood lineages." *Physiol Genomics* **34**(3): 304-314.

- Petrie, H. T. and J. C. Zuniga-Pflucker (2007). "Zoned out: functional mapping of stromal signaling microenvironments in the thymus." Annu Rev Immunol **25**: 649-679.
- Pozzi, B., S. Amodio, C. Lucano, A. Sciallo, S. Ronzoni, D. Castelletti, T. Adler, I. Treise, I. H. Betsholtz, B. Rathkolb, D. H. Busch, E. Wolf, H. Fuchs, V. Gailus-Durner, M. H. de Angelis, C. Betsholtz, S. Casola, P. P. Di Fiore and N. Offenhauser (2012). "The endocytic adaptor Eps15 controls marginal zone B cell numbers." PLoS One **7**(11): e50818.
- Pronk, C. J., D. J. Rossi, R. Mansson, J. L. Attema, G. L. Norddahl, C. K. Chan, M. Sigvardsson, I. L. Weissman and D. Bryder (2007). "Elucidation of the phenotypic, functional, and molecular topography of a myeloerythroid progenitor cell hierarchy." Cell Stem Cell **1**(4): 428-442.
- Ramos, P. C., A. J. Marques, M. K. London and R. J. Dohmen (2004). "Role of C-terminal extensions of subunits beta2 and beta7 in assembly and activity of eukaryotic proteasomes." J Biol Chem **279**(14): 14323-14330.
- Rathkolb, B., T. Decker, E. Fuchs, D. Soewarto, C. Fella, S. Heffner, W. Pargent, R. Wanke, R. Balling, M. Hrabě de Angelis, H. J. Kolb and E. Wolf (2000). "The clinical-chemical screen in the Munich ENU Mouse Mutagenesis Project: screening for clinically relevant phenotypes." Mamm Genome **11**(7): 543-546.
- Rathkolb, B., E. Fuchs, H. J. Kolb, I. Renner-Muller, O. Krebs, R. Balling, M. Hrabě de Angelis and E. Wolf (2000). "Large-scale N-ethyl-N-nitrosourea mutagenesis of mice--from phenotypes to genes." Exp Physiol **85**(6): 635-644.
- Reiner, S. L., F. Sallusto and A. Lanzavecchia (2007). "Division of labor with a workforce of one: challenges in specifying effector and memory T cell fate." Science **317**(5838): 622-625.
- Reis, J., F. Hassan, X. Q. Guan, J. Shen, J. J. Monaco, C. J. Papasian, A. A. Qureshi, C. W. Van Way, 3rd, S. N. Vogel, D. C. Morrison and N. Qureshi (2011). "The immunoproteasomes regulate LPS-induced TRIF/TRAM signaling pathway in murine macrophages." Cell Biochem Biophys **60**(1-2): 119-126.
- Reynaud, C. A., M. Descatoire, I. Dogan, F. Huetz, S. Weller and J. C. Weill (2012). "IgM memory B cells: a mouse/human paradox." Cell Mol Life Sci **69**(10): 1625-1634.
- Rieger, M. A., B. M. Smejkal and T. Schroeder (2009). "Improved prospective identification of megakaryocyte-erythrocyte progenitor cells." Br J Haematol **144**(3): 448-451.
- Rivas, D., L. Mozo, J. Zamorano, A. Gayo, J. C. Torre-Alonso, A. Rodriguez and C. Gutierrez (1995). "Upregulated expression of IL-4 receptors and increased levels of IL-4 in rheumatoid arthritis patients." J Autoimmun **8**(4): 587-600.
- Robinson, J. P. and W. O. Carter (1993). Flow cytometric analysis of granulocytes. Clin Flow Cytom Princ Appl. K. D. Bauer, Williams & Wilkins, Baltimore: 405-433.
- Rock, K. L., E. Latz, F. Ontiveros and H. Kono (2010). "The sterile inflammatory response." Annu Rev Immunol **28**: 321-342.
- Rockwell, C. E., J. J. Monaco and N. Qureshi (2012). "A critical role for the inducible proteasomal subunits LMP7 and MECL1 in cytokine production by activated murine splenocytes." Pharmacology **89**(3-4): 117-126.

- Rode, I. and T. Boehm (2012). "Regenerative capacity of adult cortical thymic epithelial cells." Proc Natl Acad Sci U S A **109**(9): 3463-3468.
- Rolink, A., E. ten Boekel, F. Melchers, D. T. Fearon, I. Krop and J. Andersson (1996). "A subpopulation of B220+ cells in murine bone marrow does not express CD19 and contains natural killer cell progenitors." J Exp Med **183**(1): 187-194.
- Rose, S., A. Misharin and H. Perlman (2012). "A novel Ly6C/Ly6G-based strategy to analyze the mouse splenic myeloid compartment." Cytometry A **81**(4): 343-350.
- Rothenberg, M. E. and S. P. Hogan (2006). "The eosinophil." Annu Rev Immunol **24**: 147-174.
- Rowe, S. J., L. Allen, V. C. Ridger, P. G. Hellewell and M. K. Whyte (2002). "Caspase-1-deficient mice have delayed neutrophil apoptosis and a prolonged inflammatory response to lipopolysaccharide-induced acute lung injury." J Immunol **169**(11): 6401-6407.
- Rubtsov, Y. P., R. E. Niec, S. Josefowicz, L. Li, J. Darce, D. Mathis, C. Benoist and A. Y. Rudensky (2010). "Stability of the regulatory T cell lineage in vivo." Science **329**(5999): 1667-1671.
- Russell, J. H. and T. J. Ley (2002). "Lymphocyte-mediated cytotoxicity." Annu Rev Immunol **20**: 323-370.
- Rutschmann, S. and K. Hoebe (2008). "Dissecting innate immunity by germline mutagenesis." Immunology **123**(4): 459-468.
- Sadik, C. D., N. D. Kim and A. D. Luster (2011). "Neutrophils cascading their way to inflammation." Trends Immunol **32**(10): 452-460.
- Sallusto, F., J. Geginat and A. Lanzavecchia (2004). "Central memory and effector memory T cell subsets: function, generation, and maintenance." Annu Rev Immunol **22**: 745-763.
- Sallusto, F., D. Lenig, R. Forster, M. Lipp and A. Lanzavecchia (1999). "Two subsets of memory T lymphocytes with distinct homing potentials and effector functions." Nature **401**(6754): 708-712.
- Sanger, F., S. Nicklen and A. R. Coulson (1977). "DNA sequencing with chain-terminating inhibitors." Proc Natl Acad Sci U S A **74**(12): 5463-5467
- Schatz, D. G., M. A. Oettinger and M. S. Schlissel (1992). "V(D)J recombination: molecular biology and regulation." Annu Rev Immunol **10**: 359-383.
- Scheffler, S., U. Kuckelkorn, K. Egerer, T. Dorner, K. Reiter, A. Soza, G. R. Burmester and E. Feist (2008). "Autoimmune reactivity against the 20S-proteasome includes immunosubunits LMP2 (beta1i), MECL1 (beta2i) and LMP7 (beta5i)." Rheumatology **47**(5): 622-626.
- Schroder, K., P. J. Hertzog, T. Ravasi and D. A. Hume (2004). "Interferon-gamma: an overview of signals, mechanisms and functions." J Leukoc Biol **75**(2): 163-189.
- Seifert, U., L. P. Bialy, F. Ebstein, D. Bech-Otschir, A. Voigt, F. Schroter, T. Prozorovski, N. Lange, J. Steffen, M. Rieger, U. Kuckelkorn, O. Aktas, P. M. Kloetzel and E. Kruger (2010). "Immunoproteasomes preserve protein homeostasis upon interferon-induced oxidative stress." Cell **142**(4): 613-624.

- Serbina, N. V., T. Jia, T. M. Hohl and E. G. Pamer (2008). "Monocyte-mediated defense against microbial pathogens." *Annu Rev Immunol* **26**: 421-452.
- Shen, B., W. Zhang, J. Zhang, J. Zhou, J. Wang, L. Chen, L. Wang, A. Hodgkins, V. Iyer, X. Huang and W. C. Skarnes (2014). "Efficient genome modification by CRISPR-Cas9 nickase with minimal off-target effects." *Nat Methods* **11**(4): 399-402.
- Shi, C. and E. G. Pamer (2011). "Monocyte recruitment during infection and inflammation." *Nat Rev Immunol* **11**(11): 762-774.
- Shivakumar, S., G. C. Tsokos and S. K. Datta (1989). "T cell receptor alpha/beta expressing double-negative (CD4-/CD8-) and CD4+ T helper cells in humans augment the production of pathogenic anti-DNA autoantibodies associated with lupus nephritis." *J Immunol* **143**(1): 103-112.
- Shultz, L. D. and C. L. Sidman (1987). "Genetically determined murine models of immunodeficiency." *Annu Rev Immunol* **5**: 367-403.
- Sidman, C. L., L. D. Shultz, R. R. Hardy, K. Hayakawa and L. A. Herzenberg (1986). "Production of immunoglobulin isotypes by Ly-1+ B cells in viable motheaten and normal mice." *Science* **232**(4756): 1423-1425.
- Sijts, E. J. and P. M. Kloetzel (2011). "The role of the proteasome in the generation of MHC class I ligands and immune responses." *Cell Mol Life Sci* **68**(9): 1491-1502.
- Slack, E., S. Hapfelmeier, B. Stecher, Y. Velykoredko, M. Stoel, M. A. Lawson, M. B. Geuking, B. Beutler, T. F. Tedder, W. D. Hardt, P. Bercik, E. F. Verdu, K. D. McCoy and A. J. Macpherson (2009). "Innate and adaptive immunity cooperate flexibly to maintain host-microbiota mutualism." *Science* **325**(5940): 617-620.
- Slifka, M. K., R. R. Pagarigan and J. L. Whitton (2000). "NK markers are expressed on a high percentage of virus-specific CD8+ and CD4+ T cells." *J Immunol* **164**(4): 2009-2015.
- Soewarto, D., M. Klaften and I. Rubio-Aliaga (2009). "Features and strategies of ENU mouse mutagenesis." *Curr Pharm Biotechnol* **10**(2): 198-213.
- Spangrude, G. J., S. Heimfeld and I. L. Weissman (1988). "Purification and characterization of mouse hematopoietic stem cells." *Science* **241**(4861): 58-62.
- Sriram, U., J. Xu, R. W. Chain, L. Varghese, M. Chakhtoura, H. L. Bennett, P. W. Zoltick and S. Gallucci (2014). "IL-4 suppresses the responses to TLR7 and TLR9 stimulation and increases the permissiveness to retroviral infection of murine conventional dendritic cells." *PLoS One* **9**(1): e87668.
- Starr, T. K., S. C. Jameson and K. A. Hogquist (2003). "Positive and negative selection of T cells." *Annu Rev Immunol* **21**: 139-176.
- Steeber, D. A., N. E. Green, S. Sato and T. F. Tedder (1996). "Lymphocyte migration in L-selectin-deficient mice. Altered subset migration and aging of the immune system." *J Immunol* **157**(3): 1096-1106.
- Stockinger, B. and M. Veldhoen (2007). "Differentiation and function of Th17 T cells." *Curr Opin Immunol* **19**(3): 281-286.
- Stohwasser, R., U. Kuckelkorn, R. Kraft, S. Kostka and P. M. Kloetzel (1996). "20S proteasome from LMP7 knock out mice reveals altered proteolytic activities and cleavage site preferences." *FEBS Lett* **383**(1-2): 109-113.

- Sumida, T., A. Sakamoto, H. Murata, Y. Makino, H. Takahashi, S. Yoshida, K. Nishioka, I. Iwamoto and M. Taniguchi (1995). "Selective reduction of T cells bearing invariant V alpha 24J alpha Q antigen receptor in patients with systemic sclerosis." *J Exp Med* **182**(4): 1163-1168.
- Sun, J. C., J. N. Beilke and L. L. Lanier (2009). "Adaptive immune features of natural killer cells." *Nature* **457**(7229): 557-561.
- Sun, M., K. Mondal, V. Patel, V. L. Horner, A. B. Long, D. J. Cutler, T. Caspary and M. E. Zwick (2012). "Multiplex Chromosomal Exome Sequencing Accelerates Identification of ENU-Induced Mutations in the Mouse." *G3* **2**(1): 143-150.
- Sunderkotter, C., T. Nikolic, M. J. Dillon, N. Van Rooijen, M. Stehling, D. A. Drevets and P. J. Leenen (2004). "Subpopulations of mouse blood monocytes differ in maturation stage and inflammatory response." *J Immunol* **172**(7): 4410-4417.
- Takada, K. and S. C. Jameson (2009). "Naive T cell homeostasis: from awareness of space to a sense of place." *Nat Rev Immunol* **9**(12): 823-832.
- Tanaka, M., N. Miyatani, S. Yamada, K. Miyashita, I. Toyoshima, K. Sakuma, K. Tanaka, T. Yuasa, T. Miyatake and T. Tsubaki (1993). "Hereditary lipo-muscular atrophy with joint contracture, skin eruptions and hyper-gamma-globulinemia: a new syndrome." *Intern Med* **32**(1): 42-45.
- Tomaru, U., A. Ishizu, S. Murata, Y. Miyatake, S. Suzuki, S. Takahashi, T. Kazamaki, J. Ohara, T. Baba, S. Iwasaki, K. Fugo, N. Otsuka, K. Tanaka and M. Kasahara (2009). "Exclusive expression of proteasome subunit {beta}5t in the human thymic cortex." *Blood* **113**(21): 5186-5191.
- Townsend, A. and J. Trowsdale (1993). "The transporters associated with antigen presentation." *Semin Cell Biol* **4**(1): 53-61.
- Ueda, Y., M. Kondo and G. Kelsoe (2005). "Inflammation and the reciprocal production of granulocytes and lymphocytes in bone marrow." *J Exp Med* **201**(11): 1771-1780.
- Van den Eynde, B. J. and S. Morel (2001). "Differential processing of class-I-restricted epitopes by the standard proteasome and the immunoproteasome." *Curr Opin Immunol* **13**(2): 147-153.
- Van Kaer, L., P. G. Ashton-Rickardt, M. Eichelberger, M. Gaczynska, K. Nagashima, K. L. Rock, A. L. Goldberg, P. C. Doherty and S. Tonegawa (1994). "Altered peptidase and viral-specific T cell response in LMP2 mutant mice." *Immunity* **1**(7): 533-541.
- Villadangos, J. A. (2001). "Presentation of antigens by MHC class II molecules: getting the most out of them." *Mol Immunol* **38**(5): 329-346.
- Wada, K., Y. Wada, F. Ishibashi, T. Gojobori and T. Ikemura (1992). "Codon usage tabulated from the GenBank genetic sequence data." *Nucleic Acids Res* **20 Suppl**: 2111-2118.
- Walunas, T. L., D. S. Bruce, L. Dustin, D. Y. Loh and J. A. Bluestone (1995). "Ly-6C is a marker of memory CD8+ T cells." *J Immunol* **155**(4): 1873-1883.
- Walzer, T., M. Blery, J. Chaix, N. Fuseri, L. Chasson, S. H. Robbins, S. Jaeger, P. Andre, L. Gauthier, L. Daniel, K. Chemin, Y. Morel, M. Dalod, J. Imbert, M. Pierres, A. Moretta, F. Romagne and E. Vivier (2007). "Identification, activation, and selective in vivo ablation of mouse NK cells via NKp46." *Proc Natl Acad Sci U S A* **104**(9): 3384-3389.

- Wang, X., A. Ottosson, C. Ji, X. Feng, M. Nordenskjold, J. I. Henter, B. Fadeel and C. Zheng (2009). "Proteasome inhibition induces apoptosis in primary human natural killer cells and suppresses NKp46-mediated cytotoxicity." *Haematologica* **94**(4): 470-478.
- Weissman, I. L. (2000). "Stem cells: units of development, units of regeneration, and units in evolution." *Cell* **100**(1): 157-168.
- Williams, L. M. and A. Y. Rudensky (2007). "Maintenance of the Foxp3-dependent developmental program in mature regulatory T cells requires continued expression of Foxp3." *Nat Immunol* **8**(3): 277-284.
- Williams, M. A. and M. J. Bevan (2007). "Effector and memory CTL differentiation." *Annu Rev Immunol* **25**: 171-192.
- Wilson, A., E. Laurenti, G. Oser, R. C. van der Wath, W. Blanco-Bose, M. Jaworski, S. Offner, C. F. Dunant, L. Eshkind, E. Bockamp, P. Lio, H. R. Macdonald and A. Trumpp (2008). "Hematopoietic stem cells reversibly switch from dormancy to self-renewal during homeostasis and repair." *Cell* **135**(6): 1118-1129.
- Wittwer, C. T., G. H. Reed, C. N. Gundry, J. G. Vandersteen and R. J. Pryor (2003). "High-resolution genotyping by amplicon melting analysis using LCGreen." *Clin Chem* **49**(6 Pt 1): 853-860.
- Wojdasiewicz, P., L. A. Poniatowski and D. Szukiewicz (2014). "The Role of Inflammatory and Anti-Inflammatory Cytokines in the Pathogenesis of Osteoarthritis." *Mediators Inflamm* **2014**: 561459.
- Woodland, D. L. and R. W. Dutton (2003). "Heterogeneity of CD4(+) and CD8(+) T cells." *Curr Opin Immunol* **15**(3): 336-342.
- Xing, Y., S. C. Jameson and K. A. Hogquist (2013). "Thymoproteasome subunit-beta5T generates peptide-MHC complexes specialized for positive selection." *Proc Natl Acad Sci U S A* **110**(17): 6979-6984.
- Yokoyama, W. M. and S. Kim (2006). "Licensing of natural killer cells by self-major histocompatibility complex class I." *Immunol Rev* **214**: 143-154.
- Yu, P., W. Lubben, H. Slomka, J. Gebler, M. Konert, C. Cai, L. Neubrandt, O. Prazeres da Costa, S. Paul, S. Dehnert, K. Dohne, M. Thanisch, S. Storsberg, L. Wiegand, A. Kaufmann, M. Nain, L. Quintanilla-Martinez, S. Bettio, B. Schnierle, L. Kolesnikova, S. Becker, M. Schnare and S. Bauer (2012). "Nucleic acid-sensing Toll-like receptors are essential for the control of endogenous retrovirus viremia and ERV-induced tumors." *Immunity* **37**(5): 867-879.
- Zaiss, D. M., N. de Graaf and A. J. Sijts (2008). "The proteasome immunosubunit multicatalytic endopeptidase complex-like 1 is a T-cell-intrinsic factor influencing homeostatic expansion." *Infect Immun* **76**(3): 1207-1213.
- Zambrowicz, B. P. and A. T. Sands (2003). "Knockouts model the 100 best-selling drugs--will they model the next 100?" *Nat Rev Drug Discov* **2**(1): 38-51.
- Zhang, Y., G. Joe, E. Hexner, J. Zhu and S. G. Emerson (2005). "Host-reactive CD8+ memory stem cells in graft-versus-host disease." *Nat Med* **11**(12): 1299-1305.
- Zhao, C. and J. D. Davies (2010). "A peripheral CD4+ T cell precursor for naive, memory, and regulatory T cells." *J Exp Med* **207**(13): 2883-2894.

- Zhao, J., G. Evans, W. Li, L. Green, S. Chu, P. Marder and S. Na (2008). "Rapid and quantitative detection of p38 kinase pathway in mouse blood monocyte." In Vitro Cell Dev Biol Anim **44**(5-6): 145-153.
- Zheng, H., D. Fletcher, W. Kozak, M. Jiang, K. J. Hofmann, C. A. Conn, D. Soszynski, C. Grabcic, M. E. Trumbauer, A. Shaw and et al. (1995). "Resistance to fever induction and impaired acute-phase response in interleukin-1 beta-deficient mice." Immunity **3**(1): 9-19.
- Zimprich, A., A. Benet-Pages, W. Struhal, E. Graf, S. H. Eck, M. N. Offman, D. Haubenberger, S. Spielberger, E. C. Schulte, P. Lichtner, S. C. Rossle, N. Klopp, E. Wolf, K. Seppi, W. Pirker, S. Presslauer, B. Mollenhauer, R. Katzenschlager, T. Foki, C. Hotzy, E. Reinthaler, A. Harutyunyan, R. Kralovics, A. Peters, F. Zimprich, T. Brucke, W. Poewe, E. Auff, C. Trenkwalder, B. Rost, G. Ransmayr, J. Winkelmann, T. Meitinger and T. M. Strom (2011). "A mutation in VPS35, encoding a subunit of the retromer complex, causes late-onset Parkinson disease." Am J Hum Genet **89**(1): 168-175.
- Zoeger, A., M. Blau, K. Egerer, E. Feist and B. Dahlmann (2006). "Circulating proteasomes are functional and have a subtype pattern distinct from 20S proteasomes in major blood cells." Clin Chem **52**(11): 2079-2086.
- Zuckermann, F. A. (1999). "Extrathymic CD4/CD8 double positive T cells." Vet Immunol Immunopathol **72**(1-2): 55-66.

8 Index of abbreviations

Å	Ångström
ALDD	Autoinflammation, lipodystrophy and dermatosis syndrome
APC	Antigen-presenting cell
BCR	B cell receptor
BHI	Brain-heart infusion
bp	Base pairs
CANDLE	Chronic atypical neutrophilic dermatosis with lipodystrophy and elevated temperature syndrome
Cas9	CRISPR associated protein 9
CD	Cluster of differentiation
CFU	Colony-forming units
CLP	Common myeloid progenitor
CMF	Clean Mouse Facility
CMP	Common myeloid progenitor
CRISPR	Clustered regularly interspaced short palindromic repeats
cTEC	Cortical thymic epithelial cell
CTL	Cytolytic T lymphocyte
CXCL1	Chemokine (C-X-C motif) ligand 1
DAB	3,3'-diaminobenzidine
DC	Dendritic cell
DKO	Double knockout
DMSO	Dimethyl sulfoxide
DN	Double-negative
DNA	Deoxyribonucleic acid
dNTP	Deoxynucleotide triphosphate

DP	Double-positive
EDTA	Ethylenediaminetetraacetic acid
ELISA	Enzyme-linked immunosorbent assay
ENU	<i>N</i> -ethyl- <i>N</i> -nitrosourea
EP	Erythrocyte progenitor
EpCam	Epithelial cell adhesion molecule
ER	Endoplasmic reticulum
ES	Embryonic stem
FACS	Fluorescence-activated cell sorting
Fc γ R	Fc γ Receptor III/II
FELASA	Federation of European Laboratory Animal Science Associations
FMO	Fluorescence minus one
5'FOA	5'fluoro-orotic acid
G-CSF	Granulocyte colony-stimulating factor
gRNA	guide-RNA
CM leu ⁻	Complete medium without leucine
GAC	Genome Analysis Center
GMC	German Mouse Clinic
GMP	Granulocyte - macrophage progenitor
GP	Granulocyte progenitor
G170W	Exchange of the amino acid number 170 from glycine to alanine
G170W	Exchange of the amino acid number 170 from glycine to tryptophan
hCG	Human chorionic gonadotropin
HDR	Homology- directed repair
HE	Hematoxylin and eosin
HSC	Hematopoietic stem cell

IFN	Interferon
Ig	Immunoglobulin
IL	Interleukin
i.p.	Intraperitoneal
IU	International unit
i.v.	Intravenous
JMP	Joint contractures, muscular atrophy, microcytic anemia, and panniculitis-induced lipodystrophy
iNKT	Invariant NKT
KLICK	Keratosis linearis with ichthyosis congenitalis and sclerosing keratoderma
KO	Knockout
<i>L.m</i>	<i>Listeria monocytogenes</i>
Lin ⁻	Lineage negative
LLO	Listeriolysin O
LMP	Low molecular weight protein
LOD	Logarithm of the odds
LPS	Lipopolysaccharide
LSK	Lineage-negative Sca-1-positive cKit-positive
LT-HSC	Long-term hematopoietic stem cell
MacP	Macrophage progenitor
MACS	Magnetic cell separation
MECL-1	Multicatalytic endopeptidase complex subunit-1
MEP	Megakaryocyte - erythrocyte progenitor
MES	2-(N-morpholino)ethanesulfonic acid
MHC	Major histocompatibility complex
MkP	Megakaryocyte progenitor

MPD	2-Methyl-2,4-pentanediol
MPO	Myeloperoxidase
MPP	Multipotent progenitor cell
mTEC	Medullary thymic epithelial cell
Neo	Neomycine
NF- κ B	Nuclear factor- κ B
NHEJ	Non-homologous end joining
NK	Natural killer
NKJO	Nakajo- Nishimura syndrome
OMIM	Online Mendelian Inheritance in Man
PBS	Phosphate-buffered saline
PCR	Polymerase chain reaction
PI	Propidium iodide
p.i.	Post infection
PMA	Phorbol 12-myristate 13-acetate
PMSG	Pregnant mare serum gonadotropin
POMP	Proteasome maturation protein
RAG1	Recombinase-activating gene 1
RMSD	Root-mean-square deviation
ROS	Reactive oxygen species
Sca-1	Stem cells antigen-1
SCID	Severe combined immunodeficiency
SLAM	Signaling lymphocytic activation molecule
SNP	Single nucleotide polymorphism
SNV	Single nucleotide variant
SPF	Specific pathogen-free

SOP	Standard operating procedure
SSC	Side scatter
STAT1	Signal transducer and activator of transcription 1
ST-HSC	Short-term hematopoietic stem cell
Suc-LLVY-AMC	N-Succinyl-Leu-Leu-Val-Tyr-7-Amino-4-methylcoumarin
<i>T.</i>	<i>Thermoplasma</i>
TAP	Transporter associated with antigen processing
T _{CM}	Central memory T cell
TCR	T cell receptor
Tdt	Terminal deoxynucleotidyl transferase
TEC	Thymic epithelial cell
T _{EM}	Effector memory T cell
TGF	Transforming growth factor
T _H	T helper cell
t _m	Melting temperature
TNF	Tumor necrosis factor
T _{reg}	Regulatory T cell
U	Unit
v/v	Volume per volume
WT	Wild type
w/v	Weight per volume
YPD	Yeast extract peptone dextrose

9 Contributions

The work presented in this thesis would not have been possible without the contributions of the following people:

I am very grateful to my collaborators Michael Groll and Eva Huber (Center for Integrated Protein Science at the Department Chemistry, TUM), for molecular analyses of the proteasome in the yeast system, as well as Wolfgang Heinemeier for yeast mutagenesis experiments. Furthermore, Eva Huber contributed to preparation of Figures 33 and 35.

Special thanks go to Tanja Klein-Rodewald and Julia Calzada-Wack from the Pathology Screen of the German Mouse Clinic who performed the pathological analyses and helped me with the histological analyses of TUB006 mice.

I also would like to thank Simon Grassmann for retroviral constructs and transduction experiments.

I further thank Andrew Macpherson and Kathy McCoy from the University of Bern for giving me the opportunity to analyze the phenotype of TUB006 mice under germ-free breeding conditions.

Furthermore, I thank Markus Ollert and Christian Anders (Klinik und Poliklinik für Dermatologie und Allergologie, Am Biederstein, TUM) for sharing their dermatological experience and analysis of the skin samples.

I am very grateful to Corinne Graf, Florian Schleicher, Christine Fürmann and Katherine Molter for excellent technical assistance, including part of the genotyping procedures, mouse handling and assistance in some laborious experiments.

Exome sequencing and data analysis were performed in collaboration with Tim Strom and Thomas Wieland from the Institute of Human Genetics, TUM.

I also want to thank Werner Panzer for irradiation of bone marrow recipients.

I further want to thank Marcus Groettrup for kindly providing MECL-1 knockout mice and anti-MECL-1 antibodies.

The initial screening of the TUB006 mouse line was performed by Svetoslav Kalodiev, the backcross to BALB/c was performed by Christina Schessl and SNP mapping approach by Christina Schessl and Matthias Klawns.

Many thanks to the animal caretakers of the mouse housing facilities at the German Mouse Clinic and the Institute of Medical Microbiology, Immunology and Hygiene.

The de-novo generation of the TUB006 mutant using CRISPR/Cas9 nickase was performed in collaboration with Thorsten Buch and Jane Beil.

10 Acknowledgement

First of all, I would like to thank my supervisors Dirk Busch and Martin Hrabě de Angelis for their supervision and for providing me the opportunity to work in their labs, for entrusting me this project, their confidence in me, and their support. Dirk's enthusiasm and invaluable immunological expertise helped me many times, when I was struggling.

I consider myself very lucky that I got to know Thure Adler, who shared his outstanding knowledge and experience in flow cytometry and mouse immune phenotyping with me. I am very grateful for his interest in my work, his enormous enthusiasm and encouragement. His advice and ideas were of great help not only for my scientific results but also for my personality.

Special thanks go to Michael Groll and Eva Huber, without whose contribution and enthusiasm the identification of the molecular basis would not have been possible.

I want to thank all members of the Busch group and the GMC, especially my PhD colleagues for the nice and relaxed working atmosphere. I am grateful for all the funny moments inside and outside the lab.

I am also very grateful to Alex Riedel for proofreading parts of my dissertation and his motivating support.

Last but not least, I thank my family and my parents for the support and confidence in me. Above all, I am most indebted to my beloved husband for his tremendous support during last years and for continuously believing in me.

I, Irina Treise, hereby declare that I independently prepared the present thesis, using only the references and resources stated. All contributions are listed. This work has not been submitted to any examination board yet. Parts of this work have been or will be published in scientific journals.

Munich, August 25th 2016

A handwritten signature in black ink, appearing to read 'Irina Treise', written in a cursive style.